TECHNISCHE UNIVERSITÄT MÜNCHEN
Fakultät für Maschinenwesen
Lehrstuhl für Leichtbau

Shape Morphing Skin Design with Applications on Mechanically Reconfigurable Reflector Antennas and Sailplane Wings

Bin Wei

Vollständiger Abdruck der von der Fakultät für Maschinenwesen der Technischen Universität München zur Erlangung des akademischen Grades eines

Doktor-Ingenieurs (Dr.-Ing.)

genehmigten Dissertation.

Vorsitzender: Univ.-Prof. Dr.-Ing. Klaus Drechsler
Prüfer der Dissertation:

1. Univ.-Prof. Dr.-Ing. Horst Baier

2. Univ.-Prof. Dr.-Ing. Kai-Uwe Bletzinger

Die Dissertation wurde am 25.06.2015 bei der Technische Universität München eingereicht und durch die Fakultät für Maschinenwesen am 29.03.2016 angenommen.

Acknowledgments

I would like to express my gratitude to my supervisor Prof. Dr.-Ing. Horst Baier for his guidance during my PhD time and his kind help during my study time. In last five years, with his guidance and encouragement I gained knowledge and experience through working on different projects, which enable me to finalize this thesis.

In the same time, I would like to appreciate the help from all colleagues at the institute. Especially I would like to thank Dr.-Ing. Leri Datashvili for his meaningful and valuable discussion and suggestions during my work. My thanks also go to the Europe Space Agency and Akaflieg München e.V. for the initializing of these challenging projects. To the colleague Markus Schatz and Stephan Endler, I would like to thank their proofreading of my thesis. Additionally I would like to thank all colleagues, partners and students, who have been cooperating with me on projects, for their supports and helps.

My heartfelt appreciation will be given to my parents for their supports in my abroad study and life. To my wife Ziwei, I would like to thank her accompany, encouragement and understanding. Without the supports from my families, I can not have accomplished this work.

Munich, May 2015 Bin Wei

Abstract

Morphing structures are able to adjust their configurations according to the actual application environments. Therefore their performance and efficiency can be enhanced in a wide range of applications. Among the numerous challenges in developing morphing structures, shape morphing skin design is one of the most challenging for the two counteracting requirements. On the one hand, the morphing skin should be flexible enough to accommodate relative large amplitude deformations, however, on the other hand it should be sufficient stiff to maintain smooth shapes during the reshaping process and in its final shapes.

To solve the task of morphing skin design, a method, tailoring material compounds and their relevant design parameters so as to satisfy the counteracting requirements of compliance and stiffness of morphing skins, is presented in this thesis. The developed analytical and numerical approaches are able to correlate the complex reshaping behavior with various design parameters to accomplish the task of morphing skin design. Besides the analytical and numerical investigations, experimental investigations to characterize flexible materials are also conducted. Moreover, the developed approaches are demonstrated and validated by two applications on a mechanically reconfigurable reflector skin and the morphing skin of a sailplane wing.

Kurzfassung

Formvariablen Strukturen sollen ihre Konfigurationen entsprechend den aktuellen Anwendungsumgebungen anpassen können. Hierdurch können ihre Leistungsfähigkeit und Effizienz in einem weiten Bereich von Anwendungen verbessert werden. Zwischen den zahlreichen Herausforderungen bei der Entwicklung von den Formvariablen Strukturen ist der Entwurf von formvariablen Häuten eine der anspruchsvollsten Aufgaben für die zwei gengenläufigen Anforderungen. Einerseits sollte die formvariable Haut flexibel genug sein, um relative große Verformungen zu realisieren, aber andererseits sollte sie ausreichend steif sein, um glatte Formen während und nach der Verformung beizubehalten.

Um diese Aufgaben innerhalb des Entwurfs einer formvariablen Haut zu lösen, wird in dieser Arbeit eine Methode zur Bestimmung von optimalen Materialzusammensetzungen und ihren weiteren Parameter zur Erfüllung von anspruchsvollen Anforderungen bezüglich der Nachgiebigkeit und Steifigkeit von formvariablen Häuten präsentiert. Die entwickelten analytischen und nummerischen Methoden sind in der Lage die komplexe Verformungsverhältnisse mit den Entwurfsparametern zu korrelieren, um das Entwurfsproblem von formvariablen Häuten anzugehen. Neben den analytischen und nummerischen Untersuchungen werden Untersuchungsmethoden zur experimentellen Materialcharakterisierung von flexiblen Werkstoffen vorgestellt. Die entwickelten Methoden werden demonstriert und validiert durch zwei Anwendungsbeispiele an einer mechanisch rekonfigurierbaren Reflektorhaut und der formvariablen Haut eines Segelflugzeugs.

Contents

List of Figures XI

List of Tables XV

Nomenclature XVII

1. Introduction 1
- 1.1. Introduction of Morphing Structures . . . 1
- 1.2. Motivation . . . 2
  - 1.2.1. Mechanically Reconfigurable Reflector Antenna . . . 2
  - 1.2.2. Morphing Wing of Aircraft . . . 4
- 1.3. Scope and Objectives of Thesis . . . 5
- 1.4. Outline . . . 5

2. State of the Art 7
- 2.1. Morphing Skins of Mechanically Reconfigurable Reflector Antennas . . . 7
  - 2.1.1. From Shape Correction to Reconfiguration . . . 7
  - 2.1.2. Morphing Skins of Reconfigurable Reflector Antennas . . . 8
- 2.2. Morphing Skins of Morphing Aircraft Wing . . . 13
- 2.3. Summary of Literature Review . . . 16

3. Fundamentals and Background 19
- 3.1. Basics of Reconfigurable Reflector Antennas . . . 19
  - 3.1.1. Fundamental Parameters of Antennas . . . 19
  - 3.1.2. Antenna Types . . . 23
- 3.2. Basics of Aircraft Wings and High-lift Devices . . . 24
- 3.3. Background of Mechanically Reconfigurable Reflectors and Morphing Sailplane Wings . . . 26
  - 3.3.1. Mechanically Reconfigurable Reflectors . . . 26
  - 3.3.2. Morphing Sailplane Wings . . . 28

4. Compound Material Design of Reflector Morphing Skins 31
- 4.1. Objectives and Approaches of Reflector Morphing Skin Design . . . 31
  - 4.1.1. Objectives of Reflector Morphing Skin Design . . . 31
  - 4.1.2. Approaches of Reflector Morphing Skin Design . . . 31
- 4.2. Investigations of Parameters to Material Design . . . 38
  - 4.2.1. Representative Unit Cell Models . . . 38
  - 4.2.2. Influence of Boundary Conditions . . . 40
  - 4.2.3. Influence of Geometry Parameters . . . 43
  - 4.2.4. Influence of Material Properties . . . 49
- 4.3. Material Properties of Reflector Morphing Skins . . . 54

4.3.1. Range of Material Properties . . . 54
4.3.2. Feasible Material Properties in Design Examples . . . 56
4.4. Material Concepts of Reflector Morphing Skins . . . 58
4.5. Extending Methods of Material Design to Morphing Wing Skins . . . 60

5. Material Characterization of Flexible Composites 61
5.1. Materials and Test Set Up . . . 61
5.1.1. Materials . . . 61
5.1.2. Test Set Up for Flexural Stiffness . . . 62
5.1.3. Test Set Up for Shear Stiffness . . . 63
5.2. Testing Results . . . 64
5.2.1. Results of Bending Tests . . . 64
5.2.2. Results of Shear Tests . . . 66
5.2.3. Fiber Microbuckling . . . 67
5.3. Summary of the Chapter . . . 68

6. Mechanically Reconfigurable Reflectors and Their Morphing Skins 69
6.1. Reflector Morphing Skin Design and Analysis . . . 70
6.1.1. Laminate Layout of Reflector Morphing Skins . . . 70
6.1.2. Layout Design with Patches . . . 72
6.1.3. Layout Design Using Triangular Lattice . . . 73
6.1.4. Concept Evaluations on Medium Size Representative Models . . . 74
6.2. Reshaping Analyses of the Engineering Model . . . 77
6.2.1. Model Description . . . 77
6.2.2. Reshaping Analyses of the Engineering Model . . . 79
6.2.3. Nonlinearity in Reshaping . . . 82
6.3. Technology Demonstrator and Reshaping Results Correlations . . . 84
6.3.1. Demonstrator Model Description . . . 84
6.3.2. Reshaping Tests and Results Correlations . . . 85

7. Sailplane Wings and Their Morphing Skins 91
7.1. Objectives and Approaches of Morphing Wing Skin Design . . . 91
7.1.1. Objectives of Morphing Wing Skin Design . . . 91
7.1.2. Approaches of Morphing Wing Skin Design . . . 91
7.2. Morphing Wing Skin Design . . . 93
7.2.1. Preliminary Analyses . . . 93
7.2.2. Detailed Analyses and Correlations with Tests . . . 96
7.2.3. Summary . . . 105

8. Conclusion and Outlook 107

A. Bibliography 111

B. Appendix 119
B.1. Results of Reshaping Analyses on the Medium Size Models . . . 119
B.2. Results of Reshaping Analyses . . . 122
B.3. Sensitivity Study on Demonstrator . . . 123
B.4. Results of Shape Correlation on Demonstrator . . . 124
B.5. Experiments of Flexible Sandwich . . . 125

B.6. Results of Stress and Strain of the Tailored CFRP Laminates 126

List of Figures

1.1. A principle sketch of the mechanically reconfigurable reflector and the morphing wing [Wittmann et al. (2010)] . . . 2
1.2. An illustration of a mechanically reconfigurable reflector [Schreider et al. (2007)] 3
1.3. Flowchart of morphing skin design with a focus on methods . . . 6

2.1. The TICRA laboratory model of 10 x 10 mm spacing wire grid surface (left) and the model covered by the RF net (right) [Pontoppidan et al. (2010)] . . . 11
2.2. The LLB laboratory model, which contains 19 actuators and has a free rim boundary [Datashvili and Baier (2009)] . . . 12
2.3. A morphing trailing edge using eccentuator concept [Müller (2000)] . . . 14
2.4. Upper: a compliant morphing wing concept of FlexSys [Kota et al. (2003)] Lower: smart droop nose [Monner et al. (2009)] . . . 15
2.5. (1): a flexible sandwich skin and its core [Bubert et al. (2010)] (2): shape memory polymers [Perkins et al. (2004)] (3): a corrugated composite skin [Yokozeki et al. (2006)] . . . 16

3.1. (a) Radiation lobes and beamwidths (b) Linear plot of power pattern [Balanis (2005)] . . . 21
3.2. Four typical parabolic reflector antennas . . . 23
3.3. Geometry of a Gregorian dual-offset reflector antenna [Cappellin and Pontoppidan (2009)] . . . 24
3.4. A sketch of airfoil NACA 4412 and its pressure distribution . . . 25
3.5. Airfoil and common high-lift devices [Howe (2000)] . . . 26
3.6. Three representative reshaping tasks [Schreider et al. (2007)] . . . 27
3.7. An image of Mü 31 of Akaflieg München [Aka (c)] . . . 29

4.1. Scheme of the compound material design for reflector morphing skin . . . 33
4.2. The force components on a small element from a plate . . . 34
4.3. Energy expressions of plates . . . 36
4.4. A representative unit cell . . . 39
4.5. Deformation plots of the plate with large deflection and artificial pure bending 40
4.6. Plate with large deflection under free movable edge . . . 41
4.7. Ratio of plate and membrane energy in large deflection . . . 41
4.8. The center cutting lines of three analyses . . . 42
4.9. The ratios of plate and membrane energy varying with thickness . . . 44
4.10. The center cutting lines of plates with different thickness . . . 44
4.11. A representative unit cell with triangular lattice . . . 46
4.12. Deformation shapes of the unit cell with triangular lattice . . . 46
4.13. Cutting lines of shell models with large deflection . . . 49
4.14. Deflection plots of unit cells with different shear modulus . . . 52
4.15. Cutting lines of unit cells with different shear modulus . . . 53

4.16. Ratios of plate energy relating to material parameters . . . 55
4.17. 50% Plate energy achieved by material parameter combinations . . . 55
4.18. Feasible material properties in the design example 1 . . . 57
4.19. Feasible material properties in the design example 2 . . . 57
4.20. Feasible material properties in the design example 3 . . . 57
4.21. Feasible material properties in the design example 4 . . . 58
4.22. The shell-membrane reflector made of triax-CFRS laminate [Datashvili (2009)] 59
4.23. Grid shell structures [Gridshell] . . . 60

5.1. A micrograph of plain woven CFRS [Hoffmann (2012)] . . . 62
5.2. Test set up of three point bending . . . 63
5.3. Relation of equivalent flexural moduli to number of layers . . . 64
5.4. Compression stress strain curves of laminates in three point bending tests . . . 65
5.5. Microbuckling on a CFRS laminate . . . 66
5.6. Stress-strain response of a biax-CFRS laminate under cyclic tension . . . 66
5.7. Stress-strain response of a biax-CFRS laminate to rupture . . . 67

6.1. Flowchart of reflector morphing skin design . . . 69
6.2. Relation of energy ratio to number of layers . . . 71
6.3. A unit cell with patches . . . 72
6.4. Medium size models: model 1: 7 full layers with 25 actuators in square lattice (left), model 2: 7 full layers with 19 actuators in triangular lattice (middle), model 3: 3 full layers plus 6 patches with 19 actuators in triangular lattice (right) . . . 74
6.5. Linear and nonlinear reshaping plots in the testing case 4 . . . 76
6.6. The FEM model of the reconfigurable reflector . . . 77
6.7. Definitions of boundary conditions on the FEM model . . . 78
6.8. A visualization of the multilayer concept in the FEM model . . . 79
6.9. Target and achieved shapes of the task Europe . . . 81
6.10. Linear and nonlinear reshaping analyses of the task Europe . . . 82
6.11. The flowchart of multi-step linear analysis . . . 83
6.12. The FEM model of the demonstrator (top view) . . . 84
6.13. The technology demonstrator [Endler et al. (2014)] . . . 85
6.14. The demonstrator with measurement markers (top view) [Endler et al. (2014)] 86
6.15. Predicted and Measured shapes of the Brazil task . . . 87
6.16. Shape pattern of the initial geometry distortions . . . 88
6.17. The updated measured and predicted shapes of the Brazil task . . . 89

7.1. Flowchart of morphing wing skin design . . . 92
7.2. The CFRP horn as the eccentuator [Wießmeier] and the idealized deflection of the sailplane morphing leading edge . . . 93
7.3. The deflection profile of a closed leading edge . . . 94
7.4. The proposed morphing skin concept of the morphing leading edge . . . 95
7.5. The flexible sandwich concept [modified from Weinzierl (2013)] . . . 97
7.6. The unit cell of the accordion honeycomb core [Xu (2012)] . . . 97
7.7. The value of local strain related to the cell angel (a) and the inclined wall length (b) [Weinzierl (2013)] . . . 98
7.8. The designed accordion honeycomb core . . . 99
7.9. The maximal strain on the designed accordion honeycomb core . . . 100

7.10. The manufactured accordion honeycomb core for tensile tests [Weinzierl (2013)]101
7.11. A demonstrator of the flexible sandwich [Weinzierl (2013)] 102
7.12. The detailed morphing leading edge FEM model [Kraus (2013)] 103
7.13. The implemented horn in the FEM model 104
7.14. The deformation of the morphing leading edge 104
7.15. The stress distribution at the contact region in different reshaping stages . . . 105

B.1. Target and achieved shapes of the task Brazil 122
B.2. Target and achieved shapes of the task ConUS 123
B.3. Predicted and measured shapes of the Europe task 124
B.4. Update measured and predicted shapes of the Europe task 124
B.5. The manufactured according core with extreme large strain [Weinzierl (2013)] 125
B.6. The demonstrator of the flexible sandwich [Weinzierl (2013)] 125

List of Tables

3.1. Frequency bands for satellite communications 20

4.1. Strain energy in the plate with large deflection and artificial pure bending . . . 40
4.2. Strain energy in plate with large deflection under free movable edge 41
4.3. Strain energy in plates with large deflection for different unit cell sizes 45
4.4. Strain energy in plates with large deflection for different unit cell shapes . . . 46
4.5. Strain energy in shells with large deflection 48
4.6. Strain energy in plates with large deflection for different material properties . 51
4.7. Strain energy in plates with large deflection for low shear modulus 53

5.1. Material properties according to the suppliers 62
5.2. Shear testing results 67

6.1. Material properties of the biax-CFRS laminate (layer number more than 3) . . 70
6.2. Shape difference between linear and nonlinear reshaping analyses of different deflections and layer number 71
6.3. Shape difference between linear and nonlinear reshaping analyses with varying number of patches 72
6.4. Ratio of bending energy and shape difference in concepts of 3 full layers with patches 73
6.5. Results overview of three reshaping analyses 80
6.6. Extreme strains in three reshaping analyses 81
6.7. Improvements of correlations between the numerical and measured shapes . 88
6.8. Reshaping results using the updated FEM models and measurements 90

7.1. Geometry parameters of the accordion honeycomb core 97
7.2. Tensile modulus of the designed accordion honeycomb core 101
7.3. Material properties of the UD-CFRP laminate (referring to the definitions of Luftfahrt-Bundesamt (LBA)) 103
7.4. Laminate layout design 103

B.1. Shape difference in the reshaping case 1 119
B.2. Shape difference in the reshaping case 2 119
B.3. Shape difference in the reshaping case 3 119
B.4. Shape difference in the reshaping case 4 120
B.5. Shape difference in the reshaping case 5 120
B.6. Shape difference in the reshaping case 6 120
B.7. Shape difference in the reshaping case 7 121
B.8. Shape difference in the reshaping case 8 121
B.9. Comparison of measured and predicted reference shapes 123
B.10. Extreme stresses (MPa) in reshaping of the leading edge, skin at the contact region 126

B.11. Extreme strains in reshaping of the leading edge, skin at the contact region . . 126
B.12. Extreme stresses (MPa) in reshaping of the leading edge, skin without interactions 126
B.13. Extreme strains in reshaping of the leading edge, skin without interactions . . 126

Nomenclature

Abbreviations

ABAQUS	software suite for finite element analysis by SIMULIA Inc
ACARE	Advisory Council for Aeronautics Research in Europe
AL	aluminum
ANSYS	Analysis System by ANSYS, Inc
ARO	Algonquin Radio Observatory
biax-CFRS	biaxially woven carbon fiber reinforced silicone
CB	carbon black
CFRP	carbon fiber reinforced plastic
CFRS	carbon fiber reinforced silicone
CTE	coefficient of thermal expansion
dB	decibel
EM	electromagnetic
ESA	Europe Space Agency
FEM	finite element method
FNBW	first-null beamwidth
G	Gain
GPS	Global Positioning System
GO	geometrical optics
HPBW	half-power beamwidth
IEEE	Institute of Electrical and Electronics Engineers
JWST	James Webb Space Telescope
LBA	Luftfahrt-Bundesamt
LLB	Institute of Lightweight Structures - Technische Universität München
MATLAB	MATrix LABoratory - commercial software from The MathWorks, Inc.

NACA	National Advisory Committee for Aeronautics
NRAO	National Radio Observatory
PIM	Passive Intermodulation
RMS	root mean square error
PO	physical optics
RSGB	Radio Society of Great Britain
PTFE	Polytetrafluoroethene
PVDF	polyvinylidene fluoride
RF	ratio frequency
TAS	Thales Alenia Space
triax-CFRS	triaxially woven carbon fiber reinforced silicone
TRL	technological readiness level
TWF	triaxially woven carbon fiber fabric
UAV	unmanned aerial vehicle
UD	unidirectional
UV	ultraviolette
WHO	World Health Organization

Symbols

Symbols	**Description**
$\alpha = \frac{h}{l}$	cell aspect ratio
$\beta = \frac{t}{l}$	inclined wall thickness ratio
γ	shear strain of plate
$\gamma = \frac{b}{l}$	depth ratio
η	the aperture efficiency
$\eta = \frac{t_h}{t}$	vertical wall thickness ratio
θ	cell angle
$\overline{\delta^2}$	the phase front variance caused by aperture surface error
ε	the effective reflector tolerance, e.g. the RMS surface error
ε	strain of plate
λ	wavelength

Symbols	Description
ν	Poisson's ratio
σ	strength of materials
χ	curvatures of shell
A	cross-section area
c	speed of light
D	aperture diameter
D	flexural rigidity
e	interval distance ratio between unit cells
E	Young's modulus
f	frequency
G	shear modulus
G_0	gain without loss
h	length of the vertical wall
h	plate thickness
l	length of the inclined wall
N_x, N_y, and N_{xy}	forces per unit length
q	lateral loads on the plate
t	thickness of the inclined wall
t_h	thickness of the vertical wall
u, v, w	deflection of plate
V	strain energy
w	deflection
X and Y	body forces or tangential forces per unit area of the middle plane of the plate

1. Introduction

1.1. Introduction of Morphing Structures

In the field of engineering, a morphing structure can be understood as such a system, which is able to change its shape/configuration in relative large amplitudes. As a major feature, its reshaping is realized by the entire system deforming, but not by relatively movements of discrete parts [Thill et al. (2008)]. According to this definition, a classical high-lift system of an aircraft wing composed of hinged aileron and/or flap can not be taken as a morphing structure. However, it could become a morphing structure through complete systematic updates, for instance, equipping advanced sensing and actuation systems as well as covering by a shape variable skin and etc. Then it can realize the desired continuous deformation in terms of surface area and camber change without open gaps in and between itself as well as no sudden cross-section change in airfoil profile.

The most known engineering structures are passive structures, whose topology, geometry and material are defined in the developing phase to achieve compromised performance under several predefined application environments. In operations, the above mentioned structural parameters can't be changed and the performance of structures can't always be optimal. To improve adjustability of systems, adaptive/smart structures are developed. According to the actual operational environments, the configurations of adaptive structures can be adjusted within relative small amplitudes via actuations. As further extensions of adaptive structures, morphing structures can change their shapes significantly, which are more suitable for practice applications.

Investigations about morphing structures are mainly focusing on mechanically reconfigurable reflector antennas and morphing aircraft wings in this thesis (see Figure 1.1). The reconfigurable reflector antenna can adjust its contour of reflector's surface according to operational requirements e.g. geographical coverage and weather conditions, thereby its usability, efficiency and economy can be improved. The morphing aircraft wing can adjust its configuration like airfoil profile, deflection of leading/trailing edge to achieve optimal performance in a wide range of operational environments. Furthermore, the continuous reshaping of the morphing wing brings advantages as higher lift-drag ratio, better loading distribution, and lower level of noise and vibration.

Generally a morphing structure could often contain three subsystems, which are morphing skin, actuation & sensing system and interface system between them. The three subsystems usually correlated with each other directly or indirectly. Compare with morphing skin, actuation & sensing system and interface system have relative higher technological readiness level (TRL) for their wide applications on adaptive structures. But for morphing skins, current investigations are mostly on the laboratory level and the maturity of the technology is still quite low. The reason can be found at the most important requirement for morphing skin: it should be flexible enough to accommodate relative large amplitude deformations, sufficient stiff to maintain smooth shapes during the reshaping process and in

its final shapes. Furthermore, there are some additional structural, functional, and manufacturing requirements for the morphing skin design on different concrete applications. These multiple and some even counteracting requirements together form the challenging task of morphing skin design.

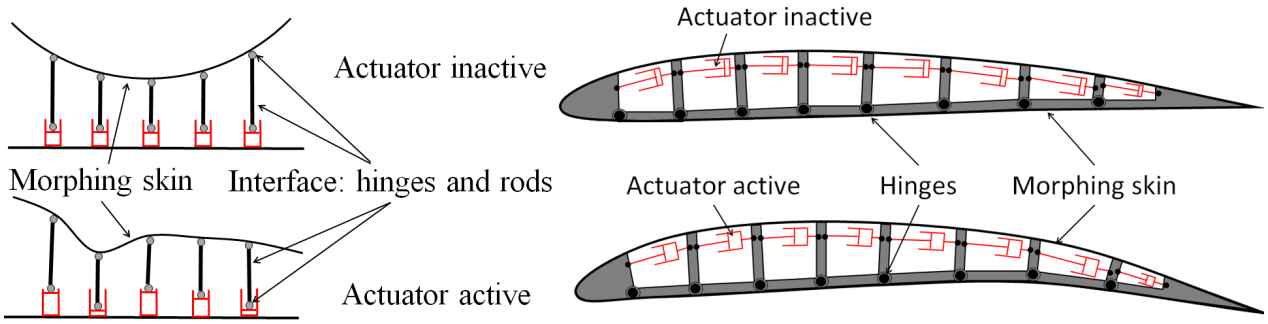

Figure 1.1.: A principle sketch of the mechanically reconfigurable reflector and the morphing wing [Wittmann et al. (2010)]

1.2. Motivation

1.2.1. Mechanically Reconfigurable Reflector Antenna

Reflector antenna is a widely applied space communication system especially in the fields of radio astronomy and telecommunication. In developing of reflector antennas, tremendous efforts have been paid to improve the efficiency, reduce the cross-polarization and achieve a satisfactory sidelobe envelope [Gu (1995)]. One of the most common solutions is the shaped reflector, whose development is benefited from reliable analytical and numerical techniques like geometrical optics (GO) and physical optics (PO). The surface contour of the shaped reflector is defined according to satellite orbit position and desired geographical coverage. Compare with the reflectors using standard shapes e.g. paraboloid and ellipsoid, the shaped reflector has higher efficiency and lower interference in geographical areas adjacent to the service area [Yoon (2002)].

The shaped reflector is a typical passive structure, whose specific tailored surface shape can't be changed during the operating period. However in practice, on the one hand, modern satellites are becoming more reliable contributed by improvements on systematic techniques. Their service life can be around 10 years and is expected to be even 15 years in future. On the other hand, the predefined radiation pattern and geographical coverage are probably changed during the service life of the satellites due to the rapid development of our world. As stated in Yoon (2002), a usual life cycle of a predefined mission scenario for antennas is about 5 years. After this period, the predefined application scenario is partly or even greatly changed and thereby the satellite antenna turns to be low efficiency and in the worst case even inefficient, which causes a great waste of such expensive communication devices. The conflict between the passive satellite antennas and varied application requirements leads to rising demands of adjustable satellite antennas.

The capability of reconfiguration can bring benefits for reflector antennas on the following aspects: allow the same satellite working in several orbit positions, adjust its radiation patterns according to actual geographical coverage and data traffic loads, and compensating for varying weather conditions [Cappellin (2007)].

The reconfigurable ability of the reflector antenna is firstly implemented by electronical means. The array-fed reflector antenna contains a beam-forming network of array fed and solo or dual standard/shaped reflectors. The generated radiation patterns are adjusted through varying power and shafting phase of individual array elements. Applications of this type of reconfigurable reflector antennas are found on international communications, regional communications and broadcasting [Altan and Rispoli (1989)]. Although they have satisfactory performance on certain applications, there are some limitations like high cost, system complexity, extra mass, and low efficiency as stated in Lawson and Yen (1988) and Clarricoats et al. (1994). To overcome these limitations, further technology development of reconfigurable reflector antennas is required.

The alternative mean is using the mechanically reconfigurable reflector in combination with a single high performance feed or small feed clusters (Figure 1.2). The reflector surface is reshaped via actuators connected at the rear side. The resulting radiation pattern can match the defined target radiation pattern with high accuracy. The mechanically reconfigurable reflector is belonging to morphing structures. The task of its morphing skin design is taken as a major example for examining and verifying the developed methodologies and technologies in scope of this thesis .

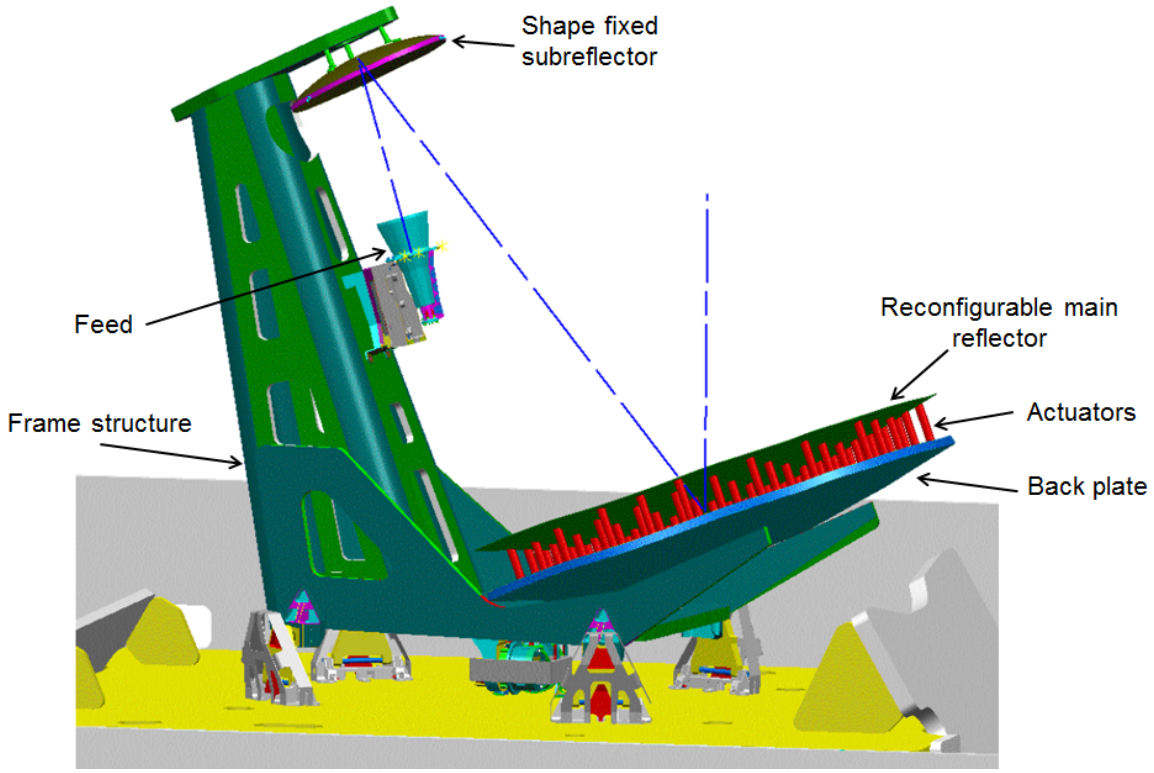

Figure 1.2.: An illustration of a mechanically reconfigurable reflector [Schreider et al. (2007)]

1.2.2. Morphing Wing of Aircraft

The civil aircraft industry shows strong economic growth rates in the last decade. Because of additional demands from rising countries with large populations like Brazil, China, and India etc., this growth rate is expected to keep robust in the next 20-25 years. At the same time, the organizations like Advisory Council for Aeronautics Research in Europe (ACARE) and World Health Organization (WHO) require the emissions per passenger kilometer and noise from civil aircraft to be dramatically reduced ($CO_2 < 50\%$, $NO_x < 80\%$, noise < 50%) [ACARE]. To satisfy the increasing demand of civil transport aircraft and achieve these goals about emission reductions at the same time, innovative aircraft designs are to be established and introduced.

One of the innovations is related to the widely applied high-lift devices of aircraft wings. Although they have quite well performance already, there are plenty of possible improvement potentials. For instance, the open gaps on the high-lift devices (mainly on the trailing edges) are one of the major sources of drag and noise increasing during deployment and operations. As stated in Wlezien et al. (1998), half of the mass and cost of civil aircraft wings are contributed by the complex high-lift devices. Not only that, the heavy and complex high-lift devices are also the reason of additional operation and maintenance cost.

A morphing wing can continuously change its configuration without open gaps, which brings benefits of improving aerodynamic performance, reducing noise level, and expanding flight envelope. The highly synthesized and integrated subsystems of the morphing wing can bring further benefits of mass saving, increase reliability, and reducing operation cost. Therefore the goals on economic and environmental aspects for the next generation aircraft can be achieved by applying morphing wings. The morphing wing aircraft shall have better performance on fuel consumption, maintenance cost, emissions and etc. Furthermore, aeroelasticity and control of aircraft can be improved by applying morphing wings. As stated by Kudva, Bartley-Cho, and many other scientists [Kudva (2004) and Bartley-Cho et al. (2004)], morphing wing aircraft have an enlarged flight envelop and increased manoeuvrability. The control of spanwise lift distribution through morphing of wings indicates the control ability of wing bending and twisting moments, which expands the control means to aircraft.

In contrast to the morphing skin of the mechanically reconfigurable reflector antenna, the skin of morphing aircraft wing is more focusing on realizing large scale reshaping amplitudes but not on extremely high shape accuracy. Further, it shall carry complex loads like pressure field imposed by the airflow together with actuation mechanisms and interactions between those. In addition to the mentioned compliant and rigidity about the morphing skin design, induced penalties like mass as well as system complexity and reliability shall be acceptable. Because of these numbers of counteracting requirements, the "design tunnel" of the morphing skin design for aircraft wings is actually quite narrow. In frame of the thesis, the morphing skin design is applied on sailplane wings. The sailplane flies only at low altitude with relative low speed. But the aerodynamics on wings can be quite complex due to its sport and dynamic flight manoeuvre. Actually, because of the slim airfoil of sailplane wings, which means limited geometry dimensions for morphing wing design, its morphing skin design can be more difficult as expected.

1.3. Scope and Objectives of Thesis

Although the morphing skin design of mechanically reconfigurable reflector antennas and morphing aircraft wings are quite different due to the complete different application environments and the resulting requirements, they have many common ground on the general aspects of methods of compound material design, analytical and numerical analysis techniques as well as correlation methods with experimental results. In this thesis, these generic methods are briefly described and discussed at first, and then demonstrated and validated on specific application examples of reconfigurable reflector skin design and sailplane morphing wing skin design.

The major objective of the thesis is exploring the method of compound material design, which is focusing on tailoring the global mechanical properties through combing different constituent materials to fulfill the required overall compliance and stiffness requirements to the morphing skin simultaneously. Besides the material tailoring, the related topics about definitions of boundary conditions, interface systems as well as actuations are investigated and discussed. Analytical and numerical techniques about how to determine the correlation between material design parameters and structural reshaping performance, how to perform reshaping analyses with considering interface and actuations, how to assess reshaping results, and how to reduce geometry nonlinearities and avoid material nonlinearities in the large amplitude reshaping are investigated and presented. Furthermore, measurement techniques to characterize the designed flexible materials, which are usually out of the range of existed testing standards, are explored and discussed. Last but not the least, the methods to correlate numerical analyses with experimental results of morphing structures are investigated.

1.4. Outline

In chapter 2, the state of the art about morphing skins of reconfigurable reflector antennas and morphing aircraft wings is described. Chapter 3 introduces the fundamentals related to morphing structures like antenna theory and aircraft wings. Furthermore, the application examples of a mechanically reconfigurable reflector antenna and the morphing wing of a sailplane are briefly introduced. The work of morphing skin design, which is tailoring material properties as well as boundary conditions to derive satisfactory skin concepts for mechanically reconfigurable reflectors is presented in chapter 4. The experimental characterization of flexible composites, which are the derived skin concepts through material design, are discussed in chapter 5. In chapter 6, the performance of the proposed morphing skin concepts is evaluated through numerical analyses first. Then these results of numerical analyses are correlated with experimental results of a technology demonstrator of the mechanically reconfigurable reflector. The second application, which is morphing skin design of a sailplane wing, is presented in chapter 7. The highlights of material design, numerical analyses and experiments of the sailplane morphing wing skin are presented in this chapter. Chapter 8 summarizes the investigations of this thesis.

The flowchart of the approaches about morphing skin design discussed in this thesis is presented in Figure 1.3. The objectives of morphing skins are generated from requirements

on functional, structural and manufacturing aspects. Respect to the defined objectives, analytical and numerical studies are performed on the representative models to derive potential material concepts for skins. Afterwards, experimental investigations are performed to characterize the derived material concepts. With the experimental validations, the material concepts of morphing skin can be basically determined. In the further stage, the morphing skin design is performed on component and structure levels to determine specific configuration, layout, and arrangement. The performance of the designed morphing skins is then evaluated through numerical analyses on the detailed numerical models. Based on the studies of the detailed models, technology demonstrators of the designed morphing skins and related substructures are manufactured. The experimental results of the demonstrators are then correlated with the numerical results to update the numerical models and indicate directions of further developments.

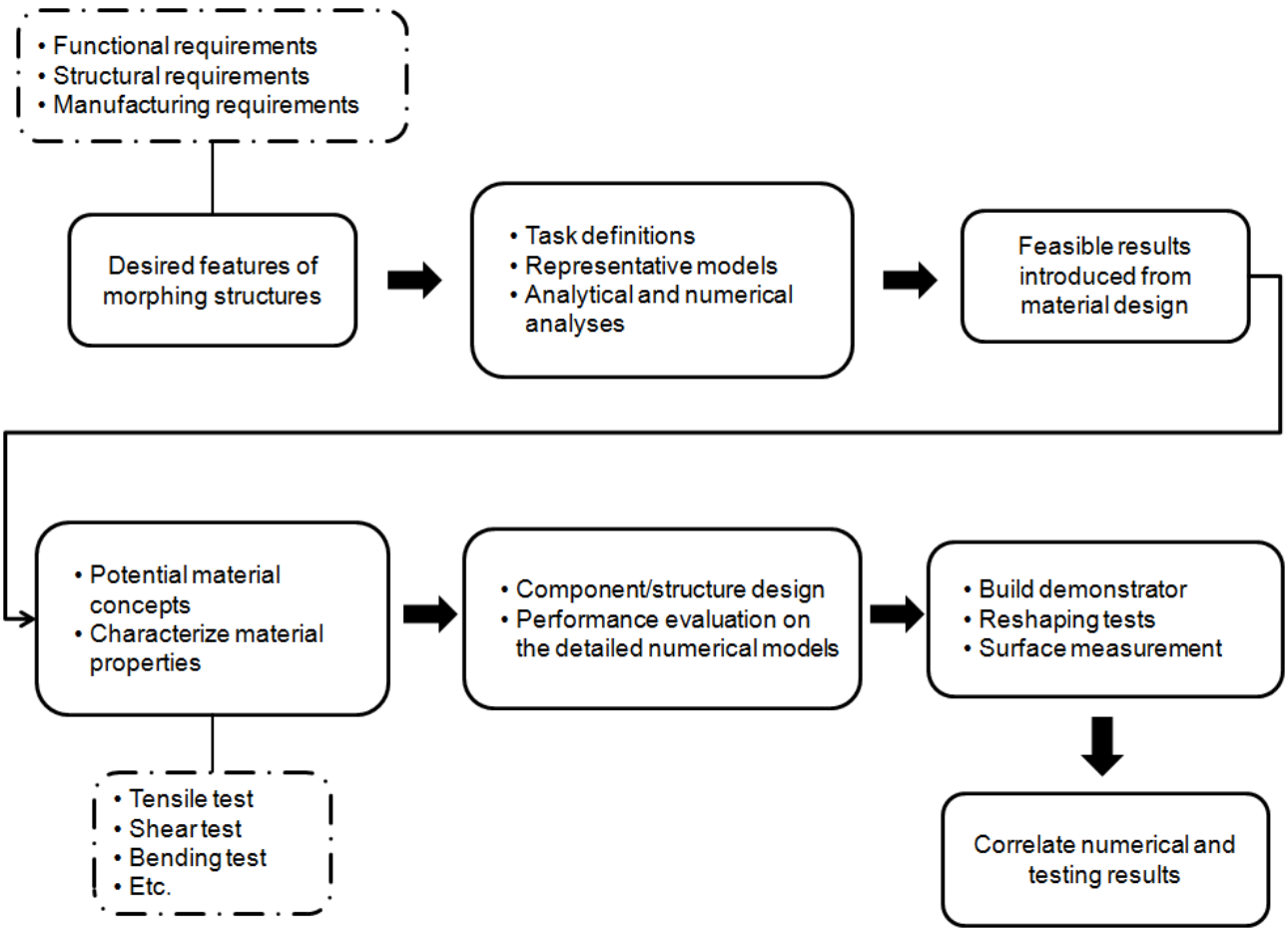

Figure 1.3.: Flowchart of morphing skin design with a focus on methods

2. State of the Art

The discussion about morphing skins shall be referred to their application backgrounds, selected actuations and interface systems together. In this chapter, morphing skin concepts and their related subsystems are reviewed in published works. Since morphing skins are quite different on mechanically reconfigurable reflector antennas and morphing aircraft wings, their reviews are presented separately.

2.1. Morphing Skins of Mechanically Reconfigurable Reflector Antennas

In early phase, the reconfigurable reflectors are mainly used on ground radio telescopes and later also on space telescopes to compensate surface errors. In fact, they should be classified as active reflectors rather than as reconfigurable reflectors. Nevertheless some conclusions introduced from these studies are still valid and can be applied on reconfigurable reflectors. The studies of mechanically reconfigurable reflectors used on satellite communications were started in 1980s and they will be reviewed in details in this chapter.

2.1.1. From Shape Correction to Reconfiguration

In order to correct the surface errors of a 140-ft radio telescope, Hoerner and Wong (1979) developed a mechanically deformable subreflector containing 4 actuators. Through their investigations on a simplified laboratory model, they observed that beam shapes and peak values were obviously changed in several testing examples contributed by millimeter range deformation of the subreflector. Inspired by this work, Lawson and Yen (1988) developed a deformable subreflector to compensate the surface errors of a 46-m radio telescope of the Algonquin Radio Observatory (ARO). Different to the concept of Von Hoerner, they followed suggestions of Legg and used a concept of piecewise deformable subreflector. Actuators are attached at the joints of the panels and drive the rigid movements of panels to realize the surface deformation. A numerical approach, which is based on the linear least squares method, is used to determine the optimal stroke lengths of actuators. An analytical example, in which a 48-plate subreflector was used, demonstrated the surface errors might be reduced to 33% of their uncorrected level.

These works indicated the capacity of adjusting radiation patterns through reflector surface reshaping via actuations. On the applications of radio telescopes, the reshaping amplitude is relative small while the surface accuracy requirement is extremely high. Therefore they are more recognized as shape correction than reshaping. Although they are not the

reconfigurable reflectors, the addressed contents such as principle of construction, reshaping control, actuations and methods of stroke length determination can be adapted on the reconfigurable reflectors.

Inspired from the works of active reflectors, the concept of applying mechanically reconfigurable reflectors to adjust radiation patterns is proposed. Different to the active reflectors, the mechanically reconfigurable reflectors require relative large reshaping amplitudes and high surface quality in terms of smoothness, which lead to the objectives of morphing structures. As mentioned in the previous chapter, there are two means to realize the desired adjustability of radiation patterns for the reconfigurable reflector antennas. The concept of the mechanically mean can be high competitive only in case it can have similar RF performance while considerable lower system complexity, mass, and cost than the electronically reconfigurable reflector antennas.

2.1.2. Morphing Skins of Reconfigurable Reflector Antennas

Clarricoats, Zhou and etc. [Clarricoats and Zhou (1991a), Clarricoats and Zhou (1991b)] started the pioneer work of developing a mechanically reconfigurable reflector antenna for satellite telecommunications in 1988. They considered two concepts initially, an adjustable mesh reflector and an adjustable panel reflector, and chosen the first one for a detailed study. The analyzed reconfigurable mesh reflector has a dimension of 1.5 m and contains 78 actuators for surface reshaping. The reflector surface is a mesh of knitted gold-plated molybdenum wires, which is widely used on most flown mesh reflector antennas. The pillowing effect was observed at the surface between control points as it is appeared on most membrane like flexible structures, which has negative influence on reflector performance in terms of creating additional side lobes and gain loss.

In investigations about pillowing, they have a first touch of material design. They varied the elastic constant of bending stiffness to tensile stiffness (D/E) to observe its influence on pillowing. Through this study they have found the amplitude of pillowing is decreased as increasing the elastic constant. They have noticed that limiting the pillowing through introducing stiffness in terms of increasing thickness introduced penalty of considerable larger actuation energy for reshaping. Therefore they have concluded, for control the pillowing of a mesh reflector it is more effective to choose appropriate button size (the area connecting with actuators) rather than introducing stiffness.

Although in their analytical predictions a free rim boundary condition was used and the results were satisfactory. As simplification a planar rim boundary constraint was actually applied and as a consequence of that, slight deterioration was observed. Further, a uniform triangular placement of actuator control points was used in this work, but authors suggested an irregular placement to reduce the intensity of a particular grating lobe and spread the energy over a wider angular spectrum. Through a parametric study about actuator number and comparing the radiation performance with the shape fixed reflector, it was found the number of actuators around 80 is a good compromise between performance and system complexity.

In the end, a scale down laboratory model with a dimension of 0.85 m was build and tested. They demonstrated a reconfiguration from a high-gain pencil beam to a shaped beam and shown excellent agreements between the predicted and measured radiation patterns. They concluded the reconfigurable reflector has a competitive performance to the

electronically reconfigurable reflector through examining it in several theoretical mission scenarios.

In their further publication [Clarricoats et al. (1994)], they demonstrated a concept of a combination of a small array feed and a mechanically reconfigurable mesh reflector. This reconfigurable reflector antennas can realize the same functions of beam shaping and beam steering as the typical array-feed antennas.

The successful feasibility study encouraged further developments of mechanically reconfigurable reflectors applying on satellite communications. They have discussed and solved some basic issues related to RF performance but some points mainly related to mechanical performance were still open. For instance, the work of material tailoring via varying the D/E to change the structure reshaping behavior is very interest but no further studies were followed. Moreover, the works about implementation of designed materials and evaluation of structure performance can hardly be found.

To overcome the pillowing effect appeared in the concept of the reconfigurable mesh reflector from Clarricoats, Pontoppidan [Pontoppidan et al. (1991) and Albertsen et al. (1994)] introduced a concept of using orthogonal interwoven wires containing bending stiffness to support the thin reflecting tricot mesh. The reconfigurable surface is defined by flexible interwoven wires in two orthogonal directions. The surface shape is determined by positions of actuators attached at intersection points of wires and the fixed rim boundary condition. Sufficient bending stiffness in surface offered a smooth contour with continuous first derivations. It was concluded, to achieve a similar RF performance the concept of orthogonal interwoven wires requires a significant less number of control points than the reconfigurable mesh reflector. An optimization of minimizing the maximal difference between the desired gain and the generated gain from the reflector surface reshaping was performed with the design variables of stroke length of each actuator. By this mean, the mechanical reshaping performance is synthesized with radiation frequency performance.

Based on the concept of orthogonal interwoven wires, Viskum et al. (1998) described a design of a dual-offset reflector by means of a shaped fixed main reflector and a mechanically reconfigurable subreflector. Through the application examples of generating two orthogonal elliptical beams, he concluded the proposed concept is feasible for these tasks and the performance can be further improved if the subreflector surface shape would be constrained (shaped) already in the optimization.

Investigations of developing reconfigurable reflectors in USA were mainly performed by the team of Washington. In 1996, Washington (1996) proposed another type of concept for a reconfigurable reflector surface, which is attaching a polyvinylidene fluoride (PVDF) film to a metallized Mylar substrate. The PVDF can be expanded or contracted via voltage exciting and then cause the reflector surface change. In his study, the beam steering and beam shaping abilities through a cylindrical reconfigurable reflector were theoretically demonstrated. However, limited by the selected actuating approach, the reconfiguration function is quite limited as compare with the concept of Pontoppidan.

Follow the strategy of Washington, Theunissen et al. (2001) synthesized a mechanical FEM description of the reconfigurable subreflector and RF performance evaluation in one program. Therefore the mechanical behavior of the reflector surface based on applied materials are taken into account during the synthesis procedure. The reconfigurable subreflector is made of flexible metallized polymer and actuated by stacked piezoelectric actuators working in ±10 mm range. Several theoretical reshaping tasks were successfully performed using the reconfigurable subreflector with 55 actuators. The major contribution of this work is synthesized the mechanical FEM model into the analysis process. But the detailed mechani-

cal performance of the reconfigurable reflector like actuation force, stress and strain was not discussed.

Based on the work of Theunissen, Washington et al. (2002) and Yoon (2002) further investigated the optimization methods to determine the optimal actuator placement and actuator stroke lengths. They proposed a method to determine actuator placement according to the maximal error between the desired and actual shapes. For the determination of optimal actuator stroke lengths, two optimization techniques, the simulated annealing algorithm and a simple univariate technique, were presented. Their results have shown the relation between the desired radiation pattern and the mechanical shape is unique. But they believe it is the global optimum and there are multiple mechanical shapes can generate nearly the same radiation patterns to the desired one.

The generated actuator placement based on Yoon's method is optimal only for these predefined tasks but not general applicable for all kinds of tasks. To maintain the maximal adjustability, a uniform distribution is recommended. The stroke length optimization seems quite computation intensive and their detailed results are not mentioned in the texts.

The researchers of TICRA [Cappellin and Pontoppidan (2009) and Cappellin et al. (2009)] performed a feasibility study of a reconfigurable reflector antenna for satellite telecommunications based on realistic mission scenarios and antenna configuration. The used antenna geometry is a dual-offset Gregorian lateral reflector antenna designed by Thales Alenia Space (TAS) and three intercontinental missions were used as testing benchmarks. They have compared three design combinations: 1. shaped sub-and main reflector for each coverage (as the reference); 2. ellipsoidal subreflector and shaped fixed main reflector; 3. reconfigurable subreflector and shaped fixed main reflector, and concluded the last one has considerable better RF performance than the second case. In investigations of actuator number, it was found using 130 actuators is appropriate to reshape a main reflector and 55 actuators is suitable to reshape a subreflector. The reshaping amplitudes for actuators in defined missions are in the range from -13 to 12 mm. Additionally, a sensitivity analysis with concerning inaccuracy of actuator positioning and thermal-elastic distortions was performed.

A laboratory model, which is 300 mm in diameter and contains 9 dummy actuators supported under a free rim boundary, is presented as a demonstrator (see Figure 2.1 left). Its surface is consist of orthogonal interwoven wires with circular cross section and its shape under actuations is predicted by an analytical approach based on Euler beam theory. Through the testing on the demonstrator, it has shown quite impressive reshaping features of smooth and continuous deformation in relative large amplitudes with few actuation energy only. To improve the reflectivity of 10 x 10 mm spacing grid, a fine RF mesh, whose spacing is 1 x 1 mm, is covered on it and served as the RF net [Pontoppidan et al. (2010)]. Although it has excellent performance in mechanical reshaping, there are still some essential weaknesses e.g. the possible Passive Intermodulation (PIM) problems and thermal distortions in space environments, which are to be solved in further investigations.

There are doubts about the geometry linear assumptions in the analyses of the orthogonal interwoven wires. As stated in Datashvili (2008), the linear assumptions and fixed translation conditions in the intersection points are too idealized for the analyses of interwoven wires. The presented numerical difficulties in the nonlinear FEM analyses in terms of surface buckling, which is actually not appeared in the physical model, indicated the free sliding among wires is to be considered. A study of relations about the sliding effect to the smooth reshaping of wires was performed on a unit cell model to understand the principle of interwoven wires reshaping [Zhou (2011)]. It was found the freedom in the intersections is the key to realize a smooth large amplitude reshaping for releasing the local concentrated

energy by this mean. However, the computation cost is not affordable for a large scale model with considering sliding effects among wires. A more appropriate understanding of the interwoven wires is classifying it to be the grid shell structure. The reshaping problem can be efficiently solved as a form finding problem by analytical means through explicit methods. Lots of examples as artistic roof design can be found in the field of civil engineering [Barnes (1999)].

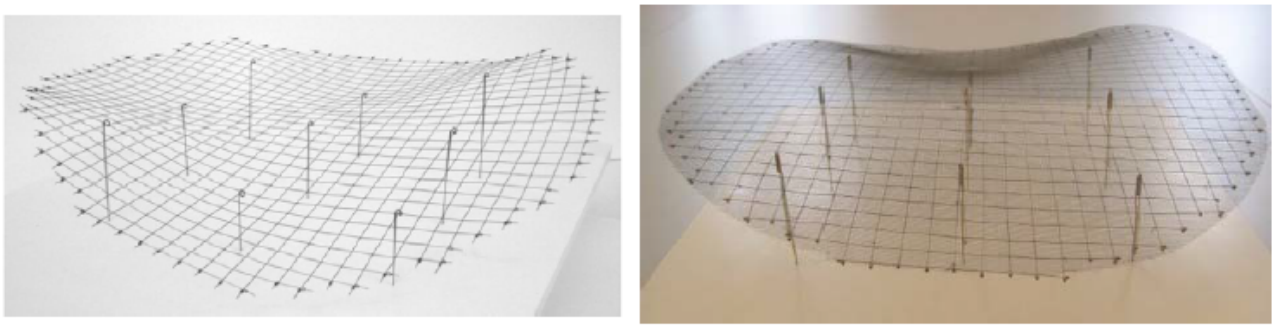

Figure 2.1.: The TICRA laboratory model of 10 x 10 mm spacing wire grid surface (left) and the model covered by the RF net (right) [Pontoppidan et al. (2010)]

Datashvili and Baier [Datashvili and Baier (2009), Datashvili et al. (2009)] surveyed existed and potential technologies about mechanically reconfigurable reflector antennas. The major critical problems in developing of a mechanical reconfigurable reflector e.g. surface material, actuator type, interface design, and reshaping approaches were discussed. Based on this survey, qualitative mechanical requirements to the reconfigurable surface material were given, which are low in-plane tensile and shear stiffness for preventing reshaping failures and reducing required bending stiffness for smooth reshaping. Other requirements related to space reflector applications like reflectivity, PIM, and CTE were given as well.

An evaluation of existed and potential surface material concepts was then assessed based on above mentioned criteria. The conclusion is the orthogonal wire grid and carbon fiber reinforced silicone (CFRS) are the most advantageous candidates.

Four types of potential actuators, linear motors, shape memory materials, piezo-electric materials and electro-active polymeric materials, were discussed and evaluated based on detailed requirements to actuators. A stepper motor was chosen as a short term possibility and the inchworm type (piezoelectric actuators) and similar concepts were considered for future development and qualification.

Based on the understanding from the technology survey, the Institute of Lightweight Structures (LLB) started investigations of a mechanical reconfigurable reflector with focus on mechanical aspects like surface material design, interface design, and actuations. Datashvili et al. (2009) proposed a reconfigurable surface concept of multilayer laminate, which is consisted of triaxially woven carbon fiber reinforced silicone (triax-CFRS). This space qualified material has low in-plane stiffness properties, low thermal expansions, and membrane like features of foldability. Rim is totally free in this concept and the boundary conditions of the reflector are statically determined through definitions on actuators and the rods.

The mechanical model is not synthesized with RF analysis in this study, instead, several target shapes derived from desired radiation patterns for mechanical reshaping were defined. Through a parameter study, some drawbacks were found in the multilayer laminate

concept. For instance, the numerical difficulties in terms of snap through in the FEM model was found, which indicated lack of bending stiffness. Therefore, this concept is modified to be a flexible sandwich containing around 2 mm silicone core among triax-CFRS layers. Linear reshaping analysis of a FEM model containing 91 actuators was performed to approach the defined target shapes. The shape difference in terms of RMS error is obtained as around 0.2 mm through a stroke length optimization using the least squares method. The amplitudes of stroke length are range from -27 to 10 mm and the maximal actuation force is around 30 N in analyses. However, the flexible sandwich concept is not preferred in practice mainly due to difficulties in manufacturing and high material cost.

Two breadboard models with 7 and 19 actuators (see Figure 2.2) were build. The numerical predicted results have shown good agreements with the measured results.

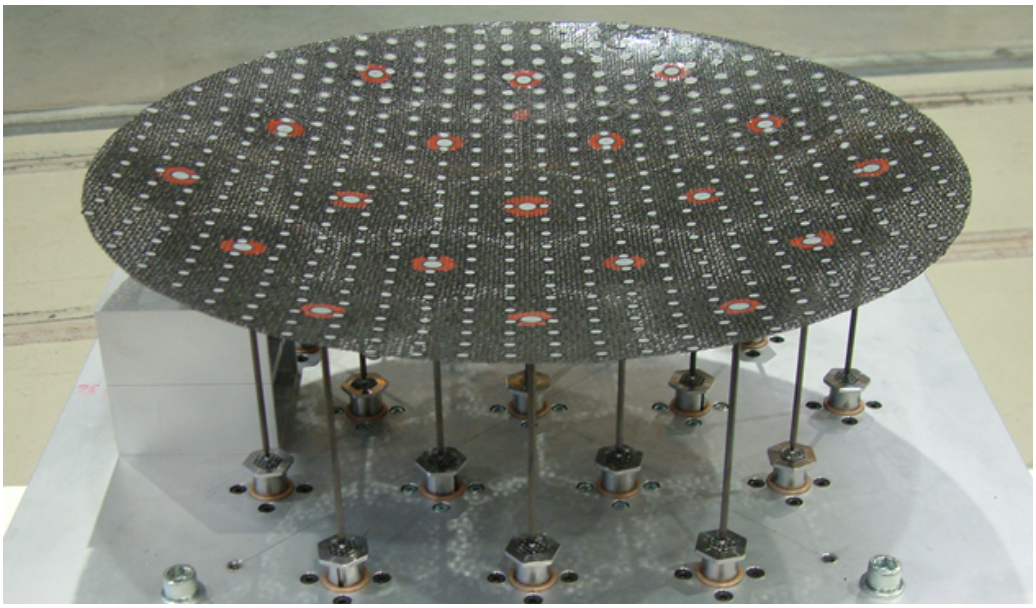

Figure 2.2.: The LLB laboratory model, which contains 19 actuators and has a free rim boundary [Datashvili and Baier (2009)]

Through these investigations, the feasibility of large scale mechanical reshaping using flexible shells was proved. The purposed concept of using the flexible composite as the reconfigurable reflector surface is still the advantageous candidate but the flexible sandwich concept is to be abandoned. There is still an open point demanding for further investigations, which is a more accurate understanding about correlations between material properties and mechanical reshaping behavior.

2.2. Morphing Skins of Morphing Aircraft Wing

The word of morphing wing sounds quite new in technology development, but actually it existed already more than one hundred years. The first powered plane from Wright brothers was equipped with flexible wings containing pulleys and cables for controlling wingtips [Weiss (2003)]. This wing warping can be referred to be one kind of wing morphing. In early stage, the wing morphing is mainly related to varying wing sweep for efficient flight at sub- and supersonic speeds. The typical examples of swing wing aircraft are MiG-23 in 1967, Grumman F-14 Tomcat in 1970 and Rockwell B-1B Lancer in 1983. Besides the penalties of mass and system complexity, one major problem in these aircraft is the change of gravity center among different configurations [Jha and Kudva (2004)]. Most modern civil transport aircraft is equipped with high-lift devices, namely leading and trailing edge devices, to gain extra lift in taking off and landing phases. These high-lift systems are passive structures and their applications are limited to the two predefined scenarios. In order to extend their application scenarios as well as improve system efficiency and performance, the technology of morphing wing is proposed for future aircraft.

A modern understanding of the morphing technology is "a seamless, aerodynamically efficient aircraft capable of radical shape change" [Thill et al. (2008)]. Generally, the scales of morphing can be classified into three types: 1. large scale morphing relates to the full wing area and sweep angle modification; 2. middle scale morphing relates to changes in wing chord like camber, thickness, twist or airfoil shape; 3. and fine scale morphing means local changes in wing shape to affect the air flow at least over this region. Associating with the above understanding of morphing wing technologies, various concepts of morphing wings and the related morphing skins are reviewed and discussed.

Monner et al. (1999) developed a variable camber concept for applications on large civil transport aircraft. A flexible rib, which consists of several rigid elements connected with revolute joints, is proposed as the kinematics for reshaping. In this concept, which is sometimes called as "finger concept", conventional metal skin is used. Linear slide bearings are equipped on the skin and the trailing edge tip to realize the required reshaping without large stretching on materials. But detailed descriptions about the skin performance are not mentioned.

Eccentuator is mentioned in several morphing leading edge and trailing edge concepts. It is actually a bent rod that transforms rotary motion into vertical force and displacement as the output. Morishima et al. (2010) investigated a morphing leading edge concept actuated by eccentuators. Several skin concepts, which are glass fiber/epoxy, carbon fiber/epoxy, and aluminum alloy, were compared through reshaping analyses under aerodynamic loads. In another morphing flap structure using eccentuator [Matteo et al. (2010)], effects of different connections between upper and lower skins were discussed. Through comparison study of different connection methods, it was found it has significant influence on reshaping quality, actuation forces, and structural stability. Müller (2000) demonstrated a morphing trailing edge of civil transport aircraft driven by eccentuators made from carbon fiber composites (Figure 2.3). Bending flexible spars are used to connect upper and lower skins to sustain the shape of the trailing edge in reshaping. The carbon fiber composite skins on the trailing edge are connected to skins of main spars with pre-stressed membranes for allowing certain relative movements. Additionally this connection region is covered by overlapped spoilers to form a continuous skin surface. The experimental results of the demonstrator have shown quite positive results on reshaping ability, structural strength and reliability. It seems to be one of the potential concepts for the near future applications.

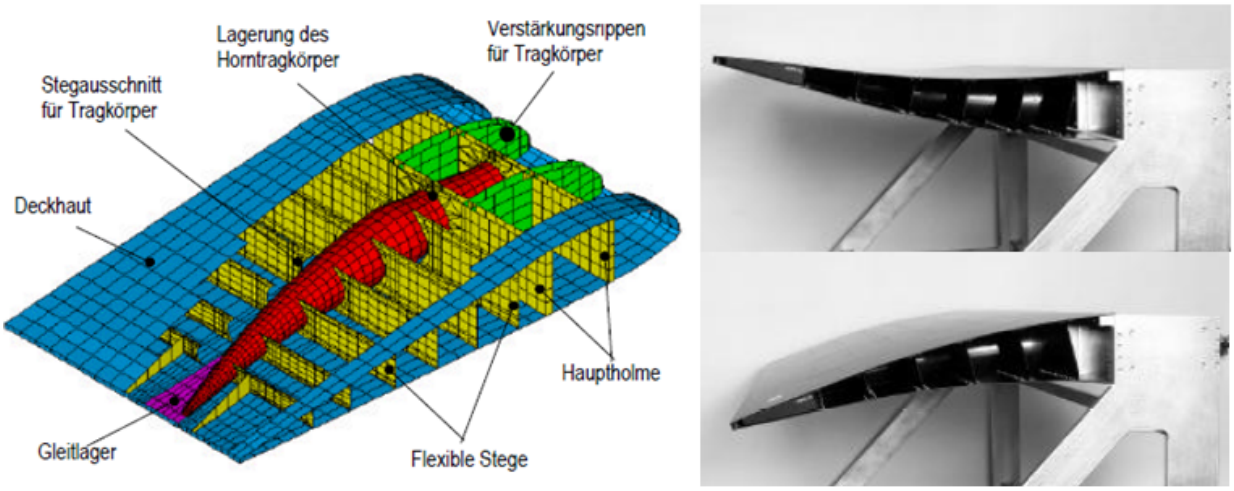

Figure 2.3.: A morphing trailing edge using eccentuator concept [Müller (2000)]

Kota [Kota et al. (2003) and Kota et al. (2006)] described a concept of morphing wing using compliant mechanisms, which is defined as "a class of mechanism that relies on elastic deformation of its constituent elements to transmit motion and/or force". A demonstrator equipped with a compliant mechanism has shown that the deflection of trailing edge between −10 and +10 degree can be achieved (see Figure 2.4 upper side). But no details about neither these mechanisms nor skins were mentioned. Baker and Friswell (2006) presented a design method of compliant structures using topology optimization. The proposed concept, which contains numerous trusses with varied cross-sections, seems to be mass intensive and quite challenging for manufacturing. Campanile (2007) developed another complaint airfoil called as "Belt-Rib" concept. The conventional spars are replaced by ribs and spokes containing flexural hinges (lumped compliance). A demonstrator is manufactured based on the proposed concept with covering by conventional metal skins. The reshaping ability of this concept seems to be quite limited.

A smart droop nose actuated by conventional kinematics is developed for applications on large civil transport aircraft by Monner et al. (2009). In this concept, a hybrid skin, which is consisted of glass fiber and carbon fiber composites, is designed and used. In testing of a 1:1 scale demonstrator, it presents a deflection ability up to 20 degree, which is typically required in practical operations (see Figure 2.4 lower side). The measurement results about strength and stability of the morphing leading edge are satisfactory as reported by Kintscher et al. (2011).

In concepts of one-dimension morphing wing, flexible sandwiches are proposed. Olympio and Dandhi [Olympio and Dandhi (2007), Olympio and Dandhi (2010)] derived analytical methods to design cellular honeycomb core with extreme anisotropic material characters. Through a proper design of the honeycomb core, it can be compliant in the deformation direction while stiff in the loading direction. Additionally, Poisson's ratio can be modified as well. A spanwise morphing wing concept using the tailored honeycomb core covered by flexible composites is presented by Bubert et al. (2010), which is able to achieve a 100% elastic elongation (see Figure 2.5 (1)). As an alternative concept to the flexible sandwich, Yokozeki et al. (2006) proposed a corrugated composite skin for these one-dimension mor-

phing wings (see Figure 2.5 (3)). He improved the concept in terms of adding CFRP roving in the longitude direction for further enhancing stiffness and covering silicone on the corrugated surface for better aerodynamics. Da Rocha-Schmidt described a shear compliant sandwich skin as the gap cover of an UAV flaps [da Rocha-Schmidt and Baier (2013)]. the skin concept consists of a shear compliant core and metal grid reinforced silicone face sheets. It has been shown in his numerical tests, the flexible sandwich skin can accommodate flap deflection between −30 and +30 degree without static and dynamic failures.

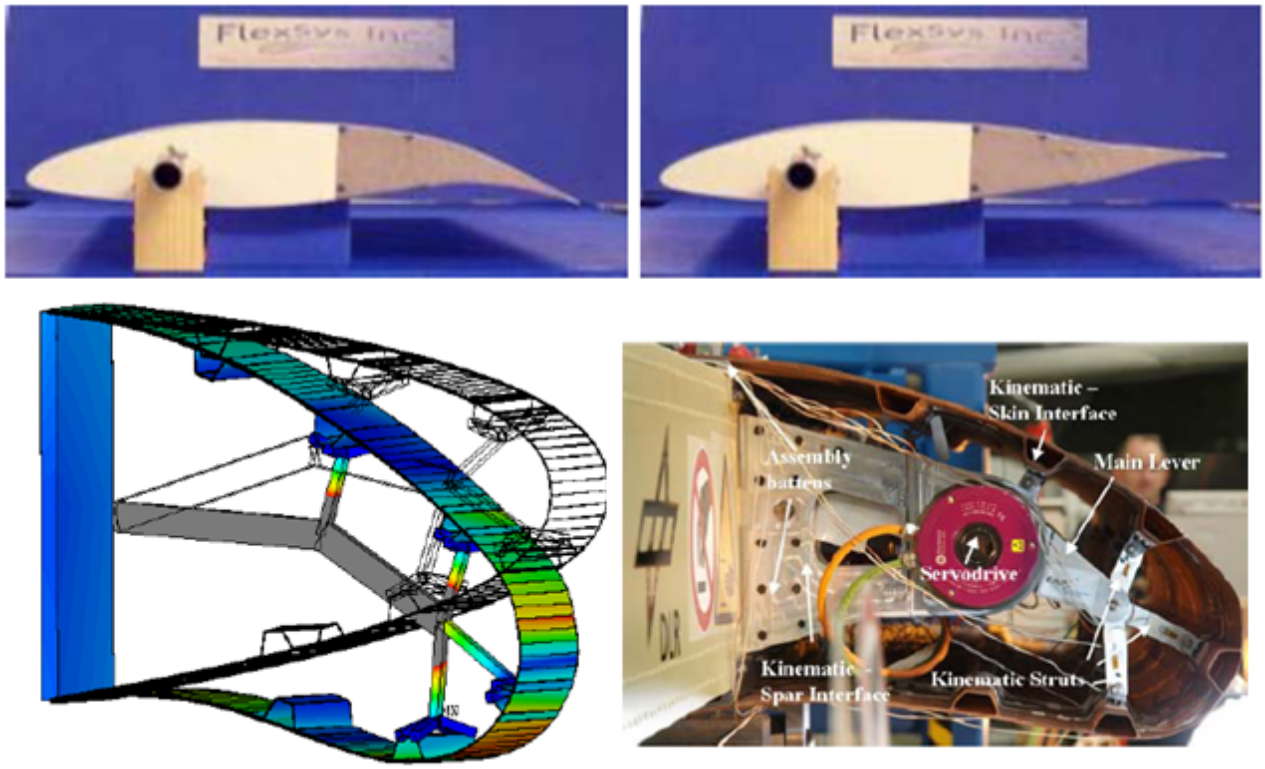

Figure 2.4.: Upper: a compliant morphing wing concept of FlexSys [Kota et al. (2003)] Lower: smart droop nose [Monner et al. (2009)]

Scott et al. (2009) introduced an inflatable morphing wing concept for expanding the span of rigid wings in high-altitude flights. Cadogan et al. (2004) presented various concepts about inflatable morphing wings. He added conventional metal skins to cover the inflatable structures for surface smoothness and meantime piezoelectric actuators on skins to deflect the trailing edge. But generally the disadvantages of inflatable structures are lack of stiffness, low in surface quality, risks of puncture and leakage. The appropriate applications for these concepts are more likely to be on low speed aircraft.

Lockheed Martin Skunk Works [Lockheed] demonstratored a Z-wing morphing concept of foldable wing to expand wing surface area. In the folding regions, a fabric reinforced silicone material is used. As mentioned by Love, the main problem of the elastomeric skin is its nonlinear behavior due to creep when actuated as found in wind tunnel tests [Love et al. (2007)]. A silicone elastomeric skin is also used in a sliding wing concept [Flanaganl et al. (2007)], which is able to change sweep from 15 to 35 degree and wing area by 40%. These elastomeric skins are usually capable for large scale morphing tasks but may contain problems on dynamic performance.

Barbarino et al. (2010) investigated a morphing trailing edge containing compliant truss structures. Several shape memory alloy rods are applied on the compliant truss structure as the active members. Perkins et al. (2004) introduced several shape memory polymers to realize wing morphing among different configurations within quite short time and therefore can bring more advantages on aerodynamics [see Figure 2.5 (2)]. These materials presented quite impressive features of deformability but generally they have limitations on reshaping amplitude and/or actuation force, and difficulties on realizing the actuating conditions in practice application environments. In short, they are still on low technical maturity level and are not suitable for near term applications.

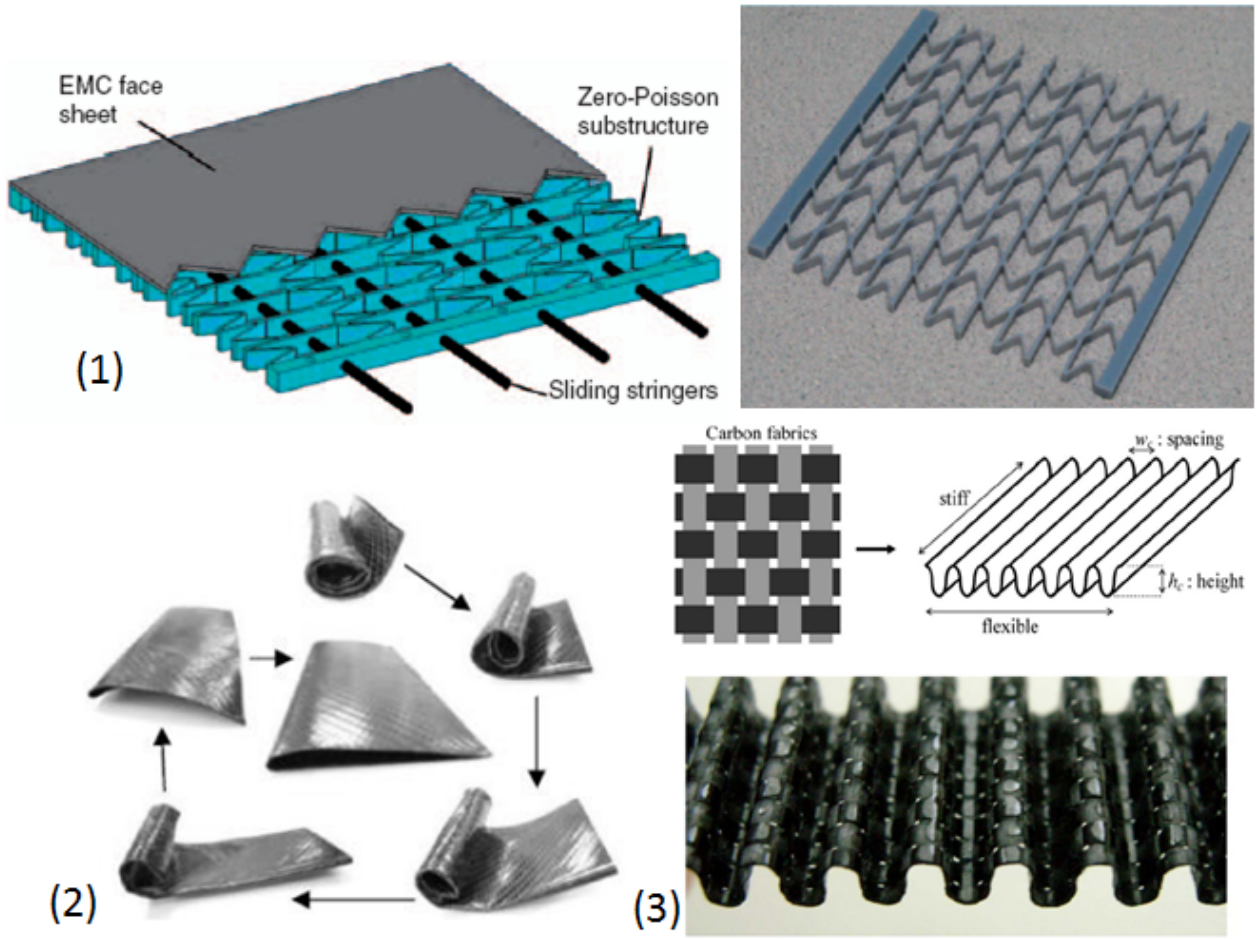

Figure 2.5.: (1): a flexible sandwich skin and its core [Bubert et al. (2010)] (2): shape memory polymers [Perkins et al. (2004)] (3): a corrugated composite skin [Yokozeki et al. (2006)]

2.3. Summary of Literature Review

To overcome drawbacks of electronically reconfigurable reflector antennas, lots of effort was paid to develop mechanically reconfigurable reflectors for satellite communications in the last 20 years. The feasibility of adjusting radiation patterns via reshaping of the reflector surface to fit the defined geographic coverage was well proved in several studies. Works

concerning the mechanically reconfigurable reflector antennas on geometry design, analyses of required deformation and actuation forces, RF performance of shaped surface, synthesis techniques of mechanical model and RF model, actuator selection, and interface design were partly or basically accomplished. The major not accomplished tasks are remained in developing and implementing a reconfigurable reflector under realistic application requirements. Among them, the most challenging task is the reconfigurable reflector skin design. In the past studies, qualitative requirements to the expected skin materials were discussed and defined. Two potential candidate materials, orthogonal interwoven wire grid and flexible composites, have shown their capabilities and meanwhile some weakness and limitations for practice applications. However, the fundamental studies about relations of material properties to structure reshaping behavior can hardly be found in the past works. A material tailoring in terms of varying material properties to adjust the reshaping responses to satisfy the defined requirements will be quite helpful to accomplish the task of reconfigurable reflector skin design.

The skin design of morphing wings is another quite challenging task with quite different goals and requirements as stated in the last chapter. Compare with the mechanically reconfigurable reflector, there are various of concepts about morphing wings and skins as reference, which range from conventional metallic panels, tailored fiber composites, elastomer, flexible sandwiches, to shape memory materials. However, most of the mentioned concepts are still on laboratory level and far away from engineering applications. Considering their potential to satisfy the total set of functional, structural, manufacturing, and certification requirements as well as sufficiently high TRL for near future applications, skin concepts like tailored composite and flexible sandwich are considered as most promising.

3. Fundamentals and Background

In this chapter, the fundamentals about antenna theory related to reconfigurable reflector antennas and basics of aircraft wings are summarized. The background information about the application examples, a reconfigurable reflector antenna and a morphing wing of sailplane, is introduced as well.

3.1. Basics of Reconfigurable Reflector Antennas

The IEEE Standard Definitions of Terms for Antennas defined the antenna as means for radiating or receiving radio waves [IEEE (1983)]. It is used to transport electromagnetic (EM) energy from transmitting source via antenna to free space, or from free space via antenna to receiver [Balanis (2005)]. The transmitting and receiving functions of an antenna are not necessary to be separated, some antennas can work with both functions simultaneously.

The antenna techniques were rapidly developed during World War II, new elements such as waveguide apertures, horns, reflectors were introduced in that time. From the 1960s to 1990s, a major impact was the introducing of analytical and numerical means to design and analyze the antenna systems. With these achievements, antennas are widely applied in communication fields. Nowadays the antennas are already parts of our daily life, which can be found overall e.g. cell phones, GPS devices, automobiles and etc.

3.1.1. Fundamental Parameters of Antennas

Frequency and Frequency Bands

The signals transmitted and/or received by antennas are electromagnetic (EM) waves. They can be represented as sinusoidal waves and propagate periodically at the speed of light in air or in space. The frequency is used to measure how fast the wave is oscillating. The multiplication product of frequency (f) to wavelength (λ) is the speed of light (c).

$$c = f \cdot \lambda \tag{3.1}$$

The EM waves are grouped into different frequency bands according to frequency and wavelength aiming to different applications. For instance, high frequency band 3-30 MHz (wavelength 10-100 m) is mainly used for shortwave radio, and super high frequency band 3-30 GHz (wavelength 10-100 mm) is mainly used for satellite communications [Antenna-Theory]. The frequency bands available for satellite communications are mainly in the range of 1 to 40 GHz. A overview table of frequency band to its typical applications defined by

Radio Society of Great Britain (RSGB) is listed as following [Microwave].

Table 3.1.: Frequency bands for satellite communications

Band	Frequency range [GHz]	Wavelength range [mm]	Typical uses
L	1 to 2	150 to 300	Military telemetry, GPS, mobile phones (GSM)
S	2 to 4	75 to 150	GSM, weather radar, deep space research
C	4 to 8	37.5 to 75	Fixed satellite service (FSS)
X	8 to 12	25 to 37.5	FSS military, terrestrial earth exploration and meteorological satellites
Ku	12 to 18	16.7 to 25	FSS, broadcast satellite service (BSS)
K	18 to 26.5	11.3 to 16.7	BSS, FSS
Ka	26.5 to 40	5.0 to 11.3	FSS

The three most commonly used frequency bands in satellite communications are C-, Ku-, and Ka-Band. Currently most of commercial satellites use C-Band while future satellites are being designed for Ku-Band. The reconfigurable reflector antennas are aiming to be used in Ku-Band.

Radiation Pattern

Radiation pattern is defined as "a mathematical function or a graphical representation of the radiation properties of the antenna as a function of space coordinates" [IEEE (1983)]. In most cases, the radiation pattern is determined in the far-field region and is represented as a function of the directional coordinate. Radiation properties include power flux density, radiation intensity, field strength, directivity, phase or polarization [IEEE (1983)].

The power density patterns are usually normalized with respect to their maximum value and plotted on a logarithmic scale or more commonly in decibels (dB). A radiation pattern is normally consisted of various lobes, which can be further classified as major, minor, side, and back lobes. An illustration of radiation lobes is shown in Figure 3.1.

A major lobe contains the direction of maximum radiation and its number may be more than one in some antennas. The rest lobes are minor lobes. A side lobe is the radiation lobe in any direction other than the intended lobe. In most radar systems, the ratio of side lobe to the major lobe is expected to be possibly low, e.g. -20 dB or even smaller.

The key function of a reconfigurable reflector is adjusting radiation patterns through surface reshaping. Then the adjusted radiation pattern can well match the desired geographic coverage for purposes of high efficiency. As stated in the last chapter, a surface reshaping within amplitudes of -15 to 15 mm can achieve the required radiation patterns in most practice missions.

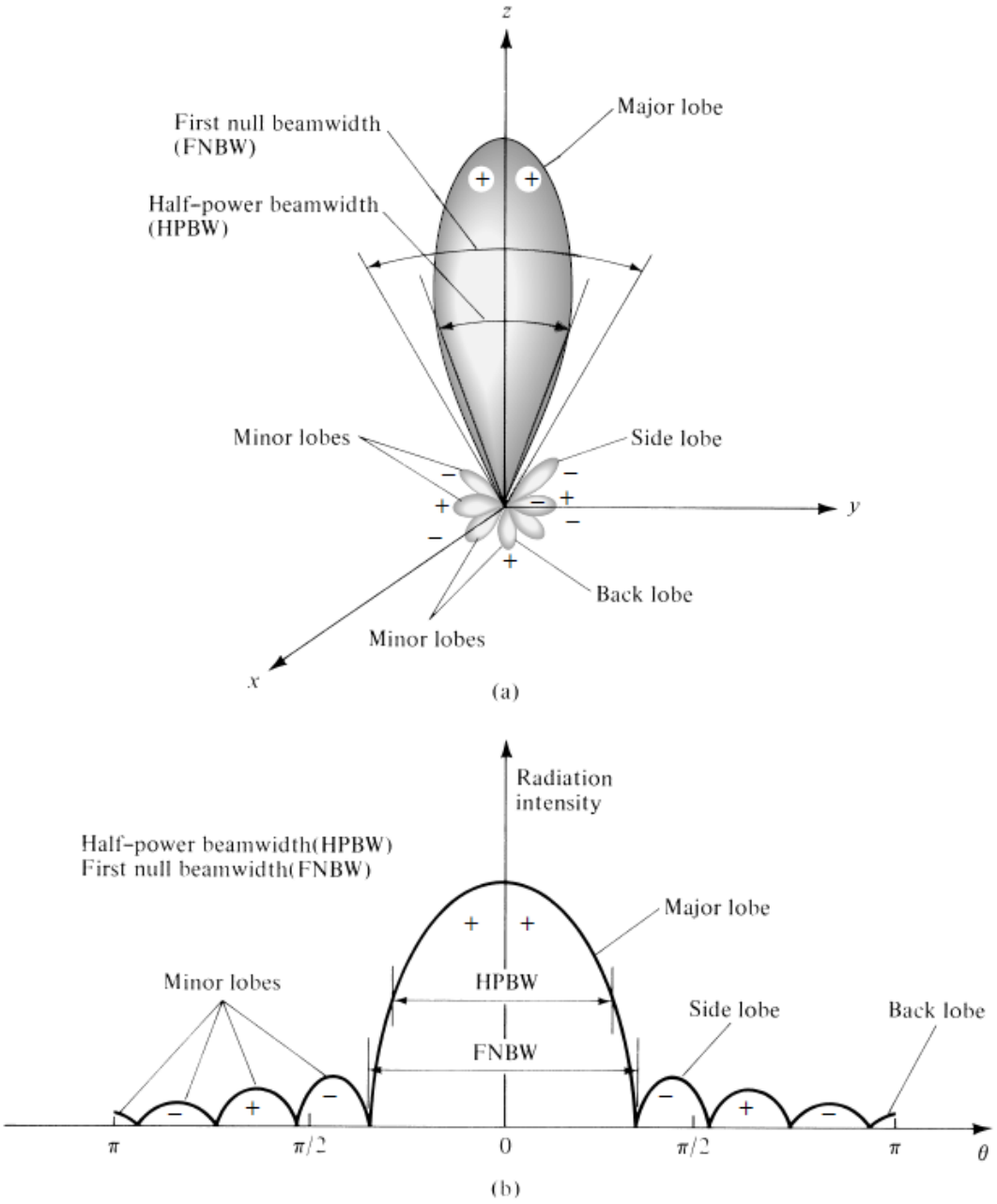

Figure 3.1.: (a) Radiation lobes and beamwidths (b) Linear plot of power pattern [Balanis (2005)]

Gain and Gain Loss

Gain (G) of an antenna is "the ratio of the intensity, in a given direction, to the radiation intensity that would be obtained if the power accepted by the antenna were radiated isotropically" [IEEE (1983)]. In most cases, the used term is the relative gain, which is compared to the gain of a reference antenna.

In practice, power gain contains two types of losses and they are impedance mismatches (reflection losses) and polarization mismatches (losses). Ruze (1966) derived a simplified

function of effective gain respecting to reflector surface distortions.

$$G = G_0 e^{-\overline{\delta^2}} = \eta(\frac{\pi D}{\lambda})^2 e^{-(4\pi\varepsilon/\lambda)^2} \tag{3.2}$$

G_0: gain without loss
$\overline{\delta^2}$: the phase front variance caused by aperture surface error
ε: the effective reflector tolerance, e.g. the RMS surface error
η: the aperture efficiency
D: aperture diameter
λ: wavelength

The loss of gain is then

$$\frac{G}{G_0} \approx 1 - \overline{\delta^2} \approx e^{-\overline{\delta^2}} \tag{3.3}$$

With help of above expressions, the tolerance of radiation pattern (gain loss) can be easily converted into surface error tolerance or vice verse. The application of these expressions is presented in a later section (see Chapter 3.3.1).

Passive Intermodulation (PIM)

Passive intermodulation (PIM) is a form of intermodulation distortion caused by passive components. PIM is a mixture product of the two (or more) high power tones at device nonlinearities like junctions of dissimilar metals, metal-oxide junctions and even loose connectors [Intermodulation]. The interference of PIM can sometimes hide the desired signals and therefore it should be removed.

Although the interference signals from PIM are at low level as compare to exciting signals, due to the fact that transmitters are collocated with receivers and often sharing the same feeders and antennas, even low level interference can cause significant problems. Therefore in design of a reconfigurable reflector surface, the PIM properties of selected materials, construction, and connections should be considered and verified by tests. As stated in Chapter 2.1.2, the concept of orthogonal interwoven wires contains many loose connections and irregular contact areas, which are the sources of PIM. Without solving the PIM problems of this concept, it is infeasible for practice applications even though it has excellent mechanical reshaping features.

3.1.2. Antenna Types

Antenna types can be briefly classified as: wire antennas, aperture antennas, microstrip antennas, array antennas, reflector antennas and lens antennas. The most well-known type is the reflector antenna, which can be further classified as: planar, corner, and curved reflector (especially the paraboloid) antennas. In frame of this thesis, only the parabolic reflector antennas are used. According to feed type, the parabolic antennas have four configurations (see Figure 3.2):

- Axial (front feed): feed locates in front of the reflector at the focus, pointing to the reflector surface
- Off-axis (offset feed): the reflector is an asymmetrical segment of the paraboloid, so the feed locates at one side of the reflector. Its advantage is mainly avoiding blocking some signals by feed
- Cassegrain: it is a dual reflectors system containing a secondary reflector in a convex form. Its feed can be located in front or at one side of the main reflector
- Gregorian: it is similar to the Cassegrain type but with a concave secondary reflector

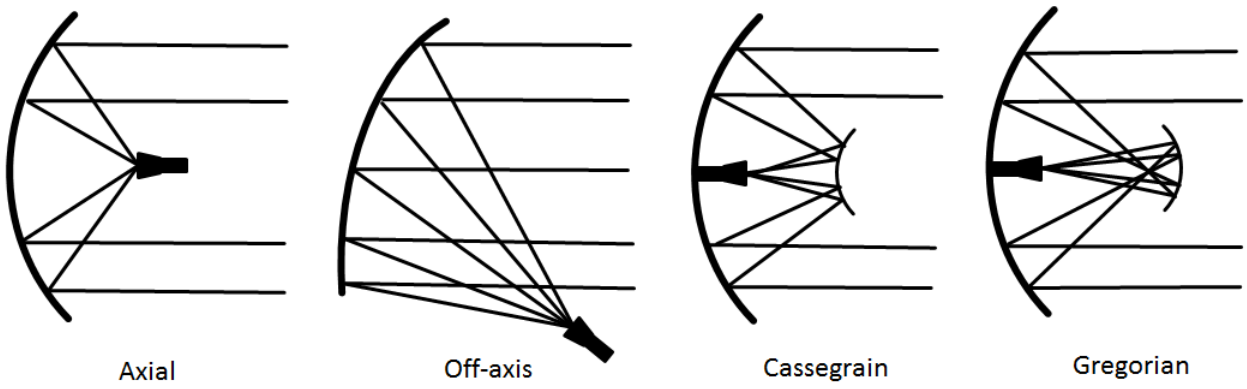

Figure 3.2.: Four typical parabolic reflector antennas

In satellite communications, the most used configurations are offset-dual reflectors. In Figure 3.3, the geometry of a Gregorian dual-offset reflector antenna is demonstrated.

The main reflector is an asymmetrical segment of the paraboloid and the subreflector is an ellipsoid with two focal points. Although the mechanically reconfigurable reflector can be one of them or both, the most often used concept in the published works is mechanically reconfigurable subreflecor.

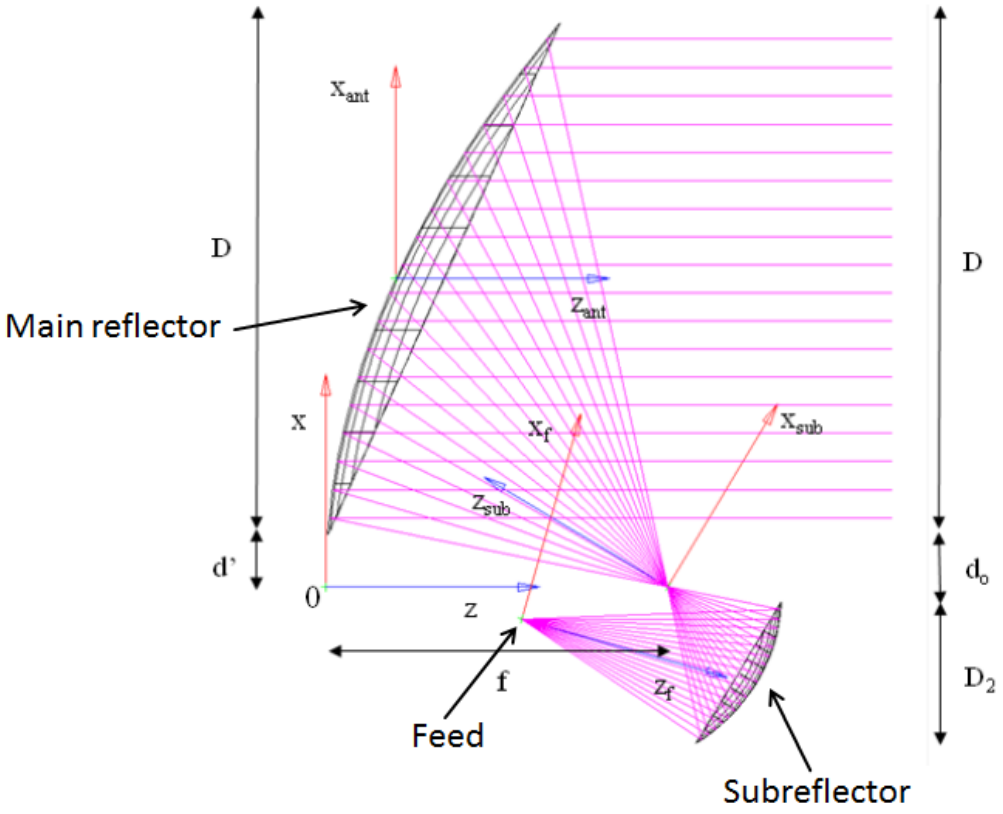

Figure 3.3.: Geometry of a Gregorian dual-offset reflector antenna [Cappellin and Pontoppidan (2009)]

3.2. Basics of Aircraft Wings and High-lift Devices

Wings are the fundamental components of aircraft, which are used to carry loads like aerodynamics in terms of lift and drag, engine thrust etc. Their basic design parameters are airfoil section including high-lift devices, planform shape and geometry, and overall size. The first term is determined through the best compromising among aerodynamics, structural, and operational requirements. The second is mainly determined by the operating Mach number of aircraft and by the airfoil shape. The third one is related to the operational environments as defined in the term one and two.

An illumination of a typical airfoil and the pressure coefficient over it is shown in Figure 3.4. The airflow pass-by an airfoil causes pressure difference on upper and lower side of the airfoil, which is lift on wing. The essential goal of airfoil design is maintaining possibly more laminar flow to gain higher lift coefficient. To achieve the defined goal, approaches range from proper airfoil shapes, shape change of leading and trailing edge, to extending of chord length are applicable.

Among these approaches, the most used is adding high-lift devices on the basic airfoil to improve its performance. There are various types of high-lift devices existed and some common forms are illustrated in Figure 3.5. The trailing edge high-lift devices are almost universal applied but the leading edge high-lift devices are used only on certain applications. Besides of complexity in mechanisms, the major reason is small gaps and steps in

leading edge position can easily cause large drag increments. Therefore, the leading edge high-lift devices are mainly used on aircraft with large surface loads on wings like large transport aircraft and some combat aircraft with requirements for short take-off and landing.

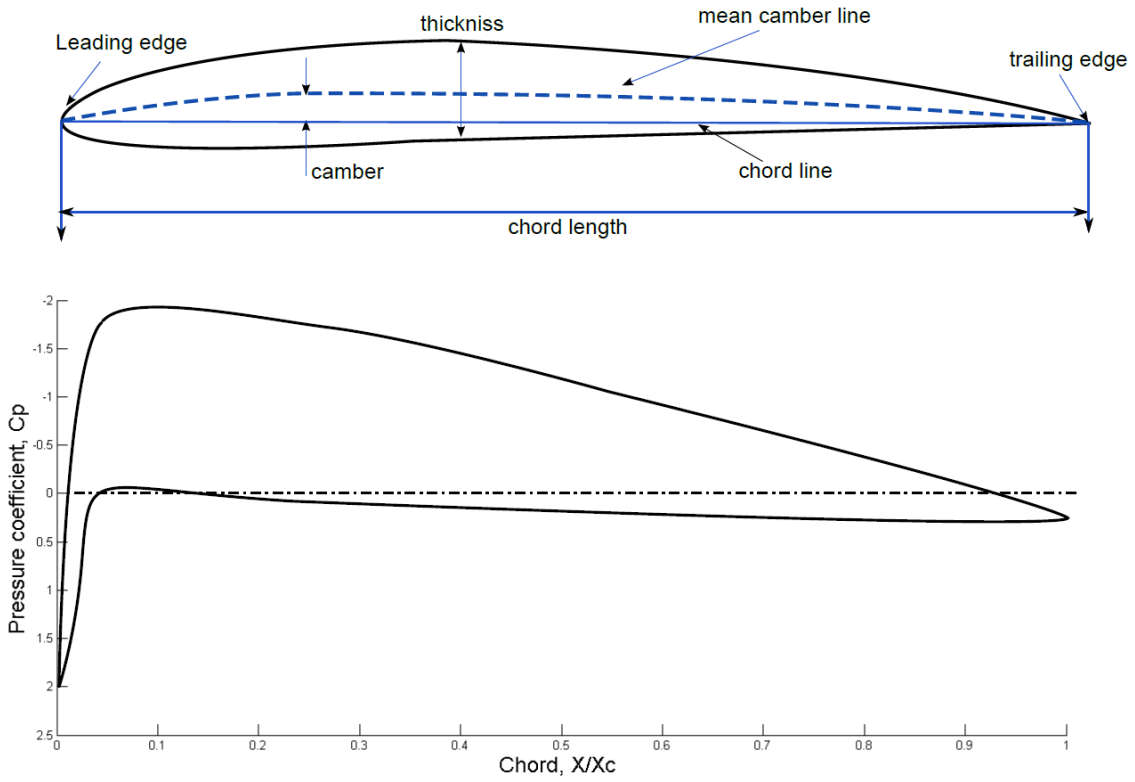

Figure 3.4.: A sketch of airfoil NACA 4412 and its pressure distribution

The trailing edge high-lift devices are range from simple systems as plain and split flaps to complex multi-slotted or Fowler flaps. Especially, these complex multi-slotted or Fowler flaps can't only change the camber but also extend the chord. They are almost standard equipments in modern civil transport aircraft. The trailing edge devices usually occupy 20% to 40% of chord length and can increase lift coefficient up to two to three times than the basic airfoil.

The leading edge high-lift devices usually occupy 10% to 20% of chord length. Its simplest form, hinged nose or droop nose, can effectively extend the angle of airfoil stall with typical deflection angle within 10 degree. Droop nose has a smoother upper surface due to a lower pivot point as compare with plain flap. Kruger flap can move the flap forwards and downwards, which extends the chord as well as changes the camber. They are stowed in the lower part of airfoil when not in operations for aerodynamic reasons. The slat/slot systems are parts of the upper surface of airfoil when in cruise status. Their deployment is moving forwards and downwards following a circular track and their functions are similar to the Kruger flap. The maximum rotation angle of slat can be around 30 degree.

The tendency of high-lift devices is morphing wing. The form variable camber will probably be achieved by combing a flexible droop nose and a flexible extendable trailing edge

flap. The latter one may not, or may, be cooperated with a slot system. As mentioned previously, these concepts can come into engineering applications only if the penalties of mass, system complexity compare to performance gains are on relative low level. It is believed, as investigations about these concepts further proceeding, theses concepts can be applied within acceptable affords on some aircraft wings in near future.

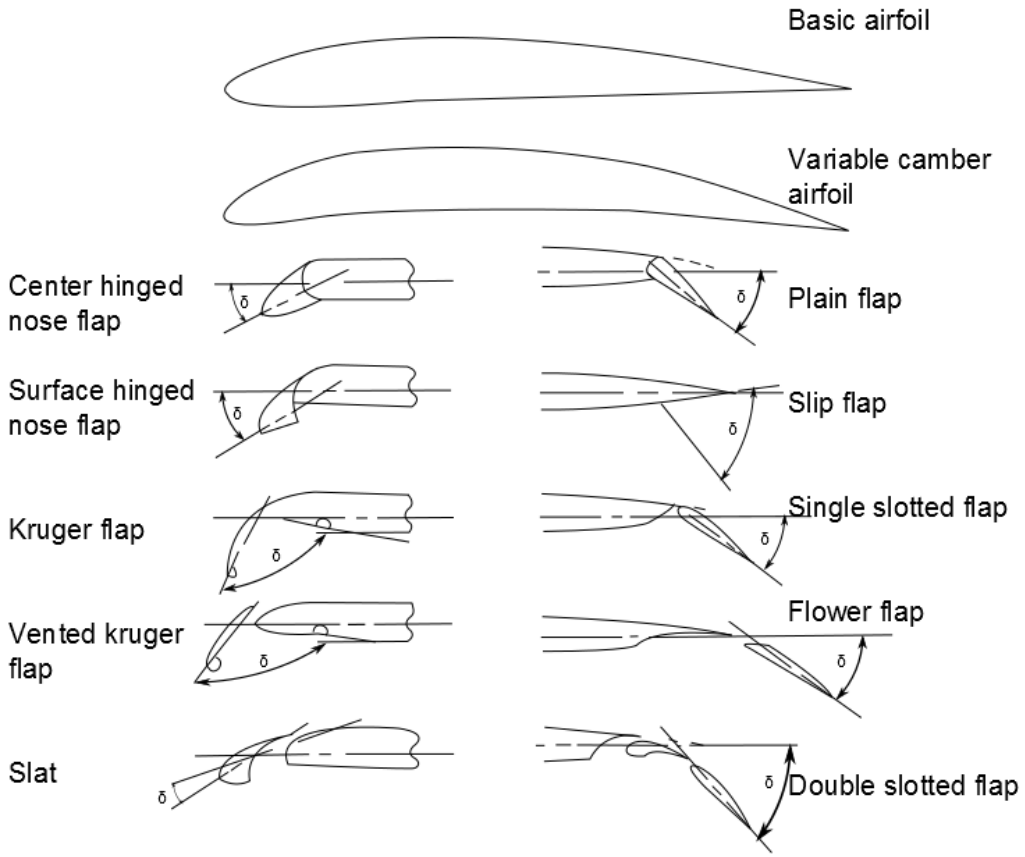

Figure 3.5.: Airfoil and common high-lift devices [Howe (2000)]

3.3. Background of Mechanically Reconfigurable Reflectors and Morphing Sailplane Wings

3.3.1. Mechanically Reconfigurable Reflectors

The investigations of mechanically reconfigurable reflector antennas in Europe are mainly guided and supported by Europe Space Agency (ESA). In last twenty years, although feasibility of mechanically reconfigurable reflector antennas was well proved and several potential concepts were demonstrated, none of them was applied in practice due to existing of various limitations in terms of thermal-elastic distortion, PIM, RF and etc. Based on recent advances on material technologies, such as the shell-membrane material CFRS from the LLB, ESA initialized a project about this topic, which is aim to explore the feasibility of a reconfigurable thin shell reflector under realistic application scenarios.

The project is carried by LLB and TAS cooperatively. During the antenna architecture design, TAS compared two dual-offset reflector concepts: lateral face antenna with a reconfigurable subreflector and earth deck steerable antenna with a reconfigurable main reflector. It is concluded that the concept of earth deck antenna with a reconfigurable main reflector of 1.2 m aperture diameter and an ellipsoid subreflector is more efficient. The antenna geometry definitions are diameter 1200 mm, focal length 850 mm, and offset 750 mm.

According to the investigations of TAS, the mechanically reconfigurable reflector antenna will be applied in the field of telecommunications and operated in Ku-Band. Its life duration is expected to be 15 years and the number of reconfiguration each year is 6 times. The losses budget for the reflector due to surface deviations is less than 0.3 dB. The maximum mass of the reconfigurable reflector antenna shall be comparative to the current products.

Three representative geographic coverage, which are derived from realistic applications and contain relative large reshaping amplitudes (in the range of -15 to +15 mm), are defined to evaluate the performance of designed reconfigurable reflectors. The three reshaping tasks are named as "Europe", "Brazil", and "ConUS", which are geographic regions of Europe, Brazil, and continent U.S. plus Hawaii and Alaska. These coverage are further divided into several regions with different gain requirements by polygonal lines. The illustrations of the three coverage are in Figure 3.6.

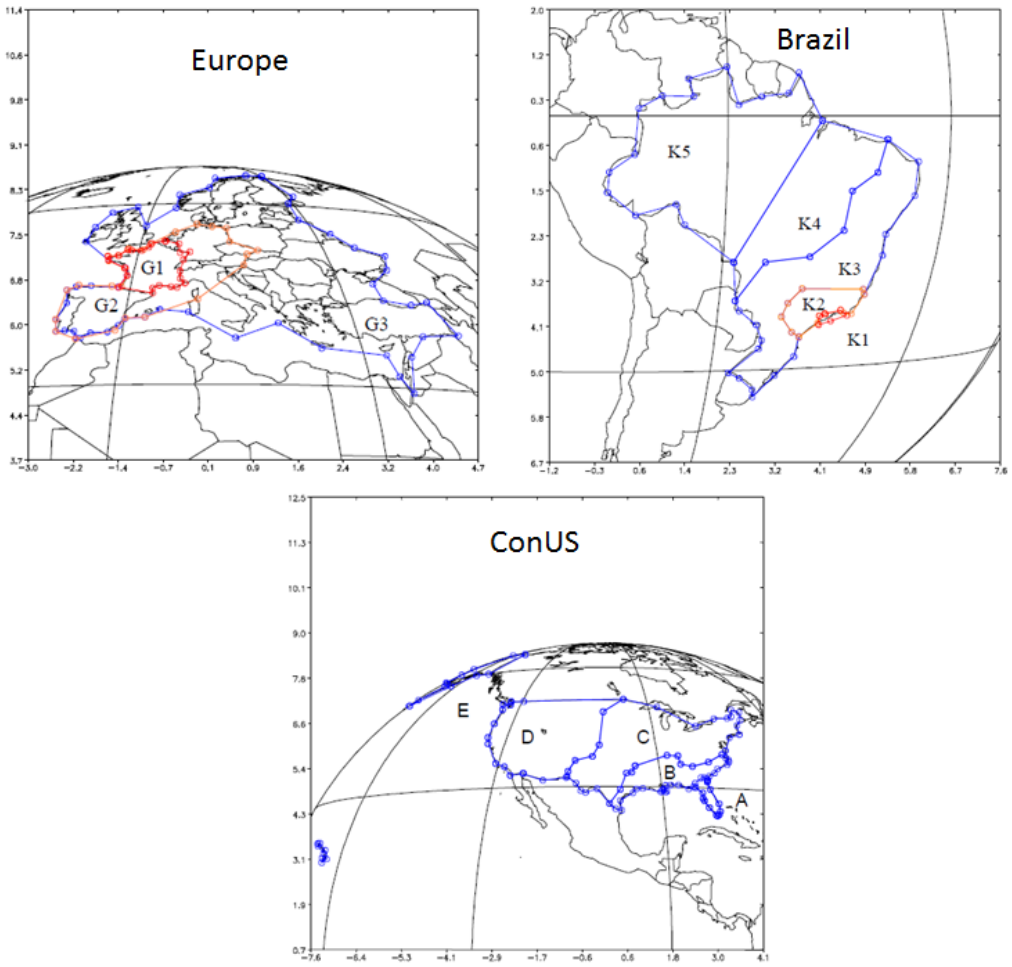

Figure 3.6.: Three representative reshaping tasks [Schreider et al. (2007)]

The above addressed requirements can be translated into mechanical requirements for material and structure design. They are classified into three aspects as functional, structural, and manufacturing requirements. As functional requirements, the relative large reshaping amplitude (as compare to reflector thickness of millimeter range) indicates at least geometry nonlinearity of the structure shall be considered. It is operated in the high frequency Ku-Band, which indicates high surface accuracy requirements. Referring to the maximum gain loss of 0.3 dB, the maximum surface error shall be smaller than 0.5 mm as the limit for applying in Ku-Band and smaller than 0.3 mm as preference. Typically, space structures should be operated in temperature range of -150 to $+150°C$, possibly small CTE values of materials are expected for small thermal-elastic distortions. Other requirements to materials like radiation resistance, aging resistance, low PIM properties, reflectivity to EM waves are expected as well.

As structural requirements, the reshaping surface shall be in material linear range and free of stability, strength and fatigue problems. The designed materials and structures should be characterized through tests according to these requirements correspondingly. The interface to actuators and boundary conditions play roles in fulfilling the structural requirements, in which proper design is required. And the corresponding sensing and actuations design/selection shall be considered according to the reconfigurable surface design. As requirements to that, possibly low actuation energy consumption and low mass are preferred in the actuation system design.

Last but not least, as manufacturing requirements, the implementation difficulties of the designed materials and structures shall be acceptable based on the existed technologies. The cost, mass and complexity of different structural designs shall be comparable to the existed products as well.

These requirements on different aspects together define the design space of material and structure design of the reconfigurable skin. Based on these requirements, approaches about compound material design for the morphing reflector skin are presented and their results are discussed in a later chapter.

3.3.2. Morphing Sailplane Wings

Akaflieg München is the student club of sailplane sports within Technische Universität München. Besides the sailplane sports, the investigations of new concepts, constructions and tests about sailplanes are their major activities too. Sailplanes are usually flying/gliding at altitude below 2000 meters with speed up to 200 km/h. For these unpowered sailplanes, the only power source is wind in terms of thermal lift and ridge lift. Therefore the aerodynamic efficiency of the glide ratio or the lift to drag ratio is the key factor to determine the performance of sailplanes.

The airfoil of sailplane wings is optimized to achieve a high lift to drag ratio through aerodynamic technologies and wind tunnel tests since quite long time. A further improvement of airfoil profile is foreseen to be minor. Therefore approaches of adding high-lift devices on wings were applied in some investigations of Akaflieg clubs over Germany. In the demonstrator fs-29 TF of Akaflieg Stuttgart, a telescope wing with ability of expanding span was presented in 1972 [Aka (d)]. The in-plane deployable trailing edge devices were equipped on the sailplane D 40 of Akaflieg Darmstadt [Aka (a)], which can extend the chord in flight for gaining more lift. Akaflieg München demonstrated a gap less Wortmann-flap sailplane

with name Mü 27 in 1979 [Aka (b)]. Although it has improved aerodynamic characters, the over heavy mass (two to three times more than common ones) and high system complexity limited the applications of this concept.

Inspirited from recent advantages in morphing wing technologies, Akaflieg München start to explore the morphing wing technologies for applying on sailplanes. As stated by Wießmeier, around 10% to 20% lift coefficient improvement can be expected by applying a gapless hinged nose on the existed wing. Based on his conclusions, the task of morphing skin design for the leading edge of a sailplane is established. The goal of this task is exploring feasible engineering solutions to a morphing leading edge for near future applications.

The wing configuration in this project is formulated on a latest concept of the sailplane Mü 31 and its image is shown in Figure 3.7. It has a span of 15 m and maximal take-off weight of 500 kg. The applied airfoil profile is DU-89-120-14-Profil and a flap with ± 25 degree deflection is equipped at the trailing edge. As suggestions from Wießmeier, around 40% of chord can be taken as the leading edge after shifting the reinforced main spar backwards. About the functional requirement, the deflection angle of the leading edge is estimated as around 10 degree downwards.

The requirements to the sailplane morphing leading edge design can be similarly formulated into requirements on functional, structural, and manufacturing aspects. It shall be able to deform in-plane and out-of-plane simultaneously in medium scale at different flight conditions. To carry the aerodynamic loads, its stiffness at least in the spanwise shall be equivalent to the existed skins. The applied skin materials shall be able to withstand temperature changing, moisture, UV etc. as existed in typical flight environments. On structural aspect, the static and dynamic loads from airflow shall be carried by the morphing skin and its related substructures without damage or degeneration on skin performance. Especially, the stability of the flexible skin in reshaping and dynamic loads like flutter shall be satisfied. Since the morphing skin is manufactured by hand laminating and cured in vacuum bags at room temperature, the labor intensity and complexity of the morphing skin manufacturing shall be acceptable. Furthermore, the maintenance of the morphing skin in terms of inspection, repairing, and replacing shall be considered as well.

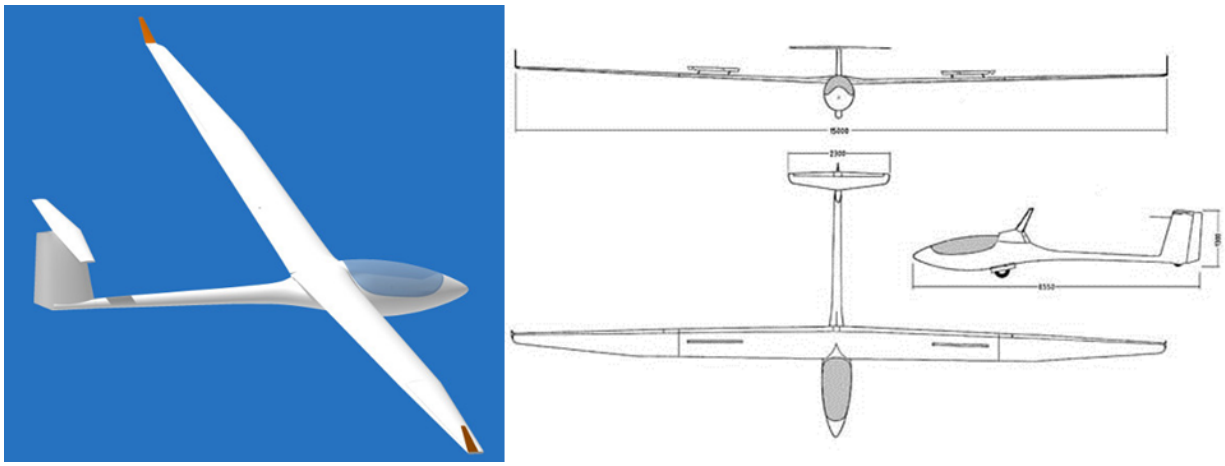

Figure 3.7.: An image of Mü 31 of Akaflieg München [Aka (c)]

4. Compound Material Design of Reflector Morphing Skins

In this chapter, the methods of compound material design, which involve tailoring different kinds of design parameters to achieve the defined objectives, are explored. To accomplish the task of reflector morphing skin design, approaches of compound material design containing correlation various design parameters with reshaping performance, deriving representative models, and assessment criterion to evaluate the derived material design are developed and presented. With help of the developed methods, parameter studies are performed to determine proper combinations of design parameters. Based on the results of the material design, potential morphing skin concepts are presented in details at last.

4.1. Objectives and Approaches of Reflector Morphing Skin Design

4.1.1. Objectives of Reflector Morphing Skin Design

The essential objective of the compound material design for a reflector morphing skin is the reshaping ability in relative large magnitude with high surface accuracy and also capable for relative high spatial frequency. As side objectives, the required reshaping energy shall be possibly low, material failure and structural instability shall be avoided.

4.1.2. Approaches of Reflector Morphing Skin Design

The desired shapes of reconfigurable reflectors are usually known. The mainly unknown are the proper material or material combinations for the reflector morphing skin, which can realize the desired reshaping. In fact, the reshaping behavior of a reflector morphing skin is mainly determined by various parameters range from material properties, geometry to boundary conditions. Therefore the essential challenging of the reflector morphing skin design is how to correlate these various material design parameters with the complex reshaping behavior.

In order to figure out their correlations, the design task of the reflector morphing skin will be simplified to enable analytical analyses. First of all, the reshaping of a reflector morphing skin can be understood as a thin shell with large deflection. As a further simplification, thin shell can be replaced by thin plate for the shallow configuration. Since the theory of

shells is derived from the theory of plates and they have many commons in theories, using plates in the preliminary analyses can keep focus on the essential problems rather than on some complex reshaping phenomena relating to the geometry of shells. In a later stage, the analyses can be easily extended to shells with the obtained knowledge from the analyses of plates. Based on the theory of plates, plates with large deflection can be expressed as two nonlinear differential equations containing information of geometry, material properties and surface shape. As additional expressions to the mathematic surface shape description, strain energy terms in reshaping can be used to better correlate design parameters with the resulting reshaping behavior. Combing the mathematic shape expressions with the strain energy expressions, those various design parameters can be well correlated with the resulting reshaping responses.

To enable analytical analyses, the analysis models shall be simplified as well. The full size reflector model contains too many variations like placements of actuators, different reshaping cases and interferences of other components, which make the analytical analyses quite complicated. Therefore representative unit cell models, which contain all essential features of the full size reflector model, are extracted from the full size model for parameter studies. With help of the representative unit cell models, parameters such as geometry range from thickness, size, shape to shell/plate configuration and boundary conditions e.g. simply supported and free movable can be evaluated with reasonable efforts. Afterwards, the design space of these parameters can be greatly reduced and the unit cell models can be updated with determined or at least partly determined geometry parameters and boundary conditions. Then in following parameter studies, the focus can be on the interested material property tailoring to find out optimal compound material concepts. To make the understanding easier, a scheme description of the methods of material design is shown in Figure 4.1.

In oder to explain the applied methods clearly, the analytical expressions of plates with large deflection and their energy expressions will be described in details in the following subsections. With help of the analytical understanding, the task of the reflector morphing skin design can be properly defined with reasonable simplifications. Using the simplified analytical and numerical models, the morphing skin design can be readily performed even containing numerous potential design parameters.

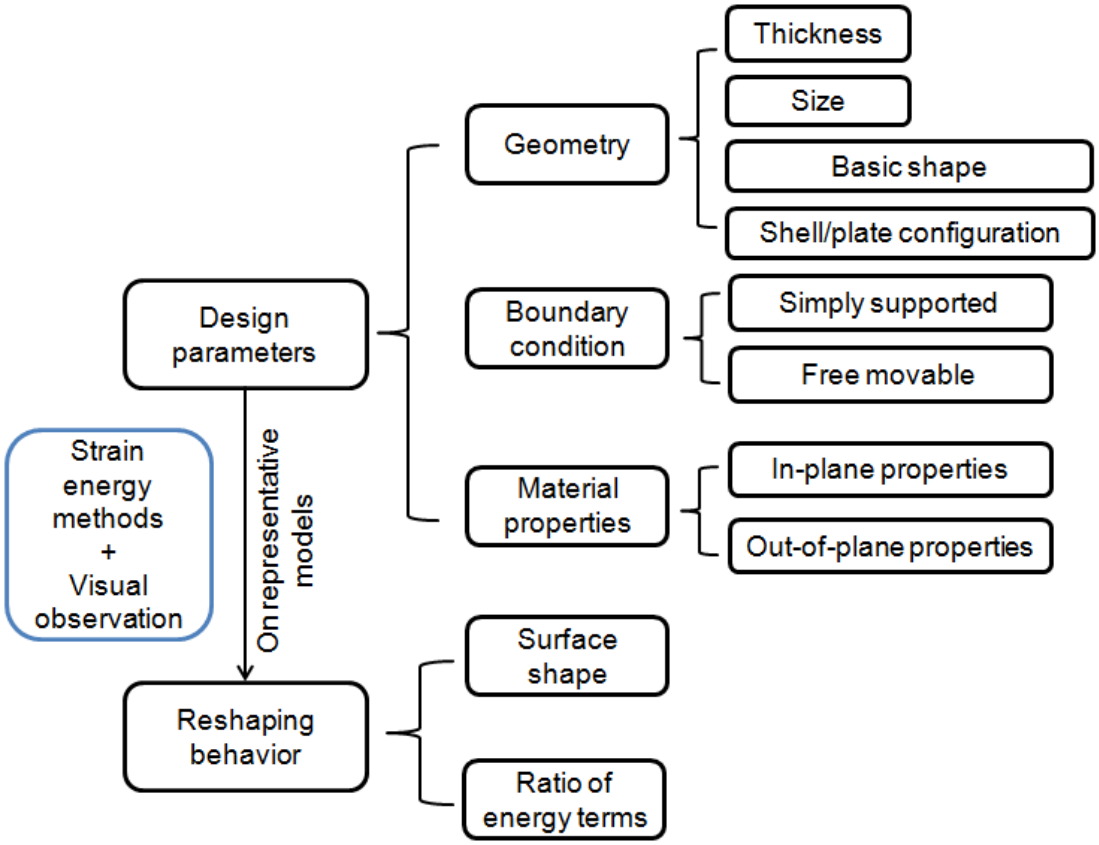

Figure 4.1.: Scheme of the compound material design for reflector morphing skin

General Equations of Plates with Large Deflection

According to theory of plates and shells [Timoshenko and Woinowsky-Krieger (1959)], the general equation of plates with large deflection can be presented as:

$$\frac{\partial^4 w}{\partial x^4} + 2\frac{\partial^4 w}{\partial x^2 \partial y^2} + \frac{\partial^4 w}{\partial y^4} = \frac{1}{D}\left(q + N_x\frac{\partial^2 w}{\partial x^2} + N_y\frac{\partial^2 w}{\partial y^2} + 2N_{xy}\frac{\partial^2 w}{\partial x \partial y} - X\frac{\partial w}{\partial x} - Y\frac{\partial w}{\partial y}\right) \tag{4.1}$$

The definitions of denotations are:
X and Y: body forces or tangential forces per unit area of the middle plane of the plate
N_x, N_y, and N_{xy}: forces per unit length
w: deflection
q: lateral loads on the plate
D: flexural rigidity
An illustration of force components on a small element cut from a plate is shown in Figure 4.2.

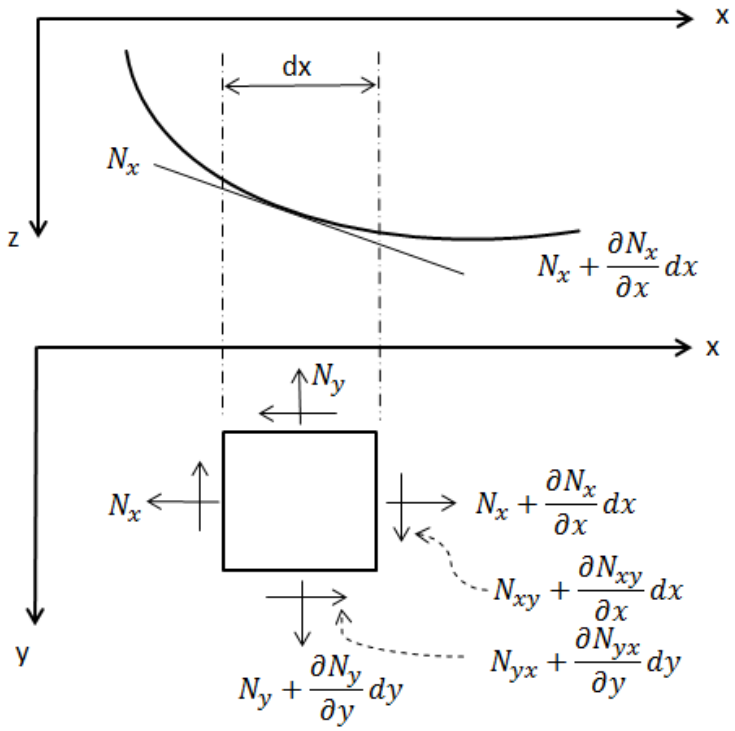

Figure 4.2.: The force components on a small element from a plate

Assuming there are no body forces or tangential forces (X and Y) acting on the x and y axes, the equations of equilibrium are

$$\begin{aligned} \frac{\partial N_x}{\partial x} + \frac{\partial N_{xy}}{\partial y} &= 0 \\ \frac{\partial N_{xy}}{\partial x} + \frac{\partial N_y}{\partial y} &= 0 \end{aligned} \tag{4.2}$$

To obtain these three force components, the strain components on the middle plane of the plate shall be derived first. In the large deflection case, which means the deflection is larger than the thickness but still considerable smaller than other dimensions, the strains consist of elongations of the middle plane stretching and elongations due to deflection. The corresponding strain components are

$$\begin{aligned} \varepsilon_x &= \frac{\partial u}{\partial x} + \frac{1}{2}\left(\frac{\partial w}{\partial x}\right)^2 \\ \varepsilon_y &= \frac{\partial u}{\partial y} + \frac{1}{2}\left(\frac{\partial w}{\partial y}\right)^2 \\ \gamma_{xy} &= \frac{\partial u}{\partial y} + \frac{\partial v}{\partial x} + \frac{\partial w}{\partial x}\frac{\partial w}{\partial y} \end{aligned} \tag{4.3}$$

The strain components can be represented using the force components by stress-strain

equations.

$$\begin{aligned}\varepsilon_x &= \frac{1}{hE}\left(N_x - \nu N_y\right)\\ \varepsilon_y &= \frac{1}{hE}\left(N_y - \nu N_x\right)\\ \gamma_{xy} &= \frac{1}{hG}N_{xy}\end{aligned} \tag{4.4}$$

where h is the thickness of plates and E is the elastic modulus.

By taking the second derivatives of the expressions in Eq. 4.3 and combing their products, a single equation containing three terms can be obtained.

$$\frac{\partial^2\varepsilon_x}{\partial y^2} + \frac{\partial^2\varepsilon_y}{\partial x^2} - \frac{\partial^2\gamma_{xy}}{\partial x\partial y} = \left(\frac{\partial^2 w}{\partial x\partial y}\right)^2 - \frac{\partial^2 w}{\partial x^2}\frac{\partial^2 w}{\partial y^2} \tag{4.5}$$

For the reason of simplification, a so called stress function (F) is introduced by Timoshenko. Therefore the force components can be rewritten as

$$\begin{aligned}N_x &= h\frac{\partial^2 F}{\partial y^2}\\ N_y &= h\frac{\partial^2 F}{\partial x^2}\\ N_{xy} &= -h\frac{\partial^2 F}{\partial x\partial y}\end{aligned} \tag{4.6}$$

where F is a function of x and y. Substituting these expressions in Eq. 4.5 by expressions in Eq. 4.4 and 4.6, we obtain

$$\frac{\partial^4 F}{\partial x^4} + 2\frac{\partial^4 F}{\partial x^2\partial y^2} + \frac{\partial^4 F}{\partial y^4} = E\left[\left(\frac{\partial^2 w}{\partial x\partial y}\right)^2 - \frac{\partial^2 w}{\partial x^2}\frac{\partial^2 w}{\partial y^2}\right] \tag{4.7}$$

To determine F and w, a second equation is required, which can be derived by substituting expressions from Eq. 4.6 in Eq. 4.1.

$$\frac{\partial^4 w}{\partial x^4} + 2\frac{\partial^4 w}{\partial x^2\partial y^2} + \frac{\partial^4 w}{\partial y^4} = \frac{h}{D}\left(\frac{q}{h} + \frac{\partial^2 F}{\partial y^2}\frac{\partial^2 w}{\partial x^2} + \frac{\partial^2 F}{\partial x^2}\frac{\partial^2 w}{\partial y^2} - 2\frac{\partial^2 F}{\partial x\partial y}\frac{\partial^2 w}{\partial x\partial y}\right) \tag{4.8}$$

The above two equations, together with boundary conditions, can be solved to determine the functions of F and w. The stresses in the middle plane of a plate can be further determined through the obtained functions of F as addressed in Eq. 4.6. Using the function w, the bending and shearing stresses can be readily obtained as in the case of plates with small deflection. Therefore, the problem of plates with large deflection is reduced to be solving two nonlinear differential equations Eq. 4.7 and Eq. 4.8. However, the solution of the two equations is generally unknown. Approximation methods such as energy method and finite element method (FEM) are usually employed to solve the equations.

Energy Expressions of Plates with Large Deflection

The strain energy of plates with large deflection is classified into two groups as in-plane energy (membrane energy) and out-of-plane energy (plate energy). The in-plane energy can

be further classified as principle axial energy and shearing energy, and similarly the out-of-plane energy is classified as bending energy and twist energy (see Figure 4.3).

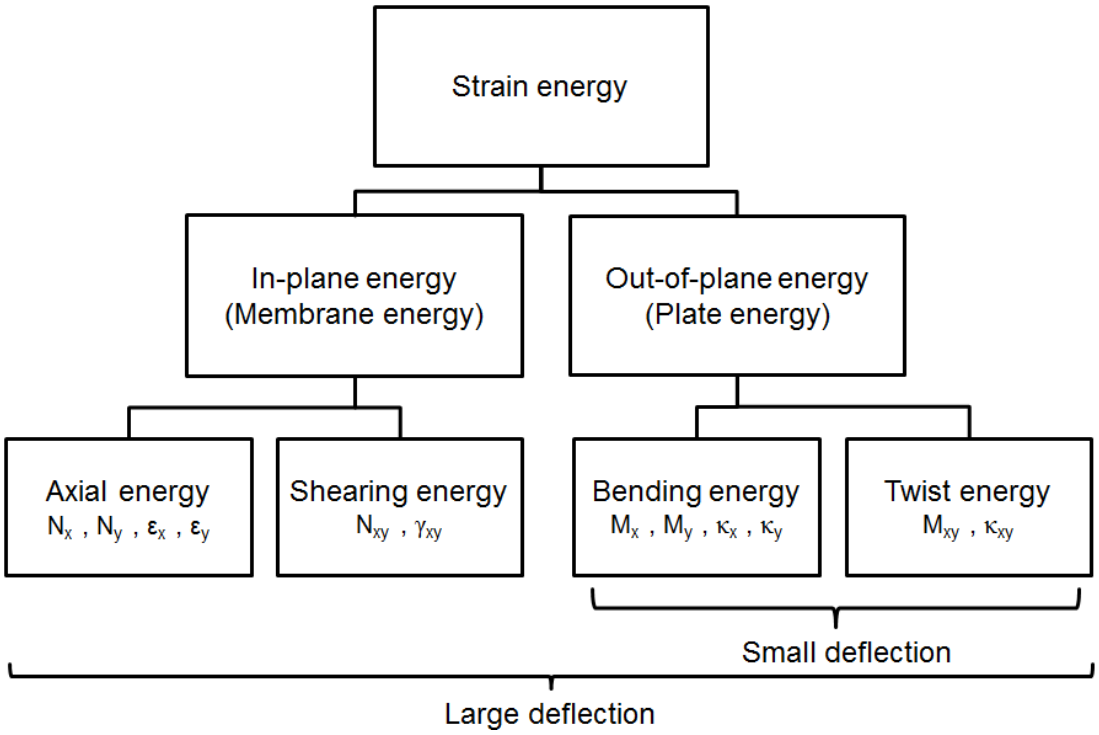

Figure 4.3.: Energy expressions of plates

The expressions of the out-of-plane energy are following definitions in plates with small deflection and they are

$$V = -\frac{1}{2}\iint\left(M_x\frac{\partial^2 w}{\partial x^2} + M_y\frac{\partial^2 w}{\partial y^2}\right)\mathrm{d}x\mathrm{d}y + \frac{1}{2}\iint\left(M_{xy}\frac{\partial^2 w}{\partial x\partial y} + M_{yx}\frac{\partial^2 w}{\partial x\partial y}\right)\mathrm{d}x\mathrm{d}y \tag{4.9}$$

and for isotropic materials they can be rewritten as

$$V = \frac{1}{2}D\iint\left[\left(\frac{\partial^2 w}{\partial x^2}\right)^2 + \left(\frac{\partial^2 w}{\partial y^2}\right)^2 + 2\nu\frac{\partial^2 w}{\partial x^2}\frac{\partial^2 w}{\partial y^2}\right]\mathrm{d}x\mathrm{d}y + D(1-\nu)\left(\frac{\partial^2 w}{\partial x\partial y}\right)^2\mathrm{d}x\mathrm{d}y \tag{4.10}$$

where the flexural rigidity D is

$$D = \frac{Eh^3}{12(1-\nu^2)} \tag{4.11}$$

The first integration term in Eq. 4.9 is the bending energy and the second is the twist energy.

The expressions of the in-plane energy can be represented analogously

$$\begin{aligned} V &= \frac{1}{2}\iint\left(N_x\varepsilon_x + N_y\varepsilon_y + N_{xy}\gamma_{xy}\right)\mathrm{d}x\mathrm{d}y \\ V &= \frac{Eh}{2(1-\nu^2)}\iint\left[\varepsilon_x^2 + \varepsilon_y^2 + 2\nu\varepsilon_x\varepsilon_y + \frac{1}{2}(1-\nu)\gamma_{xy}^2\right]\mathrm{d}x\mathrm{d}y \quad \text{(isotropic materials)} \end{aligned} \tag{4.12}$$

The terms with strains in x and y directions are defined as the principle axial energy and the term with shear strain is defined as the shearing energy.

The behavior of plates with deflection is characterized by magnitude and ratios of these energy components. In following sections details are explained through several examples.

Task Definitions

With the above presented approaches, the task of reflector morphing skin design can be initialized. First of all, the complex task definitions are to be simplified with assumptions as following.

As mentioned in the previous section, the double curved reflector is simplified as a thin plate in the initial stage. Based on the assumption of thin plates, the transverse shear stiffness and rotational inertia effects can be ignored in analyses of these structures. The criterion to determine whether thin or thick plate is the ratio of thickness to other dimensions typically like length, width, and radius of curvature. The value of this ratio for a reconfigurable reflector morphing skin can be roughly accessed as following. As referring to the published literatures [Theunissen et al. (2001) and Cappellin and Pontoppidan (2009)], a typical actuator number of a reconfigurable reflector is around 50 in a subreflector with diameter 500 mm and around 100 in a main reflector with diameter 1200 mm. Assuming in the initial analyses there are 100 actuators placed uniformly on a projected aperture plane with diameter of 1200 mm. Then the distance between two adjacent actuators is between 100 to 150 mm as a result of the assumption. As an empirical criteria for thin plates, the ratio of thickness to the distance between two adjacent actuators shall be smaller than 1/20, so the maximum thickness of a reconfigurable reflector morphing skin is estimated to be 5 mm.

The morphing skin of the reconfigurable reflector requires flexibility and stiffness simultaneously. Understanding of this demand can be better formulated in two separate understanding of the extremely flexible structures like membranes and the stiff structures like plates.

According to the theory of membranes, a membrane has only in-plane responses and no rigidity to compression and bending. Unlike to those conventional, rigid-type structures, the forms of membranes can't be imposed for the strong nonlinear interactions between their shapes and loads. Because of that, their sustainable forms are more likely to be found rather than be designed. The found forms of such structures are the equilibrium forms under defined boundary conditions, materials, and loads. In the case of no external load, the equilibrium form of a tensioned membrane can be a double curved surface with negative Gaussian curvature, which is the form of pillowing. Based on these facts, a membrane like reconfigurable morphing skin is not preferred due to complex reshaping behavior as well as poor surface quality.

In contrast to membranes, thin plates with small deflection have only out-of-plane responses (pure bending). The deflection of a plate is represented as second order derivative equations consisting of in-plane coordinates, bending moments, and flexural rigidity. The second order description of a surface indicates continuous first derivatives and geometric continuity on C^1 level. A smooth and continuous surface during and after reshaping is the desired feature for the reconfigurable morphing skin since the transmission of EM waves following geometrical and physical optics. However, as deflection grows into large amplitude, the in-plane responses of plates can't be neglected any more.

The reconfigurable reflector morphing skin shall be able to be reshaped within amplitude of 15 mm as indicated in [Cappellin and Pontoppidan (2009) and Cappellin et al. (2009)].

For a thin plate, whose thickness is expected to be around 1 mm, 15 mm deflection is belonging to a large deflection case. Different to analyses of thin plates with small deflection, the in-plane and out-of-plane responses are the indispensable components due to geometry nonlinearity in analyses of thin plates with large deflection. The reconfigurable reflector morphing skin shall present mixing features of membranes and plates simultaneously in reshaping. But the portions of the in-plane and out-of-plane responses are determined by material properties in terms of stiffness, which are actually the design tunnel of material design. A simple material tailoring was performed by Pontoppidan et al. (1991) through introducing bending stiffness by increasing thickness. As the thickness of plate growing, it presents less membrane behavior in terms of reduced pillowing amplitude. But simply increasing structure thickness is not a real feasible and effective solution, which brings penalties of mass increasing, reshaping energy consumption increasing as well as complexer reshaping behavior due to changing thin shells to thick shells.

The more reasonable approach is tailoring material properties to create certain combinations of in-plane and out-of-plane properties, thereby a thin shell can present reshaping features dominated by out-of-plane responses in the case of large deflection. As additional requirements, its thickness shall be possibly low for an acceptable actuation force inner 30 N. The unstable problems of thin shells like buckling and snap-through shall be considered and must be avoided. These together formulate the task of compound material design for reconfigurable reflector morphing skins.

4.2. Investigations of Parameters to Material Design

Parameters involving in material design can range from material properties like isotropic and anisotropic, boundary conditions like simply supported and free movable, and geometries like basic shape, plate/shell configuration and thickness. To better identify the influence of each design parameter, the investigations of these parameters are performed sequentially in the order of boundary conditions, geometry and material properties. The parameters, which have shown their positive influence on the large amplitudes reshaping, will be followed in later studies. Respect to these various of parameters, it will be too complicated and computation intensive if the parameter studies are performed on full size models directly. In order to simplify the complicated task and reduce the computation cost, representative unit cell models will be created at first.

4.2.1. Representative Unit Cell Models

The first representative unit cell model is created based on the following assumptions of the mechanically reconfigurable reflector. The reconfigurable reflector is a shallow shell, therefore it can be simplified as a plate reflector. The actuator number is assumed to be 100 with an uniform placement in square lattice as typically used in many existed concepts. Then the distance between two adjacent actuators is set to be 100 mm in this case. The representative unit cell model is determined to include 9 actuators for limiting its size but still involving the interference of adjacent actuators. Based on the above statements, the final created unit

cell model is a square plate with dimensions of 200 x 200 mm (see Figure 4.4).

Since it is more interesting to know the energy ratios among different responses rather than their physical values. The initial material properties are taken as an isotropic material with elastic modulus of 70 GPa and Poisson's ratio of 0.3 in examples (for instance, aluminum). The strain energy components of plates with large deflection are calculated through employing FEM. The obtained element strain energy results are grouped into four terms as defined in Eq. 4.10 and Eq. 4.12.

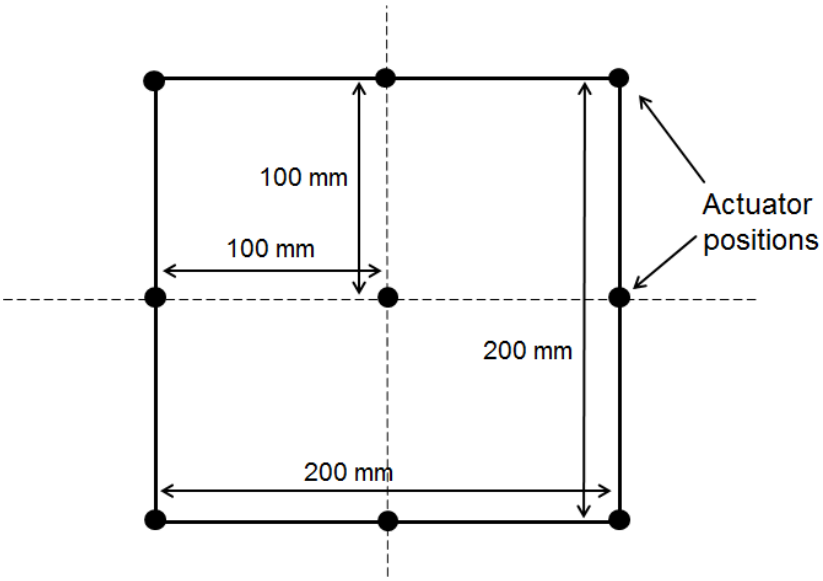

Figure 4.4.: A representative unit cell

The thickness of the unit cell is taken as 1 mm in the first example. As boundary conditions, four edges are simply supported and in the middle 15 mm deflection is applied.

The illustration of the deformed unit cell is presented in Figure 4.5 left, in which a tent like shape can be clearly observed. The local tent like shape in the center of the unit cell is more likely to be formed by stretching rather than bending. Furthermore, observing the energy amount and ratios, around 86% strain energy is membrane energy and in which around 77% is the principle axial energy, which explains the tent like reshaping contour.

Regardless of physical meanings, assuming the unit cell with 15 mm deflection is still the pure bending case, its deflection contour as well as total strain energy are significant different to the contour of the physical case (Figure 4.5 right). In the pure bending case, the curvature of the deflected plate is relatively small contributed by its smooth surface shape, which indicates a small strain value can be expected. From the comparison analyses, it can be found that if thin plates with large deflection can present close to pure bending behavior, the material can probably be maintained in linear elastic range as preferred and left only geometry nonlinearity.

As it can be observed from Table 4.1, the major strain energy is the principle axial energy in the plate with large deflection, which is mainly contributed by the fixed edges and the large deflection in the center. About the energy amount, the total energy in the plate with large deflection is around 30 times larger than it in the artificial pure bending case. And about the plate energy, it is just a minor part of total energy in the plate with large deflection

and in which the bending and twist energy are more or less the same.

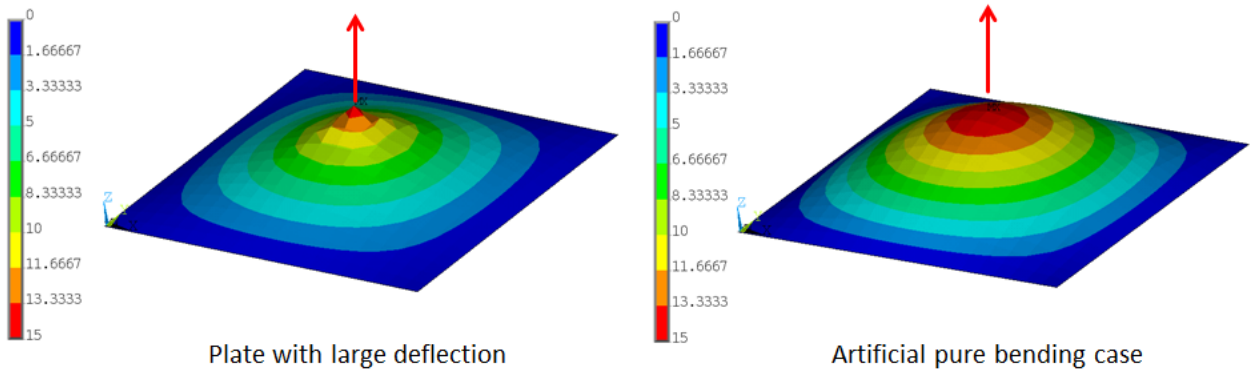

Figure 4.5.: Deformation plots of the plate with large deflection and artificial pure bending

Table 4.1.: Strain energy in the plate with large deflection and artificial pure bending

		Plate with large deflection		Pure bending case	
Type		Energy [J]	Ratio [%]	Energy [J]	Ratio [%]
Membrane energy	Principle axial	68.05	77.6	0	0
	Shearing	7.36	8.4	0	0
Plate energy	Bending	5.9	6.7	1.04	33.9
	Twist	6.39	7.3	2.03	66.1
	Total	87.7	100	3.07	100

Since the boundary condition of simply supported plays an important role in reshaping behavior, in following analyses, boundary conditions are varied to figure out their influence on reshaping behavior.

4.2.2. Influence of Boundary Conditions

The boundary condition of simply supported is changed to be in plane free movable in following analyses. It is observed, the total strain energy and reshaping contours are considerably changed as boundary condition changing. The surface contour under free movable edges is a pillow like shape with negative Gaussian curvature at the center areas (see Figure 4.6). The strain energy is around 1/4 as it in the simply supported case and the ratio of membrane energy is reduced to be around 45% only. As a visual impression, it presents a mixed feature of membranes and plates in the large deflection case.

Through tracking the energy ratio varying as deflection amplitude growing, it is observed that in the small deflection case (amplitude smaller than the thickness of plate) the major component is the plate energy. And as deflection growing, the membrane energy grows correspondingly. With the deflection further growing, the ratio of membrane energy reaches a convergence of 45% (see Figure 4.6 and Table 4.2). According to these results, an

empirical value to define a dominative component in total strain energy is estimated as 95%. That means, if the plate energy in total is more than 95%, the plate shall present the features of plates in the pure bending case regardless of large or small deflection.

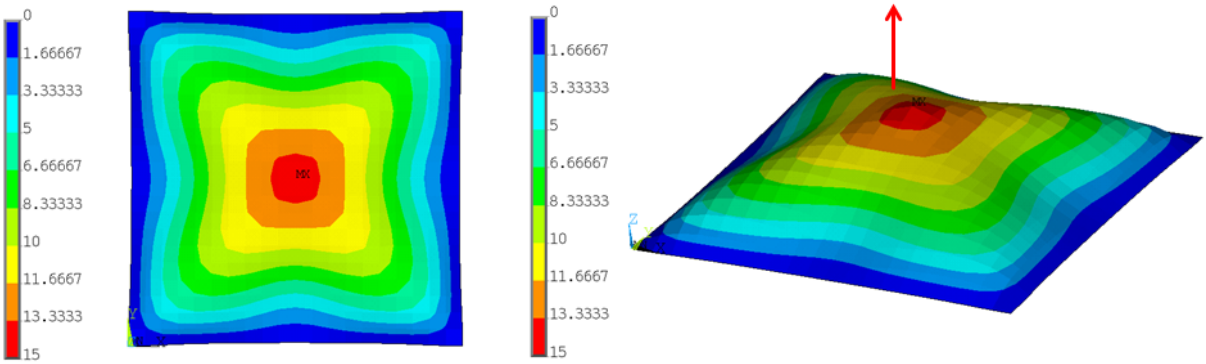

Figure 4.6.: Plate with large deflection under free movable edge

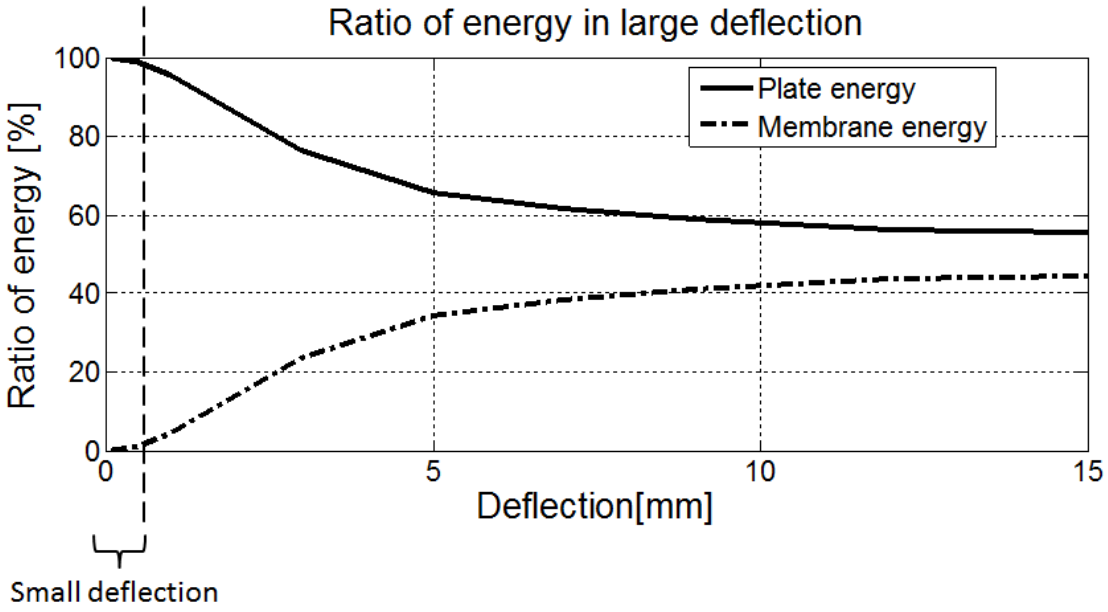

Figure 4.7.: Ratio of plate and membrane energy in large deflection

Table 4.2.: Strain energy in plate with large deflection under free movable edge

Type		Energy [J]	Ratio [%]	Sum[%]
Membrane energy	Principle axial	6.13	30.6	44.5
	Shearing	2.78	13.9	
Plate energy	Bending	4.1	20.5	55.5
	Twist	7.03	35	
	Total	20.04	100	100

The in plane free movable boundary condition has shown positive influence on reshaping performance in the large deflection case. The membrane energy, particularly its component principle axial energy, has been considerably reduced. To realize a free movable boundary condition in structures, an interface structure between actuators and the reflector surface, which allows in plane movements of the reflector surface in certain range, is required. As proposed by Datashvili et al. (2010) and Pontoppidan et al. (2010), rods are taken as interface structures to connect the reflector surface with actuators containing rotation degree of freedoms.

The center cutting lines of three analyses namely large deflection with simply supported edges, large deflection with free movable edges, and large deflection with artificial pure bending are presented as in Figure 4.8. Generally, these results are analogical to the results presented by Clarricoats and Zhou (1991a), the results of large deflection with artificial pure bending are the exact solutions given by Timoshenko and Woinowsky-Krieger (1959) and results of large deflection with simply supported edges are close to membranes in the pure stretching case. The results of large deflection with free movable edges demonstrate cutting curves with mixed features of above two results, which are global bending but local stretching. By increasing its bending stiffness, its results shall tend to approach the pure bending case.

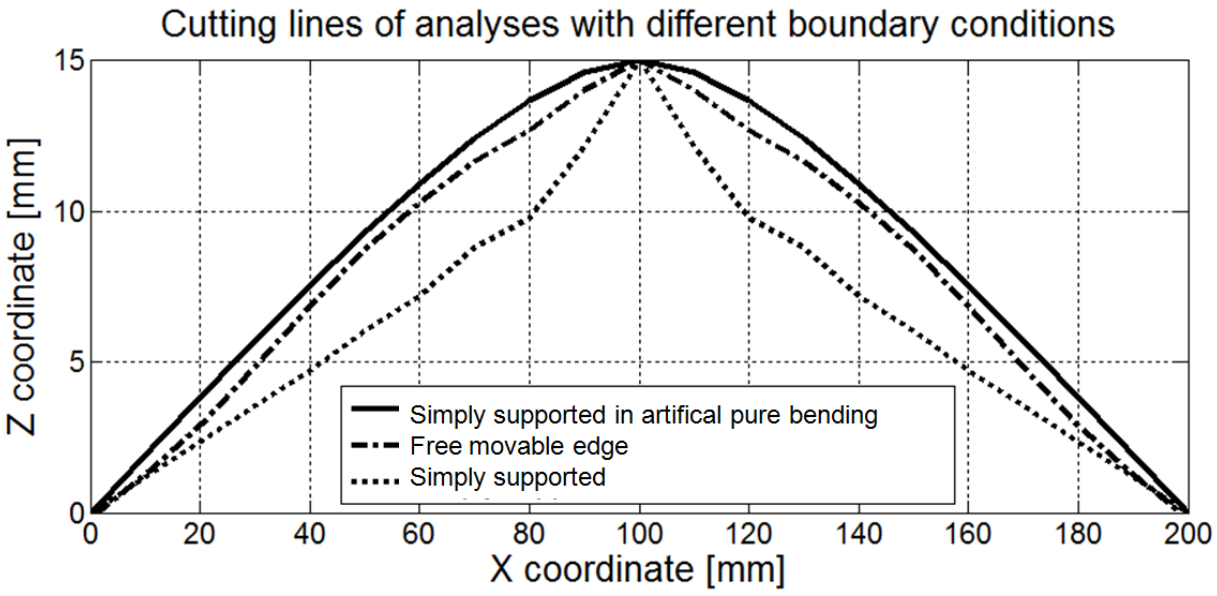

Figure 4.8.: The center cutting lines of three analyses

Two major parameters to increase bending stiffness of plates with isotropic materials are Young's modulus and thickness. Varying Young's modulus effects only the total strain energy amount while not changes the ratios of plate and membrane energy. To effect the ratio of plate to membrane energy, the ratio of bending to tensile stiffness as addressed by Clarricoats and Zhou (1991a) shall be varied. The major parameter to effect the ratio of is thickness, which is the quadratic term in the function (see Eq. 4.13). Additionally Poisson's ratio has certain influence on the ratio too. A large value of Poisson's ratio is generally helpful for increasing the ratio of bending to tensile stiffness.

$$\frac{EI}{EA(1-\nu^2)} = \frac{h^2}{12(1-\nu^2)} \tag{4.13}$$

4.2.3. Influence of Geometry Parameters

Based on the investigations about influence of boundary conditions on reshaping behavior, the free movable boundary condition will be applied in further studies. The focus in the following section is on identifying the influence of geometry parameters. Thickness is a quite effective parameter to change the reshaping behavior of plates, but actually its variable range is quite limited due to different thin/thick shell behavior and the low reshaping energy requirement. Besides thickness, other related design parameters are unit cell size, shape and plate/shell configuration. The background of the study is coming from the facts of varied actuator number, different actuator placements and the assumption of using thin plates instead of shallow thin shells in analyses.

Thickness

In varying thickness of the unit cell from 0.3 to 15 mm, following phenomena are observed: 1. the total strain energy increases rapidly due to the cubic relation of bending stiffness to thickness, 2. plate energy increases rapidly at first and then slowly proceeding to be the dominative term. Especially, when the thickness and deflection are on the comparative level ($\geq$ 10 mm), the membrane energy is ignorable, which is actually the hypothesis of plates with small deflection (see Figure 4.9).

To distinguish these energy components in reshaping, an energy component is defined as a major term when its ratio is more than 50%. Based on this definition, a trade-off of whether membrane or plate energy is the major term is found at thickness between 0.5 to 1 mm. A clear shape change of the center cutting lines can be observed between the reshaping results with plate thickness 0.5 mm and plate thickness 1 mm (see Figure 4.10).

Observing the cutting lines, the difference among the cutting lines is insignificant when thickness of plates is larger than 10 mm. Based on this fact, the empirical value of the defined dominative energy term can be released to be around 90% or even 85% in a rough assessment. Knowing from these analyses, the reshaping features of a plate can be transformed to close to pure bending by simply increasing its thickness. But this approach results penalties of large strain energy and complexer reshaping behavior, which are not preferred.

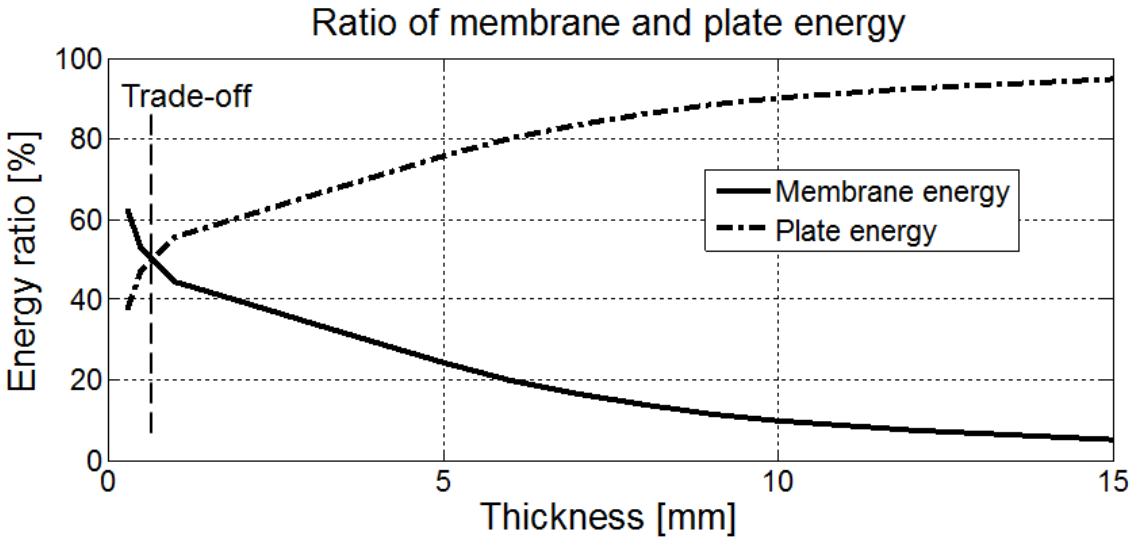

Figure 4.9.: The ratios of plate and membrane energy varying with thickness

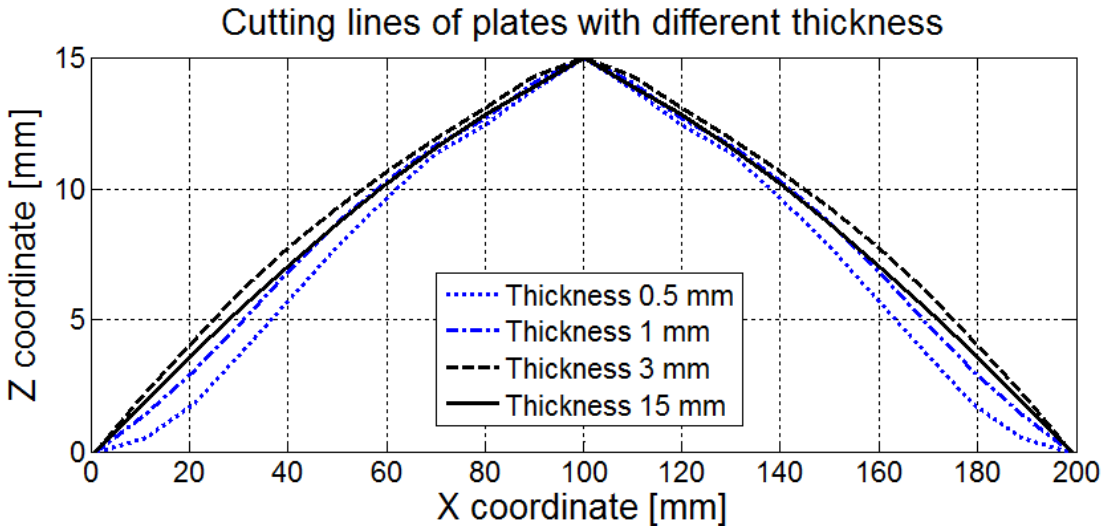

Figure 4.10.: The center cutting lines of plates with different thickness

To maintain the positive reshaping behavior of thick plates but limiting the reshaping energy demand, sandwich concepts can be proposed as an alternative. But either for thick plate concepts or sandwich concepts, the most effective term to effect the ratio of bending to tensile stiffness is still thickness. Therefore mostly the sandwich concept will be ended up with a medium thick sandwich concept, which is still not preferred. Based on the investigations about varying thickness of isotropic plates to effect reshaping behavior, it can be concluded that thickness is a quite effective term to improve reshaping features but its adjustable range is also quite limited mainly for the penalty of large reshaping energy. To find out the expected advanced morphing skin concepts, investigations shall be extended to anisotropic materials for involving design variables of material properties.

Unit Cell Size

The size of unit cell is mainly determined by actuator distance. For unit cells with the same deflection amplitude, varying the size of unit cell is actually changing the curvature of the shaped surface. Observing Table 4.3, the total strain energy is directly influenced by unit cell size but the ratios of energy components are basically not changed. That means, increasing or decreasing actuator distance in typically required range has marginal influence on reshaping behavior but considerable influence on reshaping energy amplitude.

The number of actuators is partly determined by reshaping behavior of the designed morphing skin. For example, a morphing skin with close to pure bending feature usually requires less actuators than a morphing skin with close to membrane feature to accomplish the same reshaping tasks. Less number of actuators brings benefit of less system mass as well as complexity. As long as surface reshaping error is satisfactory, actuator number shall be possibly less.

Table 4.3.: Strain energy in plates with large deflection for different unit cell sizes

	Unit cell size 140x140 mm		200x200 mm		300x300 mm	
	Energy [J]	Ratio [%]	Energy [J]	Ratio [%]	Energy [J]	Ratio [%]
Principle axial	12.9	31.6	6.13	30.6	2.68	30
Shearing	6.1	14.9	2.78	13.9	1.19	13.3
Bending	7.98	19.6	4.1	20.5	1.8	20.9
Twist	13.79	33.8	7.03	35	3.19	35.8
Total	40.78	100	20.04	100	8.94	100

Unit Cell Shape

Besides square lattice, another frequent used actuator placement is triangular lattice. For comparison, areas of unit cells with square lattice and triangular lattice are maintained as the same. The unit cell with triangular lattice has a hexagon shape with actuator distance of 124 mm and contains 7 actuators (see Figure 4.11).

The same boundary condition and amplitude of deflection as in the unit cell with square lattice are applied on this model. Two unit cells with the same thickness of 1 mm are taken in the comparison study. Based on the results presented in Table 4.4, it is found that the total strain energy of the two unit cells is on the same level and the resulting plate energy is the major term in the unit cell with square lattice while vice verse in the unit cell with triangular lattice.

Similar to the unit cell with square lattice, thickness of the unit cell with triangular lattice is varied from 0.3 to 15 mm in a parameter study. The trade-off of whether membrane or plate energy is the major term is found at around 2 mm thickness, which is larger than the value in the square lattice model. A clear shape transformation of "membrane like" to "plate like" is observed when thickness of a plate from 1 mm grows to 2 mm (see Figure 4.12).

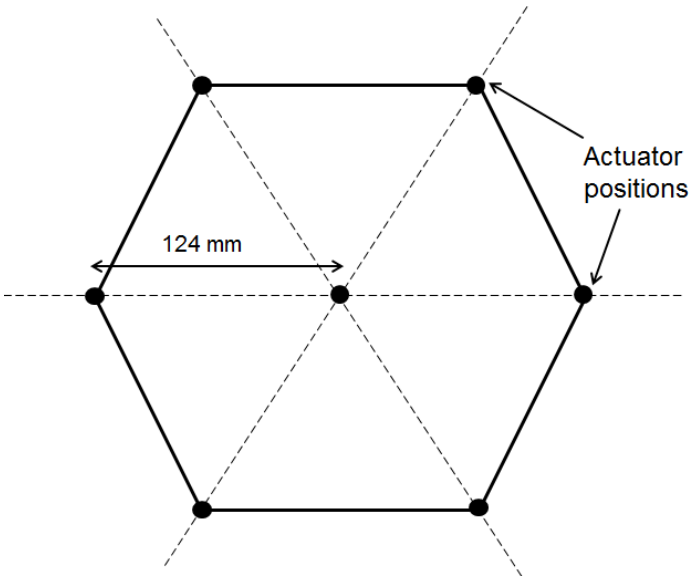

Figure 4.11.: A representative unit cell with triangular lattice

Table 4.4.: Strain energy in plates with large deflection for different unit cell shapes

	Unit cell with square lattice			Unit cell with triangular lattice		
	Energy [J]	Ratio [%]	Ratio [%]	Energy [J]	Ratio [%]	Ratio [%]
Principle axial	6.13	30.6	44.5	8.19	37.55	55.68
Shearing	2.78	13.9		3.94	18.13	
Bending	4.1	20.5	55.5	5.28	24.24	44.32
Twist	7.03	35		4.37	20.08	
Total	20.04	100	100	21.78	100	100

Observing the relations of ratios of energy components to thickness in both models, it can be found, with the same thickness the ratio of plate energy in the unit cell with square lattice is always higher than it with triangular lattice. This explains the shape transformation of "membrane like" into "plate like" occurs later in the unit cell with triangular lattice.

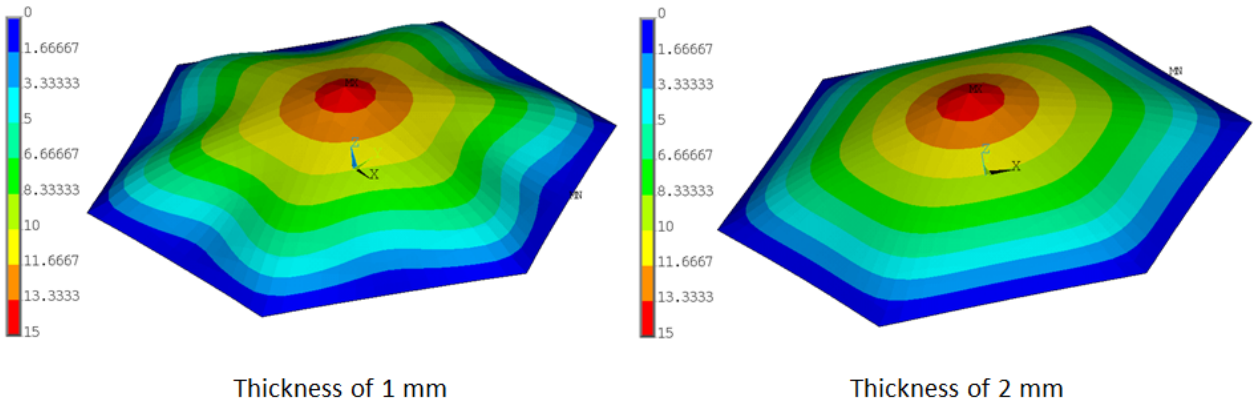

Figure 4.12.: Deformation shapes of the unit cell with triangular lattice

Therefore, to achieve similar reshaping behavior, the required thickness of a plate with triangular lattice is usually larger than the one with square lattice. That indicates eventually a higher demand on reshaping energy in plates with triangular lattice. But using triangular lattice usually requires less total number of actuators for the same reshaping area, which is a positive feature of this lattice. Based on the obtained results so far, it is difficult to determine which lattice is better or worse. Therefore the both lattices will stay in the campaign for further investigations.

Geometry Configuration

Different to plates, shells have curved geometry configuration, which adds the initial geometry stiffness into structures. The energy expressions of shells are identical to those of plates (Eq. 4.10 and Eq. 4.12). But the expressions of strains are different in shells due to effects of geometry curvatures. Strain components ε_1, ε_2, and γ of the middle surface and three curvature changes χ_x, χ_y, and χ_{xy} are presented in terms of displacement u, v, and w as follows [Timoshenko and Gere (1963)]:

$$\begin{aligned} \varepsilon_1 &= \frac{\partial u}{\partial x} & \varepsilon_2 &= \frac{\partial v}{a\partial\theta} - \frac{w}{a} & \gamma &= \frac{\partial u}{a\partial\theta} + \frac{\partial v}{\partial x} \\ \chi_x &= \frac{\partial^2 w}{\partial x^2} & \chi_y &= \frac{1}{a^2}\left(\frac{\partial v}{\partial\theta} + \frac{\partial^2 w}{\partial\theta^2}\right) & \chi_{xy} &= \frac{1}{a}\left(\frac{\partial v}{\partial x} + \frac{\partial^2 w}{\partial x\partial\theta}\right) \end{aligned} \tag{4.14}$$

where a is radius of curved shell and θ is the angle between two edges of shell.

A representative unit cell shell model is created for comparison purpose. Its projected shape is a square with dimension of 200 x 200 mm. The principle radii of the double curved shell are 1700 mm, which are the approximate radius of a paraboloid with focus length of 850 mm as addressed in Chapter 3.3. In this unit cell shell model, the same reference material, boundary conditions, deflection amplitude, and thickness as in unit cell plates are used. Different to plates with small deflection, the shells present membrane energy already in the initial small deflection case. Regardless of influence of material properties, the ratio of membrane energy in shells in the initial phase is determined by radii of curvatures and thickness of shell. For existing of initial curvatures in shells, the signs of deflection shall influence the reshaping behavior in terms of shape, energy amount, and energy ratio.

To identify the influence of deflection directions, four analyses are performed. The first two are the unit cell shell models deflecting up to $+15\,mm$ and $-15\,mm$ with geometry linear assumption, in which only the effects of geometry configuration on energy components are considered. Then, in two geometry nonlinear analyses, deflections are performed in opposite directions as well. The deflection works towards to the radius center of the shell is denoted as the positive direction and its opposite is defined as the negative direction.

In Figure 4.13, the center cutting lines of the above mentioned analyses are presented. In the geometry linear analyses, the deformations are not relevant to the signs of deflection. Their shape difference between the positive and negative deflection is caused only by the initial curved geometry. A relative large shape difference is presented in the cases of deflection in the positive direction, which can be explained as the relative large difference in energy ratios between the linear and nonlinear analyses. But in general, the contour line in the case of nonlinear analysis with deflection in the positive direction has better shape features for a high ratio of plate energy. It can be observed from Table 4.5, the ratio of plate energy in the model with + 15 mm deflection is around 80% while in the model with - 15 mm deflection is 44%.

Table 4.5.: Strain energy in shells with large deflection

Geometry linear analysis, deflection to ± 15 mm				
Type		Energy [J]	Ratio [%]	Ratio [%]
Membrane energy	Principle axial	3.27	37.04	53.12
	Shearing	1.42	16.08	
Plate energy	Bending	1.89	21.40	46.88
	Twist	2.25	25.48	
	Total	8.83	100	100
Geometry nonlinear analysis, deflection to + 15 mm				
Type		Energy [J]	Ratio [%]	Ratio [%]
Membrane energy	Principle axial	1.01	12.41	19.17
	Shearing	0.55	6.76	
Plate energy	Bending	2.33	28.62	80.83
	Twist	4.25	52.21	
	Total	8.14	100	100
Geometry nonlinear analysis, deflection to - 15 mm				
Type		Energy [J]	Ratio [%]	Ratio [%]
Membrane energy	Principle axial	16.03	39.59	55.77
	Shearing	6.55	16.18	
Plate energy	Bending	7.06	17.45	44.23
	Twist	10.84	26.78	
	Total	40.48	100	100

Tracking the variations of energy ratios relating to deflections, it is found the ratio of plate energy increases first and then decreases slightly in the positive deflection case. The explanations are following, the energy ratio is a combination product of deflection and curvature changes. When the deflection works in the positive direction, it reduces the curvature of the shell first, which increases the ratio of plate energy even when deflection is increasing. With the deflection further growing, the shape of the shell transforms from a concave to a convex stepwise and is maintained as the convex shape afterwards. Then the changes of curvatures and increasing deflection have the same effect on energy ratio, namely reducing the ratio of plate energy. When the deflection works in the negative direction, both curvature changes and the deflection increasing have the same effect on reducing the ratio of plate energy. But the reduction of the ratio of plate energy is smaller than it in the case of deflection in the positive direction. Interestingly, the ratio of plate energy increases even slightly in large deflection. The phenomenon is explained as appearance of pillowing, which forms local bending for generating plate energy.

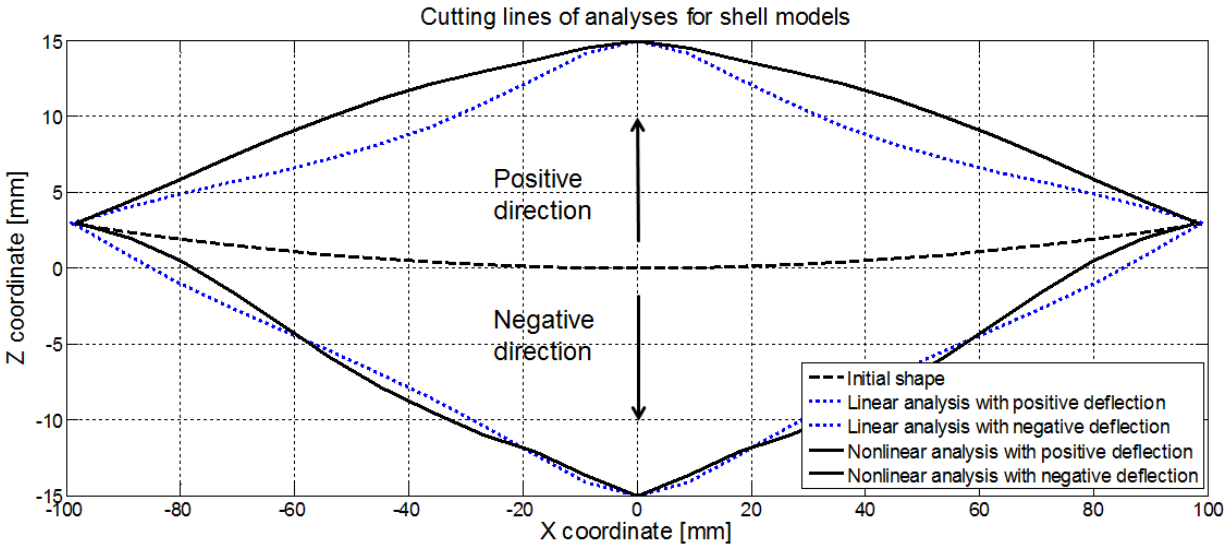

Figure 4.13.: Cutting lines of shell models with large deflection

Although there are certain difference between the reshaping behavior of shells and plates with small deflection as well as large deflection, the plate model is still recommended in the preliminary material design. The impact of a shell configuration, namely the initial geometry stiffness and not monotonous variations of energy ratios, shall be examined on the obtained results of preliminary material design.

Based on the investigations of shells, the goal of material design like high plate energy ratio in large deflection is not sufficient. Additional requirements as high ratio of plate energy in the initial small deflection and small variations of energy ratios in opposite deflections shall be added. With these updates, a relative small reshaping difference between linear and nonlinear analyses as well as deflections in different directions can be achieved.

4.2.4. Influence of Material Properties

As concluded through these parameter studies using isotropic materials, morphing skin design shall involve anisotropic materials for exploring the advanced concepts with thinner thickness, better reshaping behavior and lower reshaping energy. Before starting the investigations about material tailoring, some basics about anisotropic plates will be reviewed at first.

General Differential Equation of Anisotropic Plates

Referring to theory of plates and shells [Timoshenko and Woinowsky-Krieger (1959)], the differential equation of equilibrium for anisotropic plates is:

$$D_x \frac{\partial^4 w}{\partial x^4} + 2H \frac{\partial^4 w}{\partial x^2 \partial y^2} + D_y \frac{\partial^4 w}{\partial y^4} = q \tag{4.15}$$

with the notation

$$H = D_1 + 2D_{xy} \tag{4.16}$$

and definitions

$$D_x = \frac{E'_x h^3}{12} \quad D_y = \frac{E'_y h^3}{12} \quad D_1 = \frac{E'' h^3}{12} \quad D_{xy} = \frac{G h^3}{12} \tag{4.17}$$

where the E'_x, E'_y, E'', and G are material constants to characterize the elastic properties of plates. In the particular case of isotropy

$$E'_x = E'_y = \frac{E}{1-\nu^2} \quad E'' = \frac{\nu E}{1-\nu^2} \quad G = \frac{E}{2(1+\nu)} \tag{4.18}$$

The solution of Eq. 4.15 is determined by relations of H^2 to $D_x D_y$. When $H^2 = D_x D_y$, which is the isotropic material case, the solution is identical to the addressed in the previous section. But for the cases of $H^2 > D_x D_y$ and $H^2 < D_x D_y$, their solutions are considerable different to the solution of the isotropic material case. To obtain a more accurate understanding, analyses with different values of H^2 and $D_x D_y$ are performed and compared.

Relation of Stiffness Terms

The unit cell model as shown in Figure 4.4 and the same boundary conditions are used in following analyses. On the aspect of material properties, complete anisotropic materials are not preferred due to their complex mechanical behavior on applications. Instead, orthotropic materials with identical stiffness in both principle directions and possibly none or low coupling between the in-plane and out-of-plane behavior are preferred. In following examples, orthotropic materials with constant stiffness of D_x, D_y and $D_x = D_y$ are applied. With these assumptions, the ratio of H^2 to $D_x D_y$ can be expressed as:

$$\frac{H^2}{D_x D_y} = \left(\frac{H}{D_x}\right)^2 = \left(\left(\frac{\nu E h^3}{1-\nu^2} + \frac{2G h^3}{12}\right) / \left(\frac{E h^3}{1-\nu^2}\right)\right)^2 = \left(\nu + \frac{2G(1-\nu^2)}{E}\right)^2 \tag{4.19}$$

The ratio is determined by Poisson's ratio ν and the ratio of G/E. For most materials, their Poisson's ratios are more likely to be constants rather than can be designed. The more applicable design parameter is the ratio of G/E. Therefore in following analyses, the ratio of H^2 to $D_x D_y$ is adjusted by varying the value of G/E in terms of varying shear modulus.

Results of three analyses with different ratios of H^2 to $D_x D_y$ are listed in Table 4.6. In the case of $H^2 = D_x D_y$, the results are identical to the one of isotropic material. In the case of $H^2 > D_x D_y$, the total strain energy as well as the ratio of plate energy are increased due to stiffness increasing. But the major increased term is twist energy, which is mainly caused by the increment of shear modulus. The influence of increasing shear modulus is likely leading to a not desired direction of increasing total strain energy and twist energy. In the case of $H^2 < D_x D_y$, positive effects such as reducing total strain energy and increasing the ratio of bending energy are observed. Although the ratio of membrane energy is increased, in its components only the shearing energy is increased while the principle axial energy is actually reduced. The increased shearing energy is the product of large shear deformation and reduced shear stiffness, and it shall tend to be smaller when shear modulus is further reduced. The effect of reducing shear modulus on redistributing energy components is quite interesting and promising. If the tendency of increasing the ratio of bending energy and

meanwhile reducing the ratios of other energy components can be continued by reducing shear modulus, the expected close to pure bending behavior on thin plates with large deflection can be realized.

Table 4.6.: Strain energy in plates with large deflection for different material properties

$H^2 = D_x D_y$				
Type		Energy [J]	Ratio [%]	Ratio [%]
Membrane energy	Principle axial	6.13	30.6	44.5
	Shearing	2.78	13.9	
Plate energy	Bending	4.1	20.5	55.5
	Twist	7.03	35	
	Total	20.4	100	100
$H^2 = 4 \times D_x D_y$				
Type		Energy [J]	Ratio [%]	Ratio [%]
Membrane energy	Principle axial	12.41	32.40	36.89
	Shearing	1.72	4.49	
Plate energy	Bending	3.46	9.04	63.11
	Twist	20.7	54.07	
	Total	38.28	100	100
$H^2 = 1/4 \times D_x D_y$				
Type		Energy [J]	Ratio [%]	Ratio [%]
Membrane energy	Principle axial	2.45	24.02	54.9
	Shearing	3.15	30.88	
Plate energy	Bending	3.17	31.08	45.1
	Twist	1.43	14.02	
	Total	10.2	100	100

Based on the conclusions of above analyses, orthotropic materials with low shear modulus seem to be a promising solution for the desired morphing skin. In following analyses, shear modulus of plates are set to be sufficient small than the reference value, which is the shear modulus of isotropic materials. Observing the deflection plots in Figure 4.14, pillowing is hardly to be found as plate energy become to be the major term (more than 50%), in which the shear modulus is smaller than 1/100 of the reference value. In the analysis of models with quite low shear modulus, e.g. shear modulus is 1/1000 of the reference value, it presents smooth curves and gradients in most areas but also local singularity at the loading region. The local singularity is probably caused by lack of stiffness and it is believed that the problem of singularity can be solved by introducing a local reinforcement at the loading region.

It is shown in the cutting lines of the shaped unit cells as in Figure 4.15, when the shear modulus is 1/100 of the reference value, the local waviness of the cutting line in the reference model is turned to a complete convex curve, which is similar to the curve in the pure bending case. When the shear modulus is 1/1000 of the reference value, loading on a single node introduces a local sharp gradient change, which explains its significant difference to the curvature in the pure bending case.

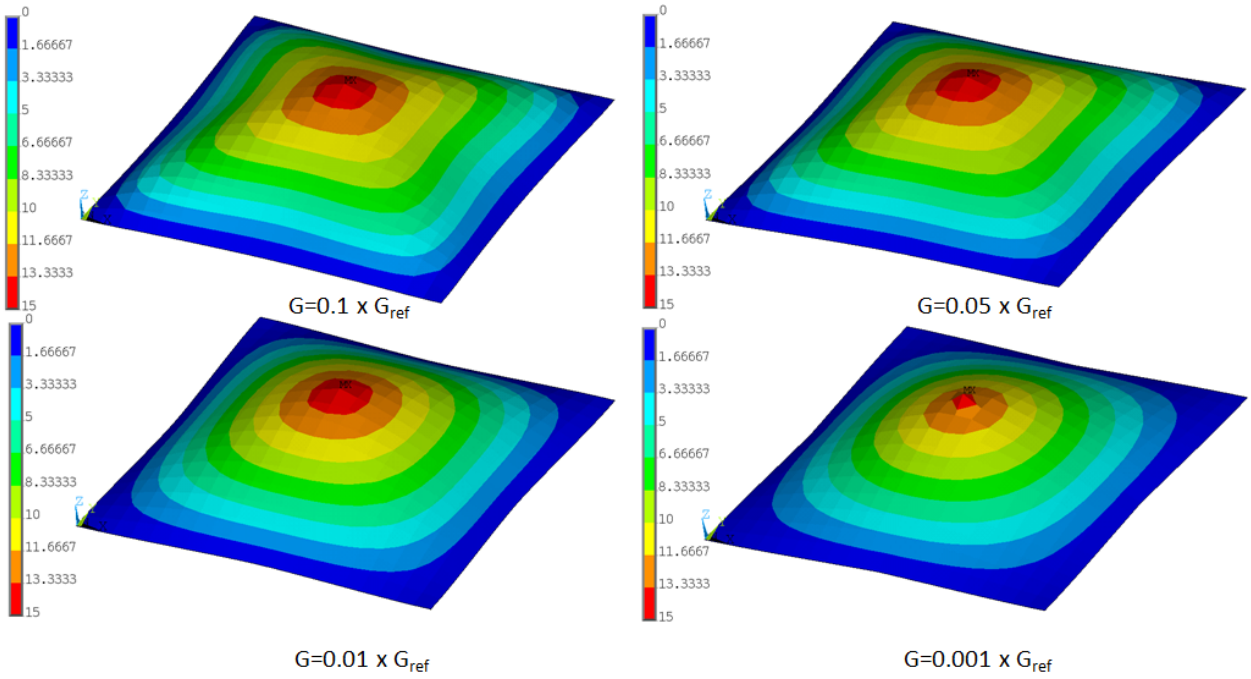

Figure 4.14.: Deflection plots of unit cells with different shear modulus

Referring to the table of strain energy (Table 4.7), as the shear modulus reducing to 0.1 and 0.05 of the reference value, the ratios of energy components like shearing and bending are keeping increasing. The major energy component is still the membrane energy and pillowing can be observed in reshaping plots. The major term of energy is transformed from membrane energy to plate energy when the shear modulus is around 0.01 of the reference value. As a result of that, pillowing in the reshaping plot is hardly observed. In this case, the shearing and bending energy are already dominative with summation of 96%. The amplitude of shearing energy shows a decrease tendency due to ignorable shear stiffness. When the shear modulus is further reduced, e.g. to 1/1000 of the reference value, the amplitude and the ratio of shearing energy are considerably reduced. The ratio of bending energy is close to be the dominative term, which is the goal of material design. Besides the improvements in reshaping, another benefit of low shear stiffness is reducing reshaping strain energy. For example, the strain energy in the analysis with the shear modulus 0.01 of the reference value is less than 1/10 of it as in the reference model.

It can be concluded from above studies, reducing shear modulus of plates has positive influence on reshaping behavior in terms of reducing reshaping energy and increasing bending features in large deflection. The orthotropic materials with sufficient low shear modulus are the feasible and advanced solution for the defined material design task. But this is just a qualitative solution, the further question is: what are the desired specific values of bending and shear stiffness? And what are the preferable relations between them? In following sections, the relations among different material parameters are investigated and several examples of material concepts are presented.

Table 4.7.: Strain energy in plates with large deflection for low shear modulus

$G = 0.1 \times G_{ref}$				
Type		Energy [J]	Ratio [%]	Ratio [%]
Membrane energy	Principle axial	1.02	15.84	57.61
	Shearing	2.69	41.77	
Plate energy	Bending	2.3	35.71	42.39
	Twist	0.43	6.68	
	Total	6.44	100	100
$G = 0.05 \times G_{ref}$				
Type		Energy [J]	Ratio [%]	Ratio [%]
Membrane energy	Principle axial	0.44	9.89	57.98
	Shearing	2.14	48.09	
Plate energy	Bending	1.7	38.20	42.02
	Twist	0.17	3.82	
	Total	4.45	100	100
$G = 0.01 \times G_{ref}$				
Type		Energy [J]	Ratio [%]	Ratio [%]
Membrane energy	Principle axial	0.04	2.16	44.87
	Shearing	0.79	42.71	
Plate energy	Bending	1.0	54.05	55.13
	Twist	0.02	1.08	
	Total	1.85	100	100
$G = 0.001 \times G_{ref}$				
Type		Energy [J]	Ratio [%]	Ratio [%]
Membrane energy	Principle axial	0.0022	0.31	13.22
	Shearing	0.091	12.91	
Plate energy	Bending	0.61	86.55	86.78
	Twist	0.0016	0.23	
	Total	0.7048	100	100

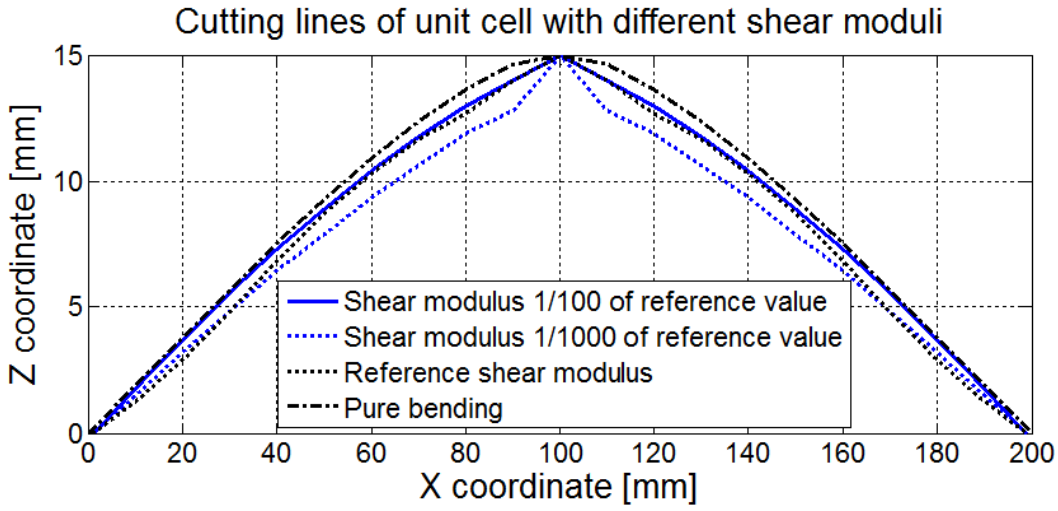

Figure 4.15.: Cutting lines of unit cells with different shear modulus

4.3. Material Properties of Reflector Morphing Skins

4.3.1. Range of Material Properties

To derive the desired material properties in a more detailed manner, a study of the essential design parameters is performed in this section. Inspired by Datashvili et al. (2010), the ratio of bending to shear stiffness is taken as a reference parameter to access the features of material properties. The expression of bending to shear stiffness for orthotropic materials is represented in Eq. 4.20.

$$\frac{D_x}{D_{xy}} = \frac{Eh^3}{12(1-\nu^2)Gh} \tag{4.20}$$

The ratio is determined by four terms, tensile modulus, shear modulus, Poisson's ratio, and thickness. Compare with isotropic materials, anisotropic materials have the additional design parameters of material properties to influence the reshaping behavior, although their influence on the ratio is only on the first order.

To better identify influence of each term, they are investigated on the same unit cell model as in the last section. The material design parameters can be further classified into three terms, the ratio of tensile modulus to shear modulus (E/G), Poisson's ratio, and thickness. As a simplification, in each set of study the Poisson's ratio is a constant and the design parameters are then reduced to E/G and thickness. As a further simplification, thickness is considered as a unit (1 mm) at first, so the ratio of E/G can be represented to the ratio of bending to shear stiffness. With these assumptions, the relation of the reshaping behavior in terms of energy ratios and reshaping contours to ratios of E/G and Poisson's ratios can be well observed.

A overview of results of the parameter study is shown in Figure 4.16. It can be found, the Poisson's ratio can significantly change the requirements of the stiffness ratio. For instance, a material with a large Poisson's ratio, typically larger than 0.5, can easily achieve a high ratio of plate energy in the large amplitude reshaping with a relative low ratio of E/G. But for a material with a small Poisson's ratio, to achieve the same amount of plate energy ratio in reshaping, it requires a considerable larger E/G ratio. Depends on the value of Poisson's ratio, the strategy in material design shall be different.

Observing the curves of plate energy ratios relating to E/G ratios, pillowing is observed when the E/G ratio is relative small. As the E/G ratio grows, the plate energy ratio is increased correspondingly and the pillowing is hardly to be found when the plate energy ratio is more than 50%. Keeping further growing of the E/G ratio, the plate energy ratio can be even larger than 80%. But afterwards local singularity is presented, which blocks the further growing of the plate energy.

As indicated from the previous studies, the most important parameter to determine reshaping behavior is the ratio of plate energy. A lower limit of 50% plate energy is recommended to avoid pillowing effects. And more than 80% plate energy is also difficult to be achieved for conventional shell structures due to local singularity, which is taken as a upper boundary. A large Poisson's ratio is recommended for requiring a smaller E/G ratio, which offers large design space for materials. A preliminary goal of material design is finding certain combinations of material parameters to maintain more than 70% plate energy in large reshaping. If aiming to a dominative ratio of plate energy (more than 90%) in reshaping, the

recommended solution is using materials with close to zero Poisson's ratio and a quite large E/G ratio, which leads to the solution of grid shell structures.

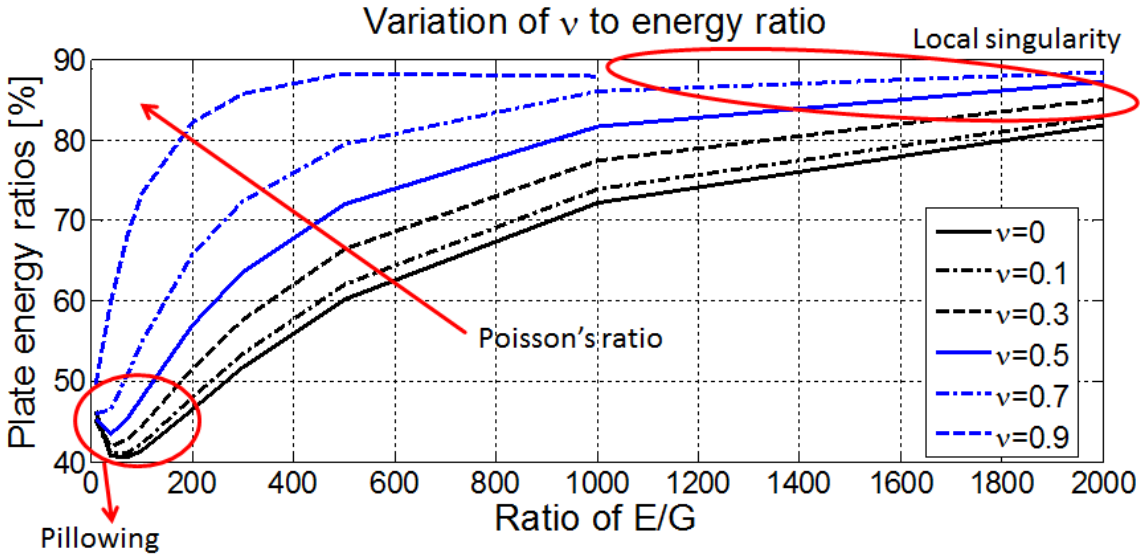

Figure 4.16.: Ratios of plate energy relating to material parameters

In the further analyses, the lower limit of 50% plate energy can be estimated by combining various thicknesses, E/G ratios, and Poisson's ratios. A overview of the design parameter combinations to achieve 50% plate energy is presented in Figure 4.17.

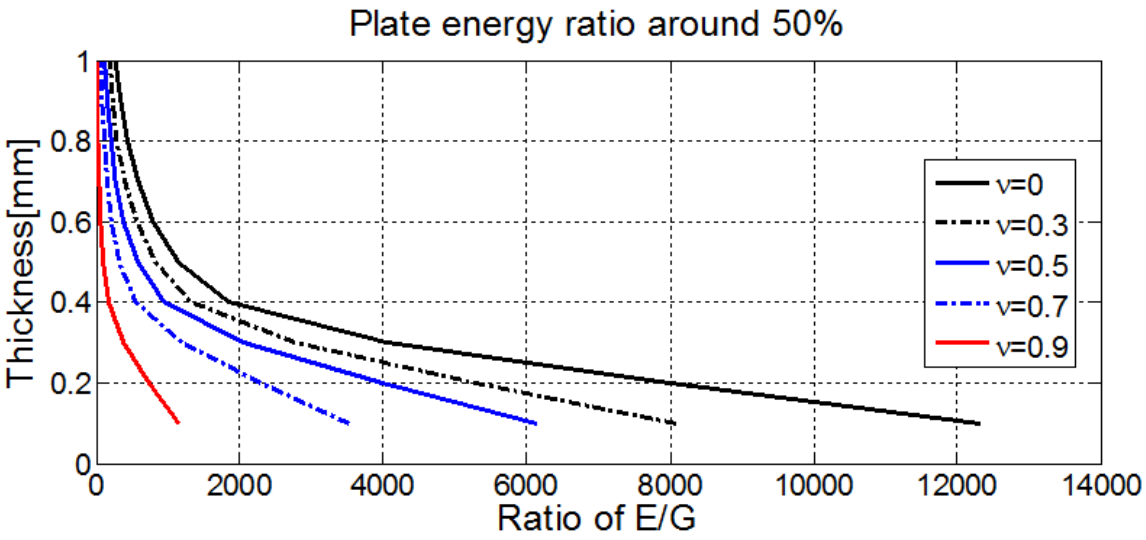

Figure 4.17.: 50% Plate energy achieved by material parameter combinations

It can be concluded, the lower limit of plate energy ratio can be readily achieved by combing relative high thickness of around 1 mm and a E/G ratio around 300. But if applying a relative small thickness of around 0.5 mm, the required E/G ratio should be considerably

enlarged due to the cubic power of thickness in bending stiffness.

Benefit from the results of this material properties' combination, the design space of materials can be reasonably reduced by limiting the material parameters in smaller ranges, e.g. large Poisson's ratios, small to medium thicknesses (0.5 to 1 mm), and medium to large E/G ratios. Then the task of reflector morphing design is reduced to find out materials or material combinations with the defined features.

4.3.2. Feasible Material Properties in Design Examples

It is shown in above analyses, the material parameters can be well correlated with each other and have different influence on reshaping behavior. From these investigations, feasible ranges of material design are basically defined but no exact solutions are indicated. To obtain a certain level concrete understanding of material parameters, four examples with predefined parameters such as thickness and Poisson's ratio are taken. The parameters in the four examples are defined as following:

Example 1: $\nu = 0.3$, thickness = 1 mm
Example 2: $\nu = 0.3$, thickness = 0.5 mm
Example 3: $\nu = 0.8$, thickness = 1 mm
Example 4: $\nu = 0.8$, thickness = 0.5 mm

The results of these examples are presented based on the work of Weidmann (2014), which is a student project guided by author. The values' range of tensile and shear modulus for these four examples can be defined through limits of E/G ratios and constraints of reshaping energy. As mentioned before, a lower limit of E/G ratio is estimated at 50% plate energy and a upper limit is estimated at 80% plate energy. The reshaping energy is estimated through computing the work of an actuation force driving 15 mm deflection. For a maximal actuation force 30 N, the work for reshaping 15 mm is 0.225 J. A smaller actuation force, like 15 N, with the resulting reshaping energy of 0.1125 J is preferred.

The feasible material properties of tensile and shear modulus for the four examples are shown in Figures from 4.18 to 4.21.

In the example 1, a E/G ratio is recommended in the range of 190 to 2000 with the defined Poisson's ratio and thickness. The available material properties for this example are shear modulus below 40 MPa and tensile modulus below 20000 MPa. In the example 2, the defined thickness is half reduced, which leads to require a higher E/G ratio with the value range from 850 to 6000. It requires a considerable higher material properties of tensile modulus up to 130000 MPa. In the example 3 and 4, requirements to E/G ratios are significantly reduced benefited by the larger Poisson's ratio. Consequently it allows larger shear modulus and lower tensile modulus.

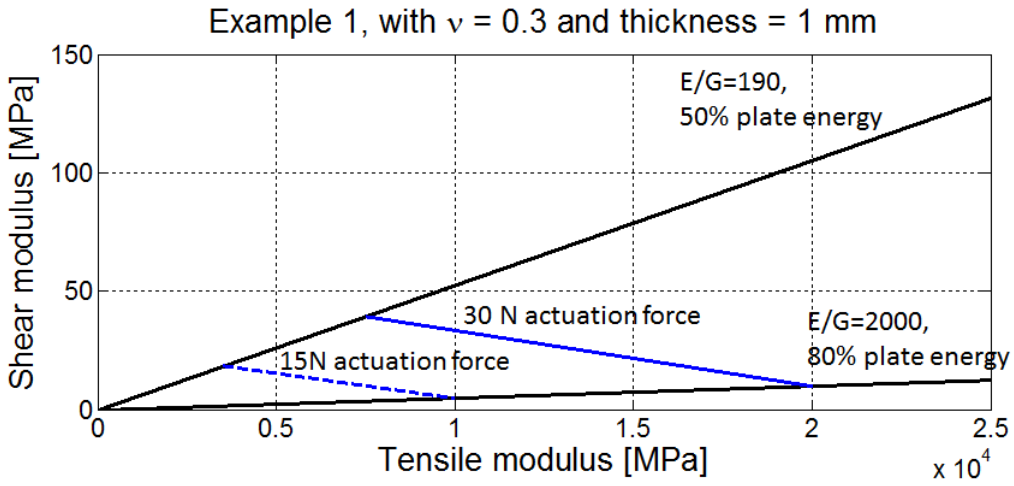

Figure 4.18.: Feasible material properties in the design example 1

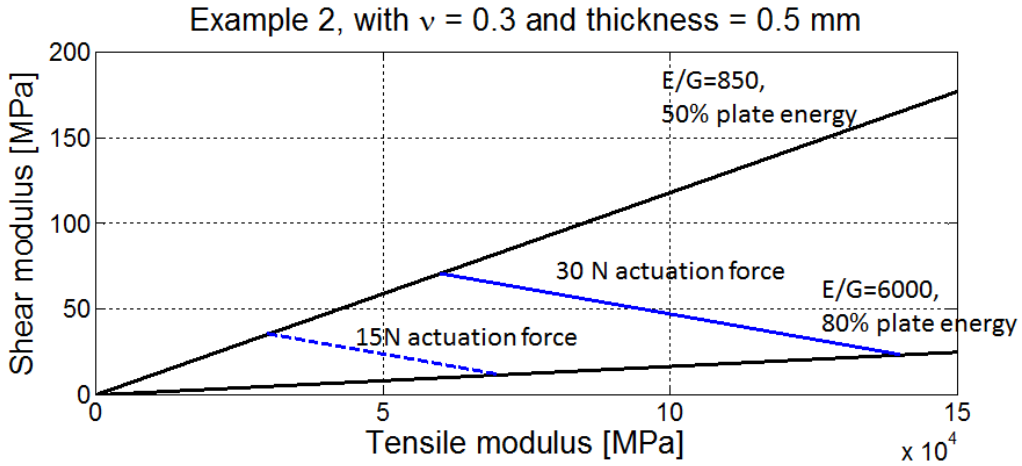

Figure 4.19.: Feasible material properties in the design example 2

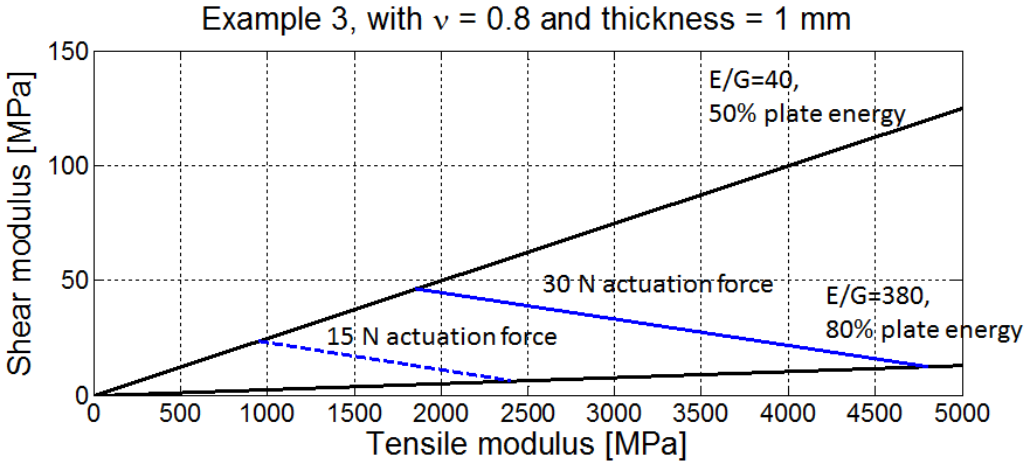

Figure 4.20.: Feasible material properties in the design example 3

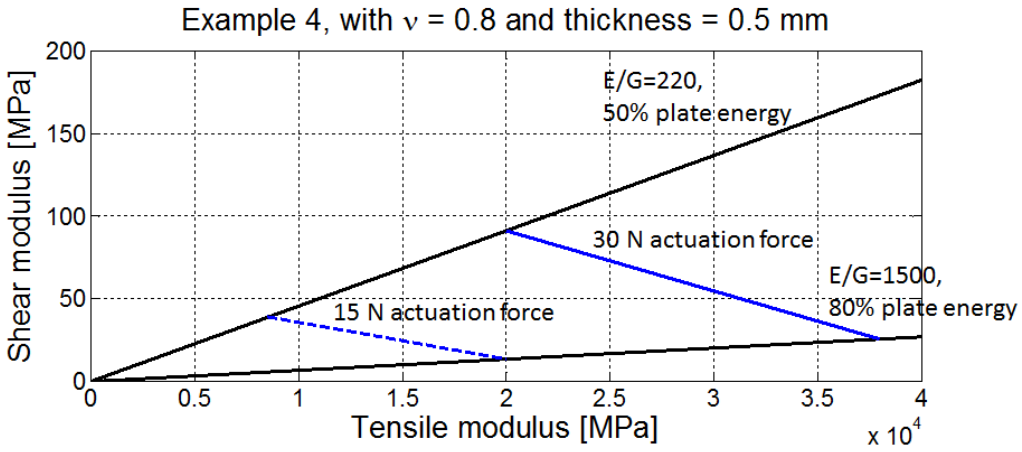

Figure 4.21.: Feasible material properties in the design example 4

Inspired by these examples, material selection shall be locked into materials with shear modulus below 100 MPa and a high ratio of E/G in the order of several hundred. Based on these results, detailed material concepts will be discussed in the following section.

4.4. Material Concepts of Reflector Morphing Skins

The design space of the specific material properties through the material design have been defined on certain level. In further steps, specific concepts will be derived based on existed technologies. One of the most promising concepts is the flexible composite, which is firstly introduced by Datashivili et al. (2006) as a deployable shell-membrane reflector. The flexible composite, namely carbon fibre reinforced silicone (CFRS), consists of two components with significant difference in mechanical and thermal-mechanical properties. The addressed concept in Datashivili et al. (2008) used triaxially woven carbon fiber fabric (TWF) impregnated with a space qualified silicone elastomer (S690 from Wacker Chemie [Chemie]).

The porous composite fabric has features of low area density (below $500\ g/m^2$), high flexibility for large scale folding, sufficient stiffness for sustaining its configuration without pretension (see Figure 4.22). In a series tests of this material [Datashvili et al. (2007)], it demonstrated quite promising mechanical and thermal-mechanical behavior. It is a quasi isotropic material with tensile modulus of around 700 MPa and shear modulus of around 200 MPa. The Mullins effect (stress and strain softening), viscoelasticity, and hyperelasticity behavior of this elastomer matrix composite were investigated by Hoffmann (2012). Its CTE can be considered as quasi isotropic and its value is close to zero when above glass transition temperature ($T_g \sim -105°C$) and $3.86 \times 10^{-6}/°C$ when below T_g. Through the RF performance tests, it is proved that it can fulfill nearly all requirements for frequencies up to 8 GHz and with some additional margins are capable for frequencies up to 10-12 GHz.

These investigations indicated the flexible composite is a feasible material candidate with great mechanical and thermal-mechanical behavior for space reflector applications. But the triax-CFRS laminate is not an appropriate one for the reconfigurable reflector morphing skins due to its low ratio of tensile to shear stiffness. The investigations of LLB [Datashvili

et al. (2009)] have shown the concept using triax-CFRS laminate ended with a flexible sandwich and has many limitations for practice applications. A high ratio of tensile to shear stiffness can be achieved through replacing the triax-CFRS by the biax-CFRS. The biaxially woven carbon fiber fabric has othotropic material properties and low shear modulus. It can be taken as the primary material candidate for reflector morphing skins. To further improve the ratio of bending to shear stiffness, laminate layout design in terms of determining ply number and configuration shall be performed.

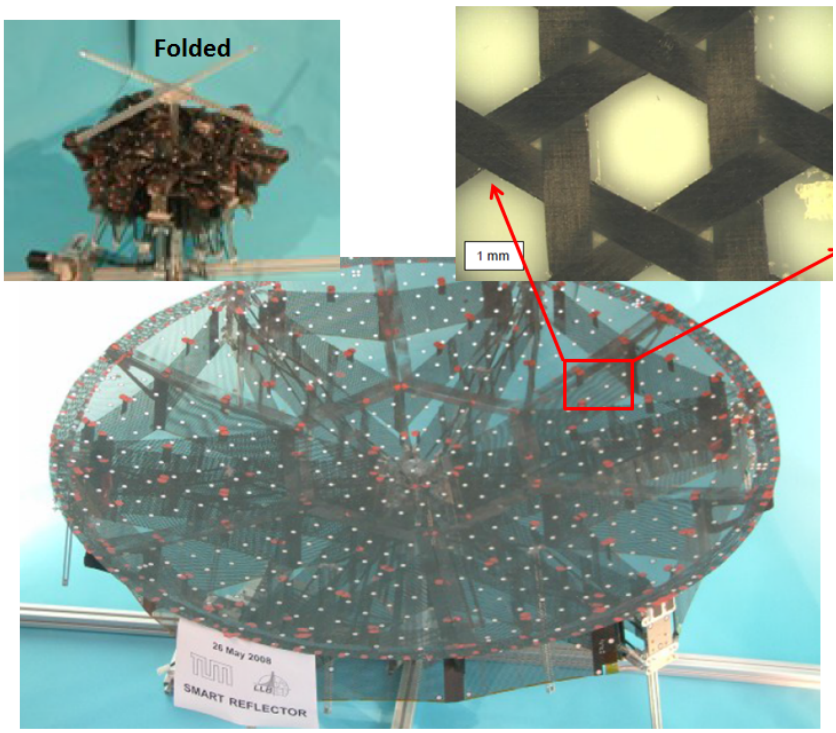

Figure 4.22.: The shell-membrane reflector made of triax-CFRS laminate [Datashvili (2009)]

As an alternative material concept, a grid shell made of CFRP tapes can be taken as a frame structure to improve reshaping behavior for achieving a higher plate energy ratio. Grid shell consists of two sets of orthogonal beams spaced equal distances in x and y directions (see Figure 4.23). The joints of their intersections can be either rigidly connected or hinged connected. The grid shell structures are widely used in the civil engineering field as double curved roofs. Actually, the concept of orthogonal interwoven wires from Pontoppidan et al. (1991) is a typical grid shell structure.

The bending stiffness of a grid shell is determined by the bending stiffness of beams and their spacing. In the case of rigid connection, the in-plane shear stiffness is determined by the torsion stiffness of beams and their spacing, and in the case of hinged connection, it is ignorable. With proper tailoring the cross-sections of CFRP tapes, spacing as well as connections, a quite high ratio of bending to shear stiffness is achievable. The grid shell is served as a frame structure and it shall be covered by biax-CFRS layers or some functional layers as the reflecting surface.

Within the frame of this thesis, the investigations of the reconfigurable reflector surface are focusing on the concept of biax-CFRS composite. The grid shell concept is taken as an

alternative concept and it will not be further discussed in this work.

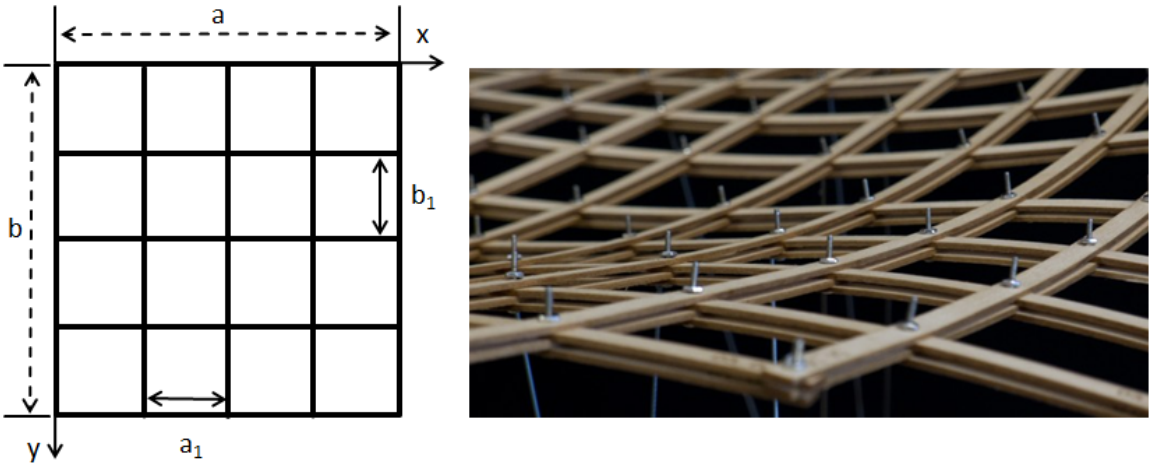

Figure 4.23.: Grid shell structures [Gridshell]

4.5. Extending Methods of Material Design to Morphing Wing Skins

The developed methods of compound material design is not limited on the application of mechanically reconfigurable reflector skins. The principles of the methods can be well extended to the application of morphing wing skins.

The required deformation of morphing wing skins can be mainly out-of-plane deformation like local reshaping, or in-plane deformation like area extending, or a mixing deformation of relative large in-plane and out-of-plane deformation like reshaping of leading and trailing edges. Although they have different design goals, their applicable design parameters are quite similar, which are geometry, boundary conditions and material properties. To correlate these design parameters with desired reshaping behavior, the developed method of energy expressions in reshaping can also be applied on the morphing wing skin design. Based on the corresponding representative models of morphing wings, feasible material combinations as well as geometry and boundary conditions can be derived to design the required morphing wing skins. With help of the predefined feasible range of material concepts, the specific morphing wing skin concepts could be determined within reasonable effort. The detailed application of the developed method on morphing wing skins will be presented in a later chapter.

5. Material Characterization of Flexible Composites

As concluded in the last chapter, the key material properties for a reflector morphing skin are flexural modulus and shear modulus. In this chapter, experimental investigations about flexural and shear properties of biax-CFRS composites are presented.

5.1. Materials and Test Set Up

Different to CFRP composites, there are rare neither experimental standards nor studies about flexible composites. To make the test set up easier, the existed testing standards of CFRP composites are taken as reference.

5.1.1. Materials

The fiber used in this study is T300 from Torayca with 1000 fiber filaments in each bundle [Torayca]. Among the available woven fabrics in market, the plain woven type is chosen for the feature of low in-plane shear modulus. The first candidate is the plain woven carbon fabric with area density of $65\ g/m^2$ [RG (c)]. A micrograph of this fabric is shown in Figure 5.1. Other candidates, which have similar or even larger spacing between fiber bundles but are different in fiber filaments number and ply thickness, are fabrics with area density of $160\ g/m^2$ and $400\ g/m^2$ [RG (a) and RG (b)].

The elastomer matrix is silicone RTV S690, which is developed for space missions as adhesive by Wacker Chemie. It is a transparent, low-modulus adhesive and has good resistance to radiation and temperature. It is suitable for hand lamination for its low viscosity and can be cured at room temperature with low shrinkage ($< 0.1\%$). The technical data of the qualified space material are listed in Table 5.1.

Although the CTE value of the silicone S690 is quite high ($\sim\ 300\,ppm.°C^{-1}$ [Sempri-moschnig et al.]), it turns to be ignorable when it is reinforced by carbon fibers. Fiber volume fraction of biax-CFRS can be between 25% to 55%. In this study, the fiber volume fraction of the manufactured specimens is around 40%.

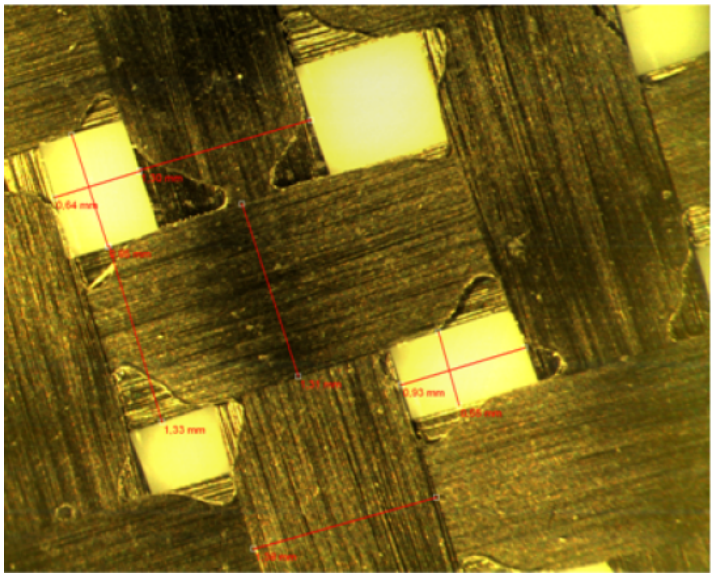

Figure 5.1.: A micrograph of plain woven CFRS [Hoffmann (2012)]

Table 5.1.: Material properties according to the suppliers

Fiber properties, T300		
Filament diameter	7	$[\mu m]$
Tensile modulus	230	[GPa]
Density	1.76	$[g/cm^3]$
Strain	1.5	[%]
Matrix properties, S690		
Viscosity (part A)	7500	[mPa S]
Viscosity (part B)	6000	[mPa S]
Density	1.06	$[g/cm^3]$
Tensile modulus	1	[MPa]
Elongation at break	150	[%]

5.1.2. Test Set Up for Flexural Stiffness

The testing standard DIN EN ISO 14125 is defined for determination of flexural stiffness for CFRP composites [DIN14125], which is taken as reference for the testing set up of bending tests (see Figure 5.2). In the three point bending tests, the dimension of specimens is 150 × 25 mm and the span of the supporting frame is 100 mm.

In oder to identify the influence of laminate thickness/layer number on flexural modulus, 7 sets of specimens with layer number 1, 2, 3, 4, 6, 8, and 12 are manufactured. Each set contains 3 specimens with the same layer number and fiber volume fraction of 40%. The measured laminate thickness shows a linear relation to its layer number. According to the measured results, the mean ply thickness is estimated as 0.107 mm, which is slightly lower than the thickness of the single layer laminate due to nesting effects.

Different to CFRP specimens, gravity influences testing results significantly, particularly for the thin specimens like 3 and 4 layers laminates. The lengths of specimens and the

supporting frame are properly selected to limit the gravity influence. For these flexible composites, a load cell with low measurement range of 500 N and high resolution of 0.2 N is selected. In tests, all specimens are deflected to 10 mm for observing their material behavior in a range which can be regarded as geometrically nonlinear.

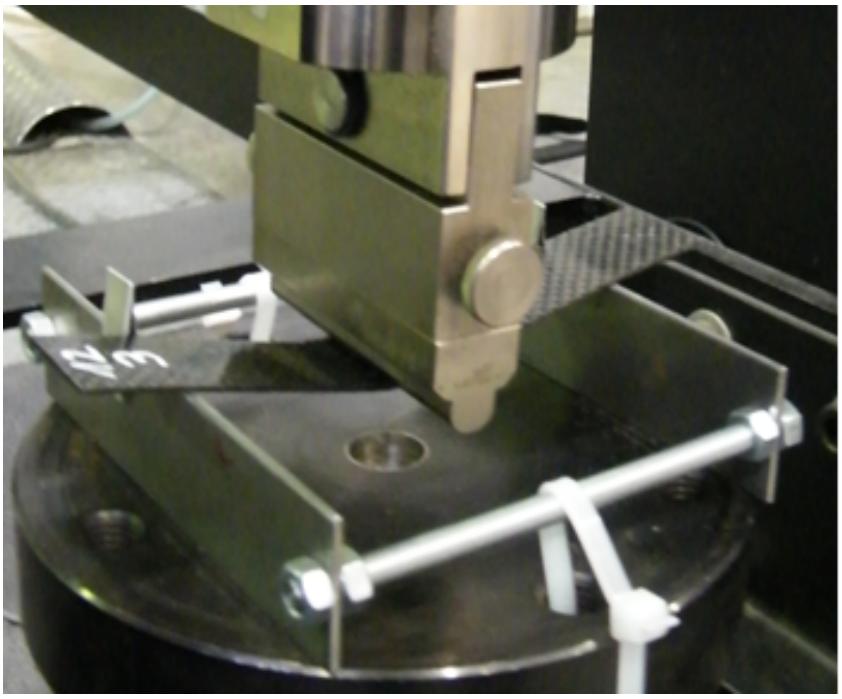

Figure 5.2.: Test set up of three point bending

The single and two layers specimens are tested by cantilever tests due to their over low bending stiffness. The test set up and descriptions can be referred to DIN53362. The rests are tested by three point bending tests.

5.1.3. Test Set Up for Shear Stiffness

Similar to the bending tests, there are 6 sets with each containing 3 specimens manufactured for shear tests. The number of layer in laminates is 1, 2, 3, 4, 8, and 12. The dimension of specimens is 250 x 25 mm as defined in DIN65466. The fiber orientation of the biax-fabric is $\pm 45^{\circ}$ to the longitude direction. Specimens are stretched in the longitude direction and the corresponding measured results such as forces and strains are recorded. For the shell-membrane type specimens, non-contact measurement techniques are preferred. In these tests, the applied system is a 3D strain measurement video system ARAMIS from GOM. The resolution of the used loading cell is 0.2 N as the same to which in the bending tests.

5.2. Testing Results

5.2.1. Results of Bending Tests

The equivalent flexural modulus of the biax-CFRS laminate can be derived from the obtained results of deflection and force according to the equations in the referred standard. It can be found, the equivalent flexural modulus of single layer laminate is significant lower than others. The value increases as laminate layer number increases and reaches a close to convergence value of 3200 MPa when laminate layer number more than 3 (see Figure 5.3). This phenomenon is also observed on CFRP composites as described by Zweben [Tsai (1979)]. The flexural modulus of thin laminate is usually smaller than its tensile modulus and it increases with layer number increasing. The difference of flexural moduli in laminates with different number of layers is explained as fabric laminate with few layers contains more undulation of yarns and inhomogeneous throughout materials. For CFRP composites, flexural modulus is converged to equal to tensile moduli as layer number increasing. This conclusion is also believed to be applicable for CFRS composites.

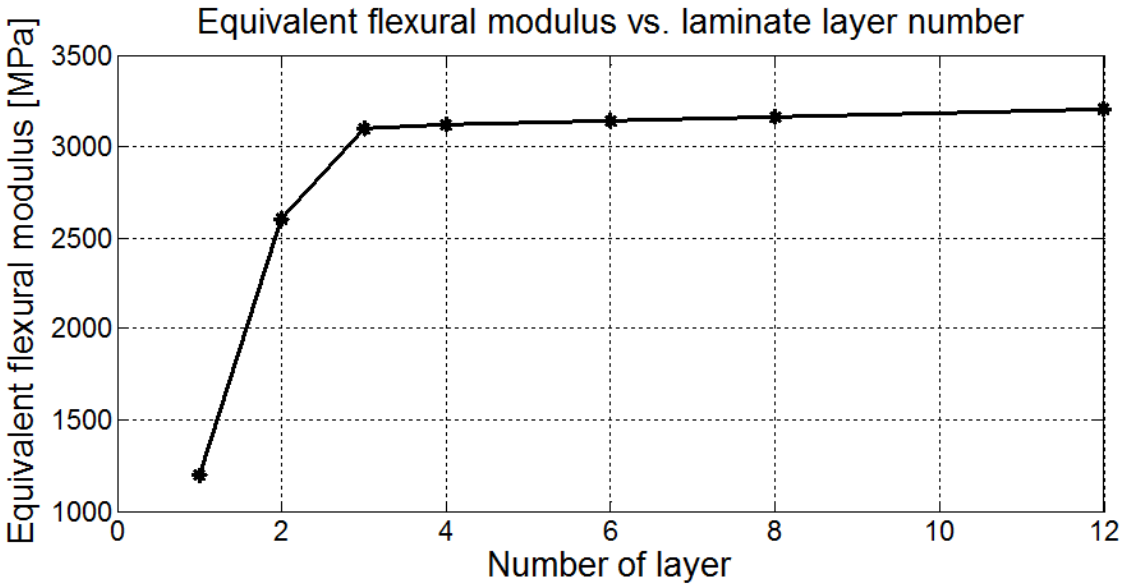

Figure 5.3.: Relation of equivalent flexural moduli to number of layers

It should be noticed, flexural modulus of CFRS composites can be considerably varied due to different manufacturing procedures and treatments after manufacturing. The difference in manufacturing can influence the nesting effects in multiple layers laminates, which causes thickness variations among specimens with the same layer number and eventually variations of flexural modulus. As concluded from the previous testing results of LLB, tempering CFRS composites in high temperature for several hours can stiffen material properties around 20% to 30%. About the applied specimens in tests, they are all manufactured at the same time with the same process but without tempering.

The obtained results of deflections and forces are converted into stresses and strains according to the equations defined in the DIN standard. The testing results are shown in Figure 5.4. They present a linear response at the low strains and their slops are rapidly reduced

when the strain beyond 0.15% (some are even beyond 0.2%). The spontaneous change of stiffness at high strains is caused by failures of fiber microbuckling. Up to 10 mm deflection, failures of fiber mircobuckling are observed on specimens of 6, 8 and 12 layers while not on 3 and 4 layers.

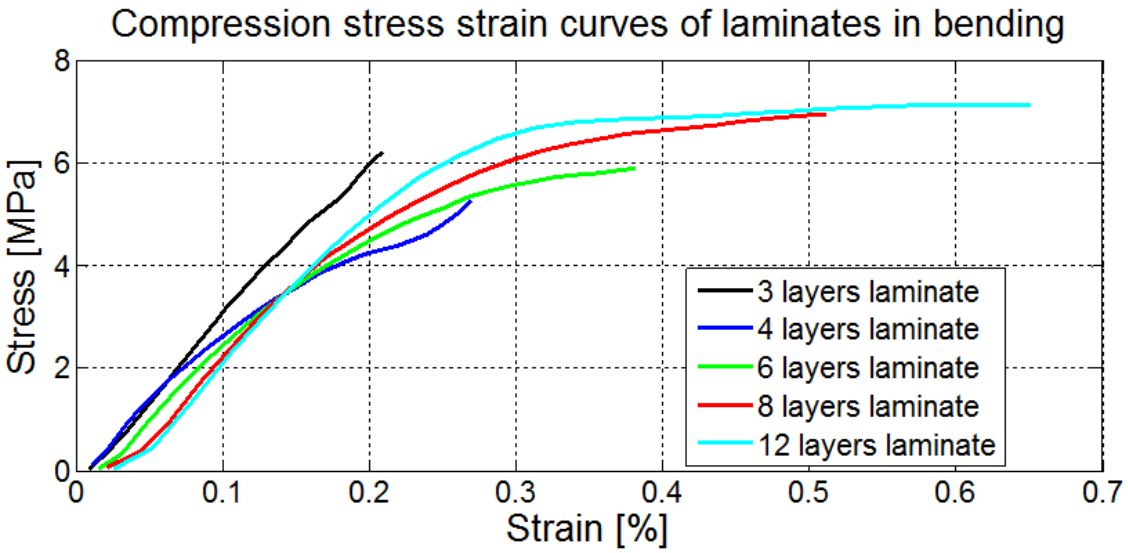

Figure 5.4.: Compression stress strain curves of laminates in three point bending tests

Fiber microbuckling is a typical failure mode of fiber composites especially with soft matrix, which was first analyzed by Rosen in early 1960s [Rosen (1965)]. Rosen concluded the critical stress for fiber composite under compression is mainly determined by shear modulus of matrix. Various works about CFRP composites were done on analytical, numerical, and experimental aspects for gaining insights of this failure. But there are rare works about CFRS composites can be found. The silicone matrix has significant difference to the conventional epoxy matrix such as quite low extensional modulus while quite large elastic strain range. It allows fiber composite bending in large amplitude without breaking while suffering fiber mircobuckling. Jimenez investigated the mechanical behavior of unidirectional CFRS composites and he concluded that the major failure of CFRS composites in large deflection is fiber microbuckling [Jimenez (2011)]. In his work, fiber microbuckling is described as a form of in-plane waviness at the compression side, which is different to the observed out-of-plane waviness on fabric CFRS composites by author (see Figure 5.5). The difference can be explained as the undulation of yarns in fabric can be taken as geometry imperfections, which initialize the out-of-plane fiber microbuckling of biaxial woven fabric composites. Some more facts of this failure is no debonding and microcracking are observed in the silicone matrix after fiber microbuckling. After releasing external loads, the materials can be recovered without noticeable failures.

Figure 5.5.: Microbuckling on a CFRS laminate

5.2.2. Results of Shear Tests

The specimens are driven three loading-unloading cycles up to 5% shear strain and then for rupture. Stress softening is observed between the first and the second cycle. According to this, the residual shear strain is estimated as 0.8%. After the first cycle, a good repeatability of stress-strain response can be observed (see Figure 5.6).

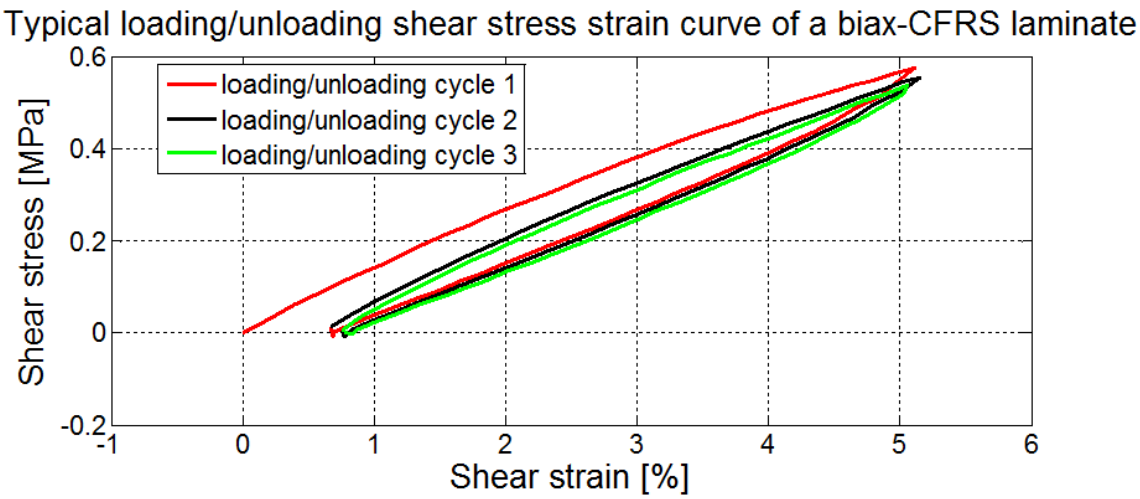

Figure 5.6.: Stress-strain response of a biax-CFRS laminate under cyclic tension

The phenomenon of stress softening is generally existed in all filled rubbers, which is called as Mullins effect. It was observed for the first time in tension tests of filled rubber by Mullins and his co-workers in 1960s [Mullins (1969)]. After fifty years of this finding, there is still no general agreement either on physical source or the mechanical modeling of this effect [Diani et al. (2009)]. As a conclusion found in many publications [Govindjee and Simo (1991)], the phenomena of stress softening and hysteresis increase with filler content increasing. Testing results of Mullins and Harwood [Mullins and Tobin (1957) and Harwood and

Payne (1966)] have shown the Mullins softening are reversible but requiring a high temperature or a solvent exposure to heal. Besides, the Mullins effect can be considerably reduced through treatments of tempering and/or placing in Ethylene atmosphere for several hours [Hoffmann (2012)].

Observing the stress-strain response in the rupture testing (Figure 5.7), it presents a linear response when shear strain below 7%. Moreover, no breaking of specimens are found even when shear strain is beyond 30%. In fact, the rupture strain of specimens are mostly found between 50% to 90%, which is a remarkable feature of CFRS laminates.

Shear moduli of laminates can be obtained by converting measured forces and strains. The values of shear modulus are quite small and they present a slight dependency on the number of layers in laminates due to nesting (see Table 5.2). The low value of shear modulus is a positive feature for the selected material, which is required in the material design.

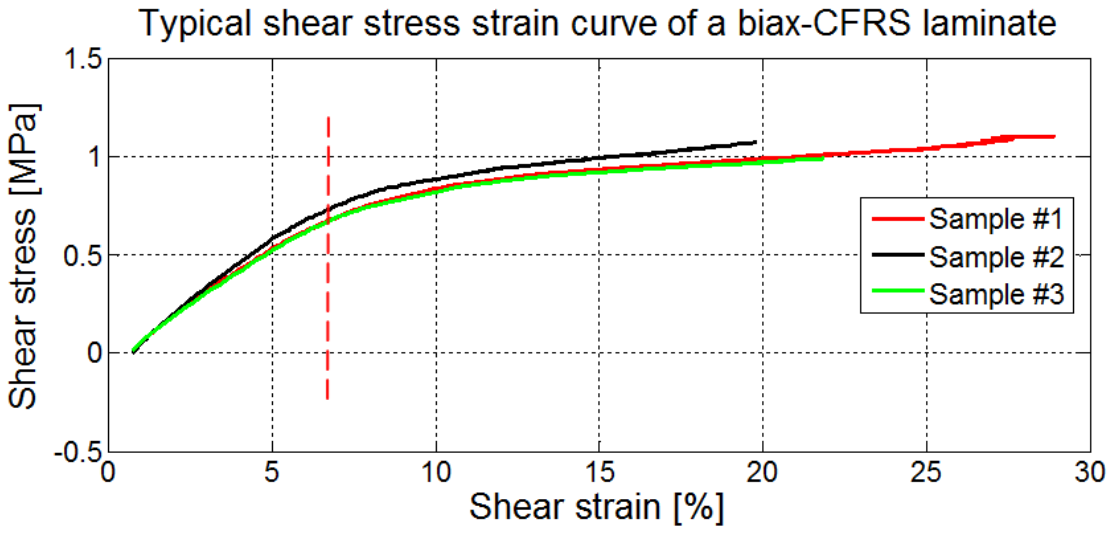

Figure 5.7.: Stress-strain response of a biax-CFRS laminate to rupture

Table 5.2.: Shear testing results

Number of layers	Shear modulus [MPa]
1	4.98
2	5.60
3	6.72
4	8.85
8	9.36
12	11.75

5.2.3. Fiber Microbuckling

The biax-CFRS laminates are quite sensitive to compression loads due to the failure of fiber microbuckling. The estimated critical strain is around 0.15% from the performed three point bending tests. Beyond this strain, a linear material model can not be further applied. In

practice, it is preferred to limit the maximal compressive strain lower than 0.15% for using a linear material model rather than a nonlinear material model. Especially the required nonlinear orthotropic material model with different properties in tensile and compression loads is quite complex and difficult to be implemented in FEM analyses.

Through repeating the tests on the tested specimens it is found the relation of force to deflection is the same to those in the previous tests. That means, the fiber microbuckling has no essential influence on the flexural modulus in the initial linear stage as well as the maximal compressive strain. This can at least partly prove the argument of no induced material failures through fiber microbuckling.

Considering the coincident positions of fiber microbuckling and loading head and their potential interference in the performed three point bending tests, the estimated value of critical strain is probably not accurate. For obtaining a more accurate value of critical strain, four point bending test is proposed for further investigations. Different to three point bending test, four point bending test contains a constant bending moment region between two loading heads, which can be quite helpful to observe the growing process of fiber microbuckling. Additionally, part of specimens can be tempered to observe its effects on flexural modulus and fiber microbuckling.

5.3. Summary of the Chapter

Bending and shear tests are performed on the biax-CFRS laminates with fabric area density of $65\ g/m^2$. The selected candidate material has low flexural modulus and extremely low shear modulus, which are the expected features as derived in material design. The used testing standards are served only as reference purpose. The testing results are all examined through analytical and numerical analyses additionally. Through these tests, the limit strains in bending and shear for linear material models are defined. They will be used as structural limitations in the morphing skin design using biax-CFRS laminates.

Fiber microbuckling is the major failure of biax-CFRS laminates. An accurate understanding of this phenomenon and deriving the accurate critical strain value are not reached in frame of this study. A micro and/or meso level numerical model shall be created to observe the phenomena of fiber microbuckling and gain more insights. It is very interesting to know the influence of parameters like woven type, number of filament in bundles, fiber volume fraction, and undulation of yarns (caused by handing and manufacturing) on fiber microbuckling. More related tests are foreseen to gain more accurate understanding of this phenomenon in further works.

Limited by the project schedule, the tests are only performed on one type of biax-CFRS composites. The obtained flexural and shear moduli of this candidate are quire promising and can be used in the following reflector morphing skin design. In the next chapter, the performance of the reconfigurable reflectors made from the tested biax-CFRS laminate is evaluated through numerical analyses and experimental validations.

6. Mechanically Reconfigurable Reflectors and Their Morphing Skins

In this chapter, the reflector morphing skin design is further explored through numerical and experimental investigations. The design of reflector morphing skin is starting from laminate layout design of the biax-CFRS composites. The derived morphing skin concepts are then evaluated on numerical models range from medium size to full size for different objectivities and with different reshaping requirements. The related tasks such as stroke length optimization, nonlinearity in reshaping, and approaches to reduce the computation cost of nonlinear analyses are discussed and their results are presented. In the end, the numerical results are correlated with the testing results of a build demonstrator. Based on lessens learned from these investigations, update concepts of reflector morphing skins are proposed. The flowchart of the reflector morphing skin design is presented in Figure 6.1.

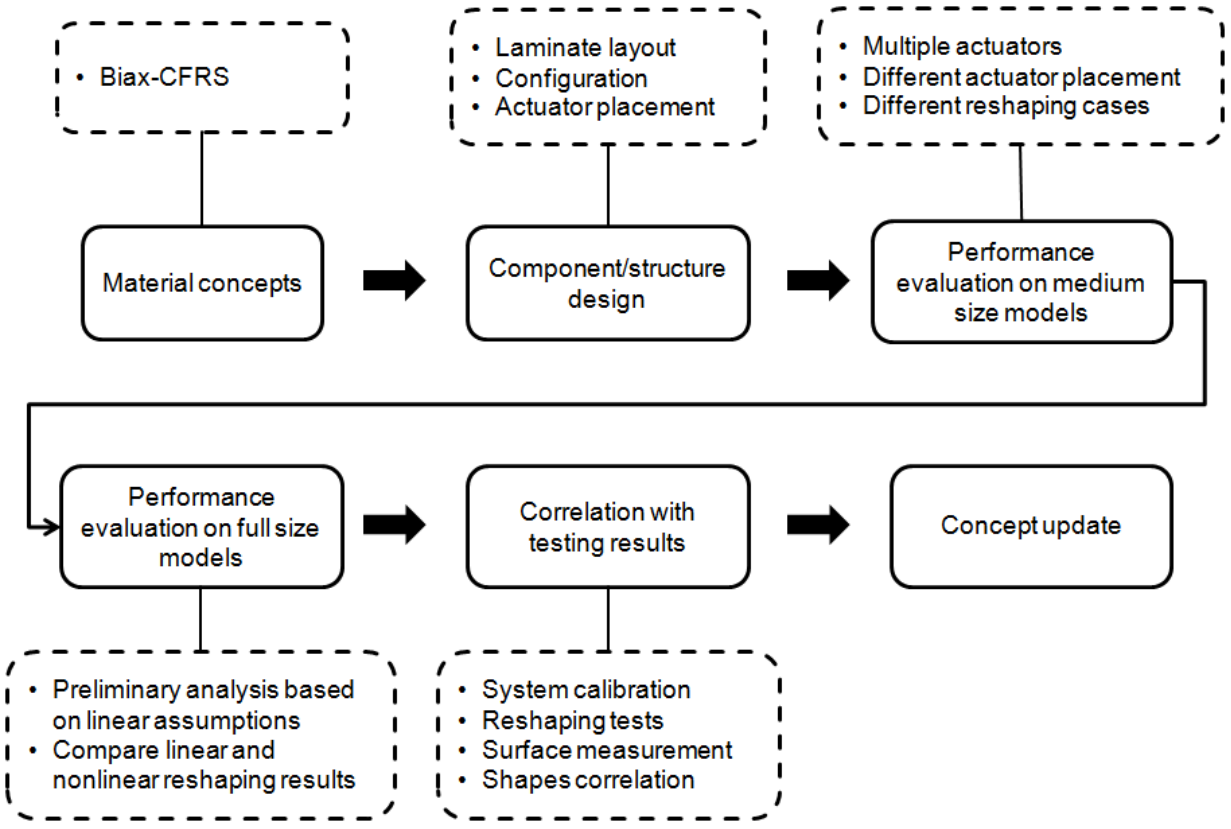

Figure 6.1.: Flowchart of reflector morphing skin design

6.1. Reflector Morphing Skin Design and Analysis

Start with the selected material for reflector morphing skins, further investigations are focusing on concept implementation and performance evaluation. Besides the unit cell models, the medium size representative models are also initialized to explore complexer reshaping behavior involving more actuators.

6.1.1. Laminate Layout of Reflector Morphing Skins

To determine the required laminate layer number, the unit cell model with square lattice and the free movable boundary conditions as in previous analyses is used. The comparison criteria for analysis results are energy ratios, energy amount, reshaping shapes, and total thickness.

The available layer number in this study is defined from 3 to 9. Single and double layers are not considered due to over low bending stiffness and more than 9 layers concept is not preferred due to a high risk of fiber microbuckling and high actuation force. The material properties of the biax-CFRS laminate with more than 3 layers are listed in Table 6.1.

Table 6.1.: Material properties of the biax-CFRS laminate (layer number more than 3)

$E_{11} = E_{22}$* [MPa]	ν_{12}	G_{12} [MPa]	$G_{13} = G_{23}$ [MPa]
3200	0.8	$4\,to\,13$**	10 ***
* flexural modulus			
** depends on the number of layers			
*** assumed value			

Observed in the data of material properties, the biax-CFRS laminate has a E/G ratio of around 300 and Poisson's ratio of 0.8. As indicated in Figure 4.17 about the relation of plate energy to material parameters, the minimum thickness for this material to achieve around 50% plate energy under 15 mm deflection is between 0.4 to 0.5 mm. Therefore the minimum number of full layers can be estimated to be 4 for its mean layer thickness of 0.107 mm. Observing the energy ratio of the unit cell model with 15 mm deflection in Figure 6.2, the crossover of membrane energy and plate energy is found at around 4 layers, which fits to the conclusion of material design.

The shape difference between linear and nonlinear reshaping analyses of the same concept is compared for reshaping performance evaluation. The shape comparison is performed by comparing the interpolated Z coordinates of achieved shapes on the equally spaced grid data in x and y directions. The RMS of shape difference between linear and nonlinear analyses is used as the comparison criterion.

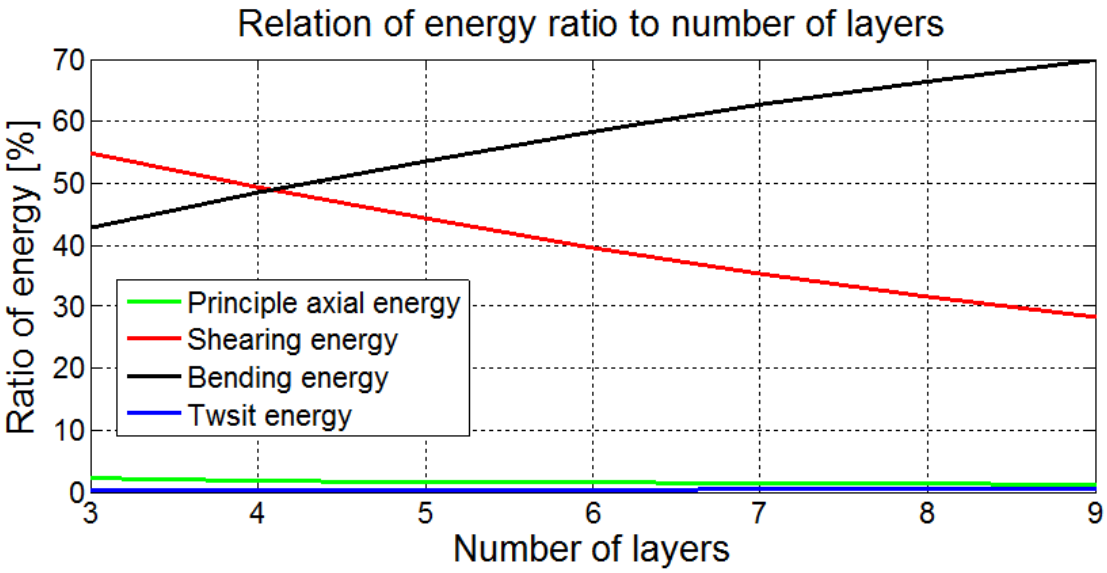

Figure 6.2.: Relation of energy ratio to number of layers

It can be observed from Table 6.2, the RMS values decrease as layer number increasing. The applied 15 mm deflection is the the maximal value in reshaping but in practice it present probably on several actuators only. In fact, the frequent used deflections for most actuators are below 10 mm. Therefore the shape comparison is also performed with applying 10 mm deflection, in which considerable reductions of RMS values are observed.

Table 6.2.: Shape difference between linear and nonlinear reshaping analyses of different deflections and layer number

15 mm deflection	Number of full layers			
Shape difference [mm]	3 layers	5 layers	7 layers	9 layers
Max.	0.9166	0.4591	0.2730	0.1875
Min.	-0.5800	-0.4543	-0.3481	-0.2480
RMS	0.4249	0.2391	0.1588	0.1093
10 mm deflection	Number of full layers			
Shape difference [mm]	3 layers	5 layers	7 layers	9 layers
Max.	0.3194	0.1468	0.0839	0.0569
Min.	-0.2487	-0.1771	-0.1290	-0.0885
RMS	0.1569	0.0839	0.0547	0.0363

As a compromise among reshaping behavior, actuation energy, risk of fiber microbuckling, and shape difference between linear and nonlinear reshaping analyses, the number of full layers is recommended as 7 and 8.

6.1.2. Layout Design with Patches

As a complement to increasing number of full layers, patches can be added locally to increase bending stiffness considerably while only marginally increasing in-plane stiffness [Datashvili and Baier (2009)]. To realize the mentioned features, patches shall be placed surrounding with actuators with proper tailored dimensions and configurations. The determination of patch size is depending on the number of patches and the distance between actuators. A sketch of a unit cell model with patches is shown in Figure 6.3.

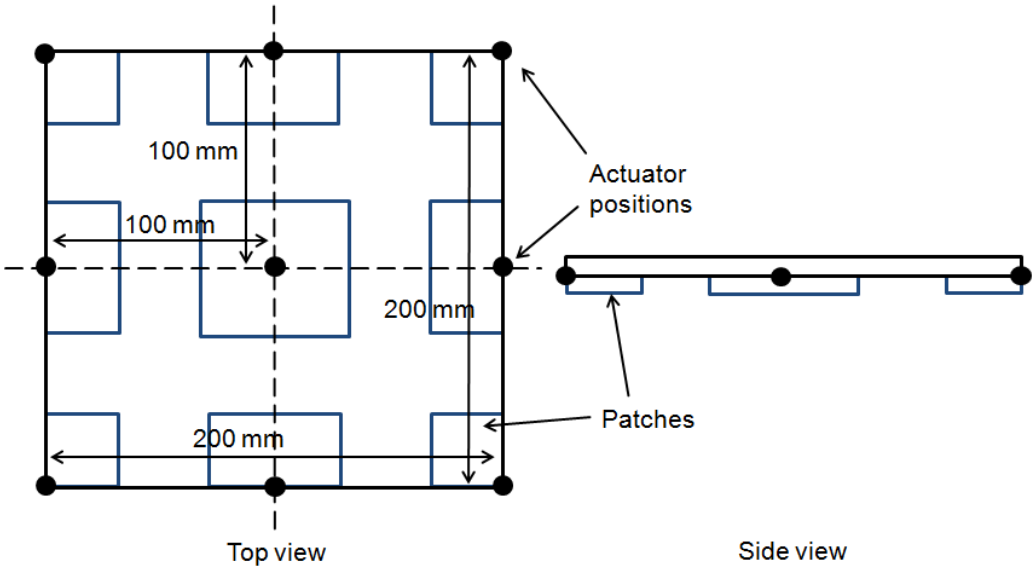

Figure 6.3.: A unit cell with patches

The 7 full layers concept is chosen as the baseline. Variations like adding 1, 2, and 3 patches are compared with the baseline in reshaping analyses. It can be observed, adding one patch on the full layer concept has an effect of translating certain membrane energy to plate energy. However in this case, the shape difference between linear and nonlinear reshaping analyses is not reduced as ratio of bending energy increasing as expected. Contrarily, it increases considerably (Table 6.3), which is mainly caused by the asymmetric layout due to adding patches.

Table 6.3.: Shape difference between linear and nonlinear reshaping analyses with varying number of patches

15 mm deflection	Number of patches			
Shape difference [mm]	7 full layers only	1 patch	2 patches	3 patches
Max.	0.2730	0.3162	0.2685	0.2257
Min.	-0.3481	-0.5614	-0.6287	-0.6872
RMS	0.1588	0.2693	0.3138	0.3507

In short, adding patches has a positive effect of increasing the ratio of plate energy but meanwhile reducing the reshaping similarity between linear and nonlinear analyses. As

goals of laminate layout design, the major one is a relative high ratio of bending response in large deflection, and the secondary one is high similarity between linear and nonlinear analyses for reducing computation complexity and cost. The number of patches shall be determined by a compromise between the above mentioned two goals.

As a variation of the full layer concept, the total layer number is maintained while some full layers are replaced by patches. Benefits of this change are maintaining the required ratio of plate energy and reducing the risk of fiber microbuckling for less number of full layers. In the following parameter study, 3 full layers concept is chosen as the baseline and three variations with different number of patches are compared. For simplification, in each variation two identical patches are added at the same time. The ratio of plate energy is increased from around 43% in the concept of 3 full layers to 70% in the concept with adding 6 patches. Meanwhile the shape difference between linear and nonlinear reshaping analyses is increased from 0.42 to 0.89 mm (Table 6.4).

The ratio of plate energy in the concept of 3 full layers plus 6 patches is quite the same to the concept of 9 full layers. The increasing difference between linear and nonlinear analyses indicates not ignorable nonlinear behavior in reshaping.

Table 6.4.: Ratio of bending energy and shape difference in concepts of 3 full layers with patches

15 mm deflection	Number of patches			
Energy ratio [%]	3 full layers only	2 patch	4 patches	6 patches
Membrane	56.94	40.40	33.29	29.72
Plate	43.06	59.60	66.71	70.28
Shape difference [mm]	3 full layers only	2 patch	4 patches	6 patches
Max.	0.9166	1.0015	0.7825	0.5874
Min.	-0.5800	-1.2601	-1.5986	-1.8235
RMS	0.4249	0.6509	0.7854	0.8896

As a short conclusion about the concepts derived through the laminate layout design, two concepts are chosen for further investigations. One is the concept of 7 full layers and the other is the concept of 3 full layers plus 6 patches. The concern of the first concept is the risk of fiber microbuckling and the second is relative strong geometrical nonlinearity in reshaping especially in the region containing only 3 full layers.

6.1.3. Layout Design Using Triangular Lattice

As mentioned previously, actuator placements like square or triangular lattice have similar effect on reshaping behavior. Analogical investigations about number of layers and patches are performed on the unit cell model with triangular lattice. Quite similar conclusions about the minimum number of full layers and effects of patches are obtained on this model.

6.1.4. Concept Evaluations on Medium Size Representative Models

The proposed biax-CFRS laminate concepts are further investigated on medium size representative models. The medium size model is a symmetric paraboloid with projected diameter 720 mm and focal length 850 mm. Three concepts of reflector skins with different laminate layouts and actuator placements are implemented on the medium size models (see Figure 6.4). The number of actuators are chosen as around 20 on the medium size models to observe complex reshaping behavior.

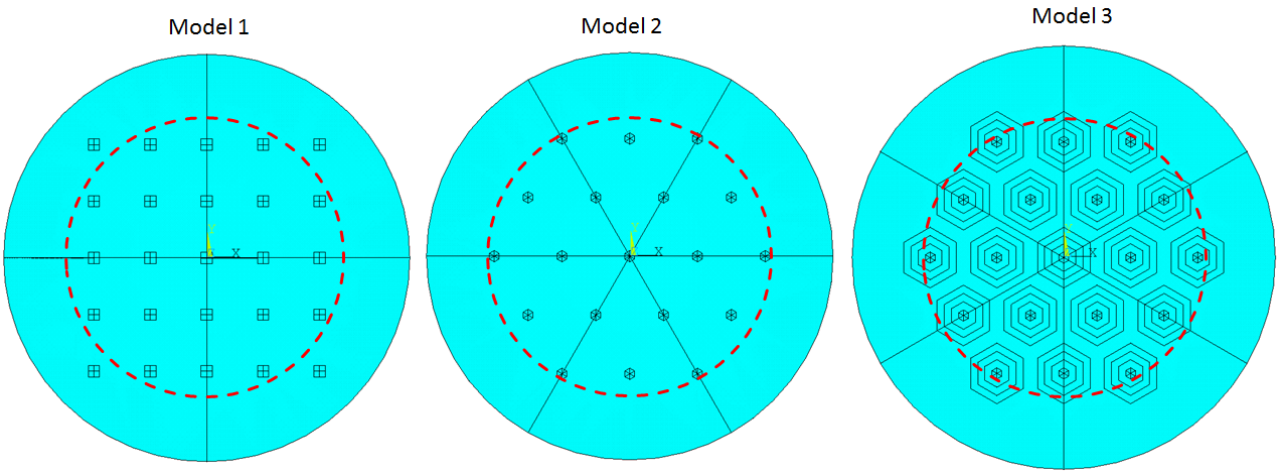

Figure 6.4.: Medium size models: model 1: 7 full layers with 25 actuators in square lattice (left), model 2: 7 full layers with 19 actuators in triangular lattice (middle), model 3: 3 full layers plus 6 patches with 19 actuators in triangular lattice (right)

The actuator distance in model 1 is set as 100 mm and in model 2 and 3 are 120 mm for the reason of the same control area. Pads, which are made of stiff CFRP with thickness of 0.6 mm, are added at the rear side of the third layer to reinforce the loading regions. Their diameters are taken as 20 mm and their shapes are adjusted to the applied actuator lattice correspondingly. A circular area with projected diameter 500 mm (red rim in the figure) is chosen as the comparison area in the three models. The outside of the rim, whose deformation is not fully controlled by actuators, is excluded in evaluations.

As boundary conditions in reshaping analyses, the center actuator is fully fixed except the translation in Z direction. Additionally the last actuator in the X axis is fixed on rotation around X axis to block rigid body movements. Stroke lengths are given to all actuators in the Z direction to realize surface reshaping. The reshaping results are evaluated by comparing the linear and nonlinear analyses results of the same model. Although the linear reshaping behavior is not the goal of material design, reshaping shapes in linear analyses are generally smooth in geometry and can be taken as reference in the preliminary phase.

The reshaping magnitude is set to be 10 mm, which is smaller than the value in the unit cell models but closer to the mostly required values on real applications. The stroke lengths for actuators are separately defined in a series of testing cases and in them the default value is zero. The testing reshaping cases are defined as follows:

- Case 1 and 2: the center actuator has a stroke length of +10 mm in the case 1 and -10 mm in the case 2. These analyses are mainly used to observe the reshaping behavior of local deformation and the impact of shell configuration.

- Case 3 and 4: the center and its adjacent actuator (in the X direction) both have the same stroke lengths of +10 mm in the case 3 and -10 mm in the case 4. The reshaping shapes actuated by two actuators and the impact of shell configuration are accessed.

- Case 5: the center and its adjacent actuator have opposite inputs of +10 and -10 mm. The difference of deflection is reached as 20 mm, which can be taken as a over large reshaping.

- Case 6: three sets of random stroke lengths with mean values of zero and standard deviation of 3 mm are applied in the reshaping analyses. These random shapes are not comparable to the typical required shapes in practice. But in the preliminary phase without knowing of target shapes, they can be taken as testing benchmarks.

- Case 7 and 8: testing cases are similar to the case 6 but with different mean values. The mean value is 5 mm in the case 7 and -5 mm in the case 8.

Totally there are 8 cases, 14 different shapes and 28 analyses (linear and nonlinear analyses for each shape) defined for each model. The reshaping quality is evaluated through comparing RMS values of shape difference between linear and nonlinear analyses. The detailed results are listed in the appendix (section B.1 in Appendix). Only some highlights of the results are presented in this section.

In the cases of two actuators deflecting in the same direction with the same magnitude (case 3 and 4), RMS results are generally worse than these in the case 1 and 2. It is interesting to observe that the model 2 (with triangular lattice) is less sensitive to the impact of shell configuration in terms of quite similar RMS results in the case 3 and 4. This effect is introduced by the triangular actuator placement, in which, the area between two adjacent actuators can be directly effected by actuators in the perpendicular direction. Therefore the surface reshaping can be better controlled by actuators.

It can be observed in Figure 6.5, the model 3 has a peak deflection between two adjacent actuators in the linear analysis while a smooth shape in the nonlinear analysis. In this 3 full layers plus 6 patches concept, the middle area between two adjacent actuators has the lowest bending stiffness. As a response to the bending moment from actuators in reshaping, its deflection is considerable higher than other regions. But in the nonlinear analysis, the bending stiffness is updated as deflection growing. Therefore no over large deflection appears. This is also the major reason of relative large reshaping difference between the linear and nonlinear analyses in this concept.

The worst RMS results are presented in the testing case 5, which are around 0.5 mm in the model 1 and 2 and around 1.6 mm in the model 3. As a conclusion obtained from this case, a relative large deflection difference between two adjacent actuators shall be possibly avoided.

In the random reshaping testing cases 6, 7 and 8, the RMS values are range from 0.1 to 0.6 mm in the model 1 and 2. The stroke lengths of the model 3 are identical to the model 2. Therefore it can be compared with the results of the model 2. Its results are generally 2 to 3 times worse than the results of the mode 2.

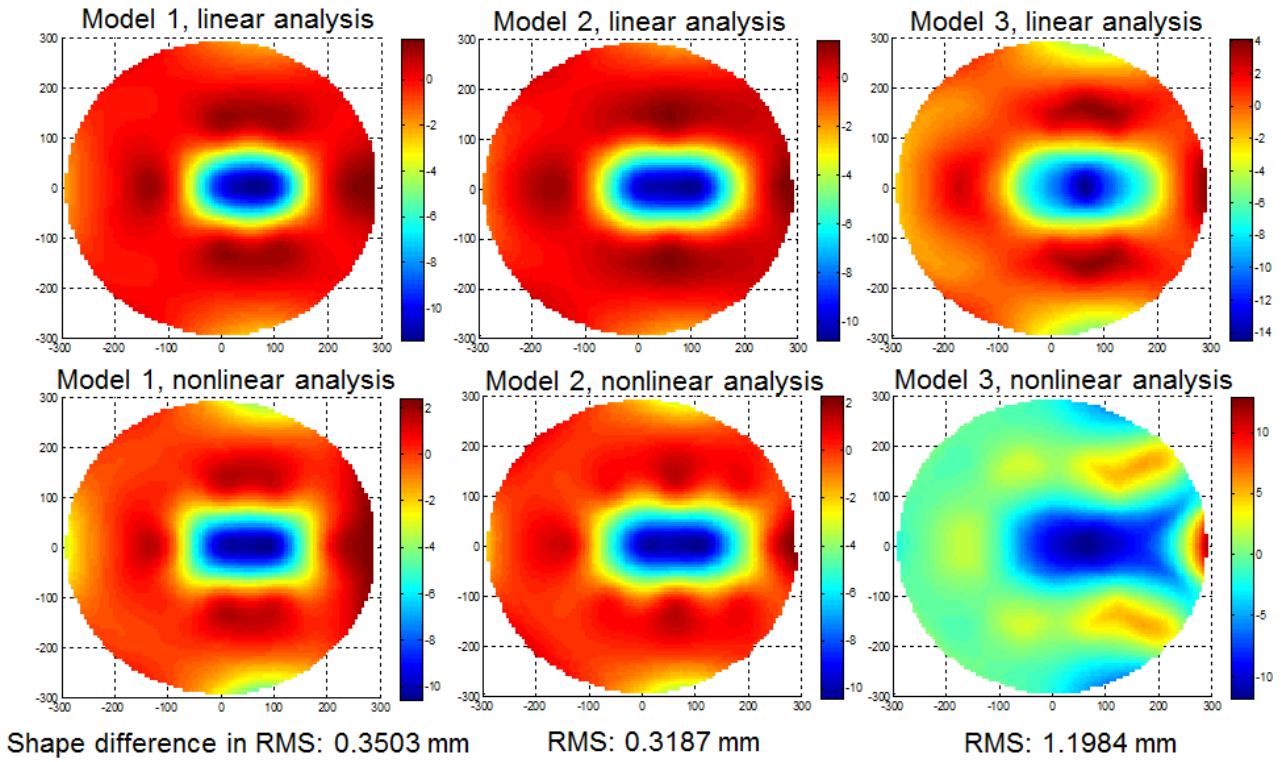

Figure 6.5.: Linear and nonlinear reshaping plots in the testing case 4

As a short summary of these investigations, concepts using the same full layers either in square lattice or triangular lattice have quite similar RMS results. The concept using square lattice is generally slightly better in RMS results but has larger difference between reshaping in opposite directions. For the same target control area, the concept using triangular lattice requires less actuators and has better adjustability about actuator positions to fit the circular target area.

Based on these understandings, triangular lattice is preferred to be the actuator placement concept. The concept with patches has strong geometry nonlinearity in reshaping due to stiffness variation in different regions and asymmetrical layout. It contains less full layers, therefore the risk of fiber microbuckling failures and reshaping energy demands are also less. With the reinforcement by patches, the energy ratio between shearing and bending energy is comparable to the full layers concepts containing the same total layer number.

Although full layers concepts have significant high similarity between linear and nonlinear analyses, geometry nonlinearity must be considered for the proposed concepts in further investigations. As a conservative consideration, the concept 3 full layers plus 6 patches is chosen as a baseline for the reflector morphing skin. Once the structure performance in terms of reshaping accuracy, strength, and actuation forces are more accurately understood through analyses on the full size engineering model, full layers concepts can be taken as improving concepts.

6.2. Reshaping Analyses of the Engineering Model

On the engineering model of the mechanically reconfigurable reflector, the performance of the designed morphing skin is studied through reshaping to the typical practical tasks.

6.2.1. Model Description

The engineering model is an offset main reflector, whose geometry definitions can be found in Chapter 3.3. The skin concept, 3 full layers plus 6 patches, and the triangular actuator placement are applied on this model. To enhance the reflectivity of radio frequency and the electrical conductivity of the composite reflector surface, a 0.3 mm carbon black filled silicone [Endler et al. (2012) and Datashvili et al. (2013)] is added as the front layer. An illustration of the model is presented in Figure 6.6.

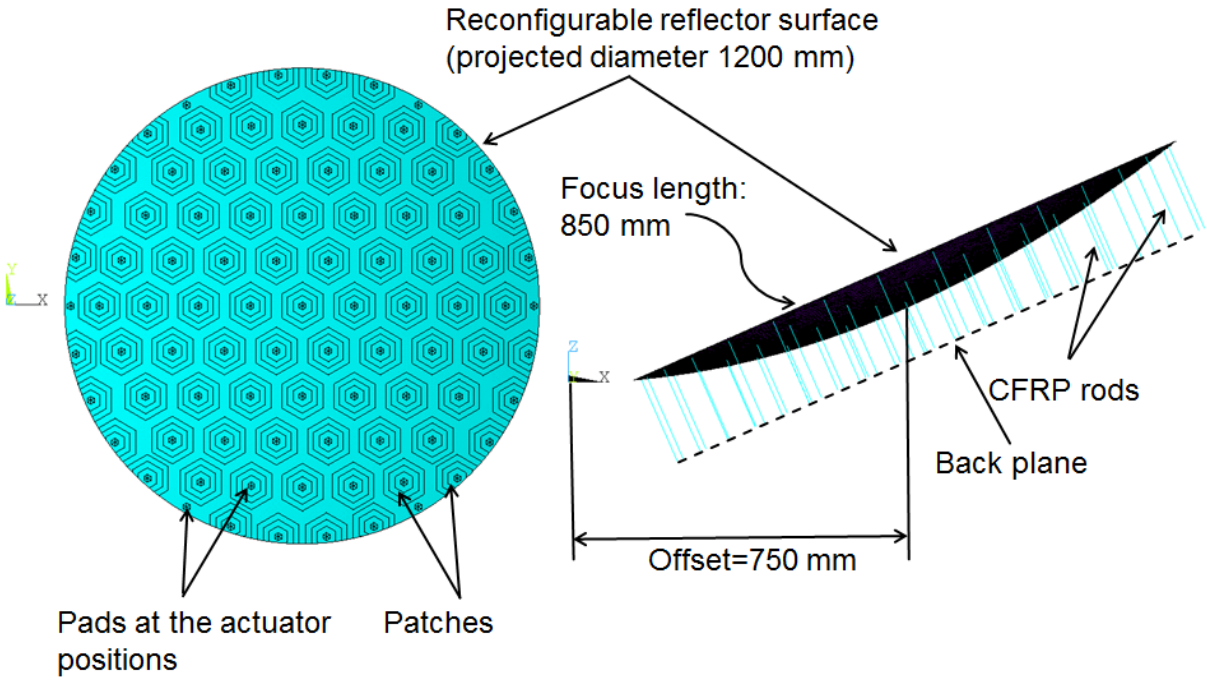

Figure 6.6.: The FEM model of the reconfigurable reflector

There are totally 91 actuators placed in triangular lattice. As found in the last chapter, the actuator placement at rim area has considerable influence on reshaping performance. Therefore a modified actuator placement is used in the engineering model. The actuators in the center region are equally placed in triangular lattice with projected distance of 132 mm. The placement of actuators at the rim area is modified to fit the circular rim of the engineering model. Limited by available space at the rim region, six actuators are placed with only pads but no patches. The CFRP rods connect the reconfigurable reflector surface with actuators, which are arranged to be perpendicular to the flat backplate. The flat backplate is chosen mainly for reasons of manufacturing simplification. Other backplates, like curved one can

be used for a compacter configuration but resulting no noticeable difference on reshaping.

The boundary conditions of the FEM model are defined in the local coordinate system (defined at the center of the reflector model, see Figure 6.7) as follows:

- Z direction of all rods are used for applying the stroke lengths of actuators
- Translations between the reflector surface and CFRP rods are coupled
- In-plane translations and rotations around Z of all nodes at the bottom are fixed
- The rest rotations of the center rod is fixed
- The rotation around X of one rod at the far side in the X direction is additionally fixed to prevent rigid body movement

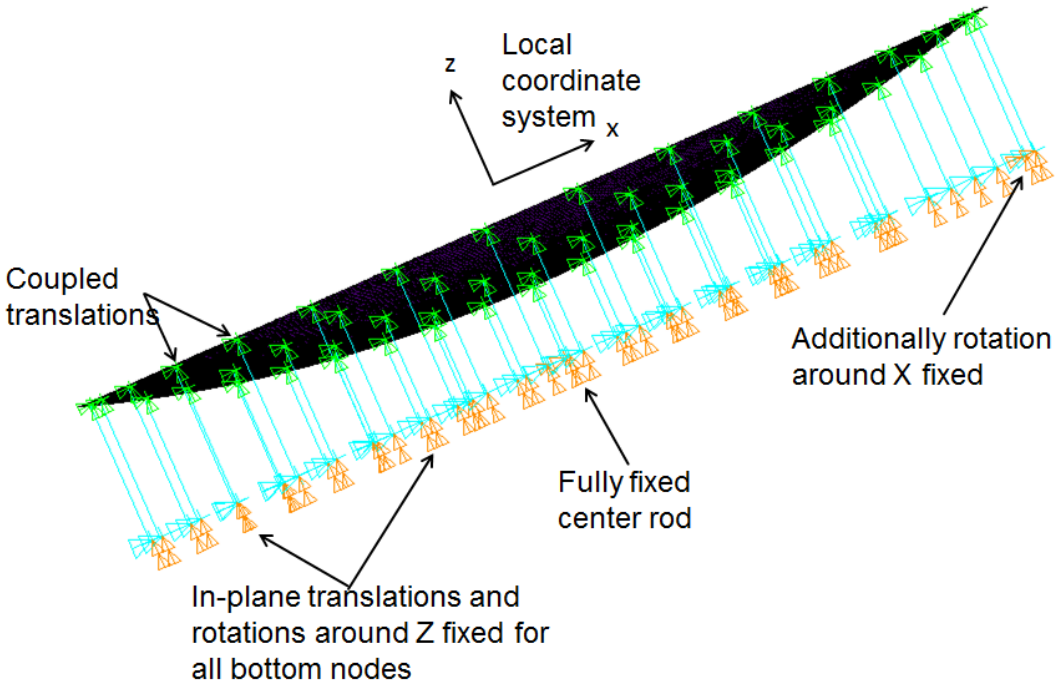

Figure 6.7.: Definitions of boundary conditions on the FEM model

The FEM model is created in ANSYS software. Layered shell elements (SHELL181) are applied to model the reflector surface and 3-D beam elements (BEAM188) are used to model the rods. The layout of the multilayer concept is illustrated in Figure 6.8.

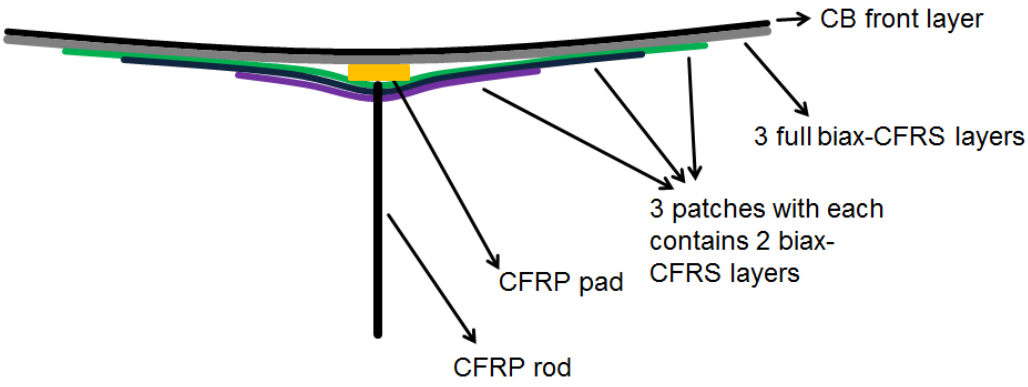

Figure 6.8.: A visualization of the multilayer concept in the FEM model

6.2.2. Reshaping Analyses of the Engineering Model

Three target shapes are defined by TAS for the three representative geographic coverage as stated in Chapter 3.3. These shapes are generated through a radio frequency optimization software without considering mechanical behavior of the reflector. The three shapes, "Europe", "Brazil" and "ConUS", contain shape variations in Z direction within -15 to 15 mm. In reshaping analyses, the reflector surface shall be reshaped to the target shapes via actuations as close as it can.

The first challenging task of the reshaping analyses is how to determine the stroke lengths of actuators for optimal reshaping results. The task of determination of stroke lengths can be formulated as an optimization problem:

$$\begin{aligned}&\text{Goal}: min.\, R(\triangle u) = \sqrt{\tfrac{1}{n_u}(u_{goal} - u_{achieved})^2}\\ &\text{Design variables}: x_i\\ &\text{Constraints}: x_{min} \leq x_i \leq x_{max},\ F_{min} \leq F_i \leq F_{max},\ \varepsilon_x,\ \varepsilon_y,\ \varepsilon_{xy}\end{aligned}$$

u_{goal} is the target surface displacement, $u_{achieved}$ is the achieved surface displacement and n_u is the number of measurement points. Design variables are the stroke lengths of actuators x_i. As constraints, F is the actuation force and ε is the strain of biax-CFRS layers.

The computation cost of an optimization containing 91 design variables in geometry nonlinear systems is generally quite high. Moreover, to identify local and global optimum or find a better local optimum, the optimization shall be performed at least several times using different initial values and parameter settings. The high computation cost is not affordable in the engineering practice of the mechanically reconfigurable reflectors. To realize reshaping analyses within reasonable computation efforts, the simplification approach as stated in Lawson and Yen (1988) and Datashvili et al. (2010) is applied. In this approach, the system is assumed to be linear and therefore the efficient least square method can be applied.

The first step in the stroke length optimization is forming a surface response matrix to inputs of actuators. In this step, unit stroke length is applied to one actuator while the rest are stayed on their initial positions at each time. The change of the surface shape due to the actuation of a single actuator is then saved as a part of the response matrix. After repeating this process for each actuator, the full influence matrix can be established. Using the

influence matrix in the least square method, the optimal stroke lengths for the three defined target shapes can be obtained at the same time. This computation is quite efficient for its limited number of calculation iterations and the linear assumption of structures.

The optimal stroke lengths for the three target shapes are in the range of -16 to 15 mm. The surface difference between the target and achieved shapes is expressed as RMS, which is 0.52 mm in the Europe task, 0.74 mm in the Brazil task, and 1.29 mm in the ConUS task. These values are beyond the maximal RMS requirement of 0.3 mm, which is resulted from the RF requirement of gain loss less than 0.3 dB. In spite of this, they are not the critical point in the preliminary analysis stage. In a later stage, coupled analyses containing mechanical models and radiation frequency analyses will be performed to improve and eventually achieve the required RF performance. The structural performance in both stages is analogous for their comparable stroke lengths. Applying the optimized stroke lengths on the FEM model, preliminary mechanical performance such as actuation force, extreme values of strains can be evaluated. A overview of these results for the three reshaping tasks is in Table 6.5. It should be noticed, the actuation forces in the three analyses are all below 5 N, which allows a wide selection range of actuators.

Table 6.5.: Results overview of three reshaping analyses

Target shape	Shape difference in RMS [mm]	Stroke length max./min. [mm]	Actuation force max./min. [N]
Europe	0.521	6.43/-16.38	2.04/-1.45
Brazil	0.748	9.33/-12.68	1.68/-1.49
ConUS	1.292	12.08/-15.03	2.89/-4.39

Observing these surface contours between the target and achieved shapes (Figure 6.9 and other figures in section B.2 of Appendix), the shape difference is mainly found at the rim and the regions with large shape variations. The reshaping results of the task Europe and the task Brazil are satisfactory while massive shape difference is observed in the task ConUS. In fact, the target shape ConUS is treated as the critical case for its large geographic coverage.

The results of strains are examined layer by layer. As shown in the material characterization of the biax-CFRS specimens, when the maximal compression strain is larger than 0.15%, the flexural stiffness is significantly reduced. Additionally the maximal shear strain shall be smaller than 7% for ensuring linear material assumptions. These two values are defined as the maximal strain values for biax-CFRS layers in the reshaping analyses.

To distinguish different strain terms, the strains in two fiber directions are denoted as X and Y direction and the shear strain is denoted as XY direction. As found in the three reshaping analyses, the extreme strains are located at the three full layers region without patches. The reason of the large local strains can be explained as follows. The strain values are determined by curvatures and thickness of the shaped surface. The three full layers region has lowest bending stiffness but it has largest bending moments from adjacent actuators working as combination manners. Due to the large local bending moments, the surface curvatures of this region are quite large.

The maximal compression strain is either at the first or the last full biax-CFRS layer (here is the third layer). In the Europe task, it is 0.13% in the fiber direction, and in the Brazil task, the maximal compression strain is slightly higher with the value 0.15%. In the ConUS task,

the maximal compression strain is 0.2%, which indicates local stiffness degenerations are probably occurred. The maximal shear strains in the three analyses are all below 3%, which reserve enough margins to the shear strain limitation. Extreme strains in the region of three full layers for the three reshaping analyses are in Table 6.6.

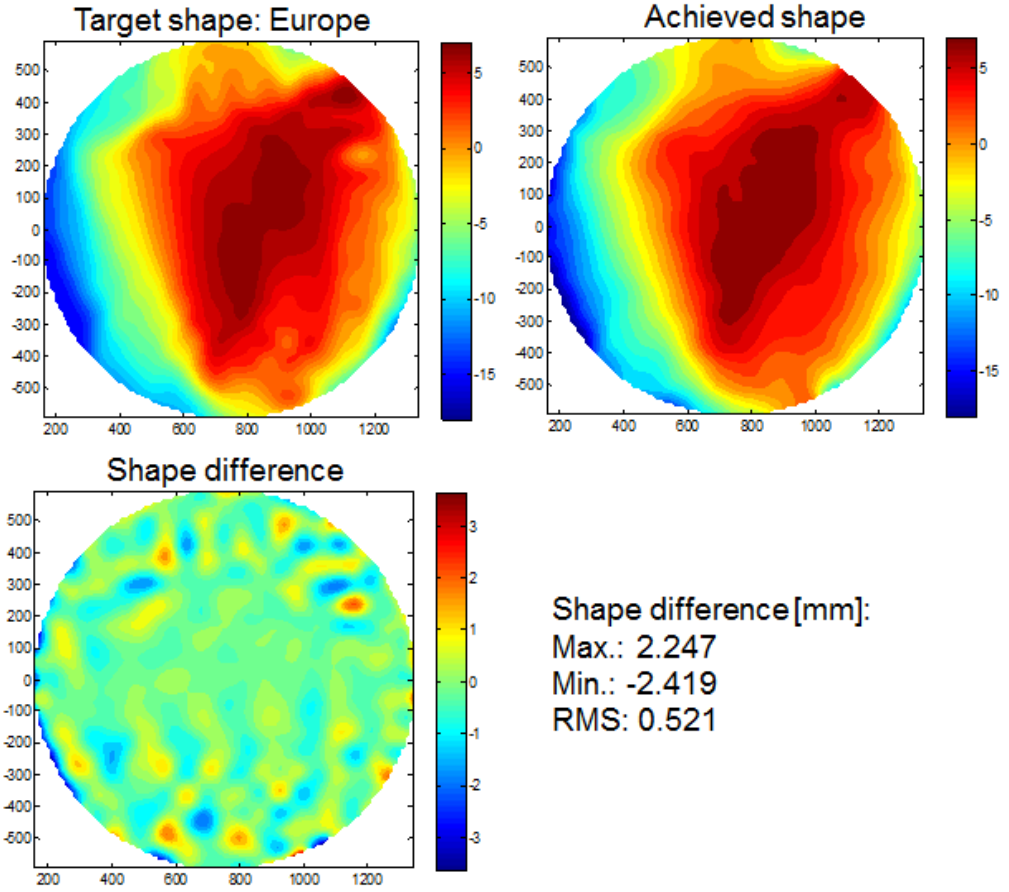

Figure 6.9.: Target and achieved shapes of the task Europe

Table 6.6.: Extreme strains in three reshaping analyses

Strain [%]	Max. in X	Min. in X	Max. in Y	Min. in Y	Max. in XY	Min. in XY
Europe	0.106	-0.128	0.089	-0.076	2.747	-2.228
Brazil	0.153	-0.146	0.178	-0.176	2.344	-2.516
ConUS	0.186	-0.201	0.194	-0.197	3.287	-3.297

6.2.3. Nonlinearity in Reshaping

As concluded in the analyses of the medium size models, the geometry nonlinearity in reshaping can not be ignored. To identify the difference between linear and nonlinear analyses, reshaping analyses using the same stroke lengths for linear and nonlinear analyses are performed and their results are compared. The task Europe is taken as an example, in which a clear shape difference between the linear and nonlinear analyses is observed (Figure 6.10). The largest magnitude of shape difference on these local regions is around 2 to 3 mm. The RMS value of the shape difference is 0.767 mm, which is in the same range of the predicted value on the medium size model. Compare the results of actuation forces and strains, no noticeable difference is found between the linear and nonlinear analyses. But because the shape accuracy is the fundamental requirement to the reconfigurable reflectors, the relative large shape difference between the linear and nonlinear analyses is not acceptable. Although the nonlinear analysis is quite computation intensive, it is the essential process to obtain correct reshaping results.

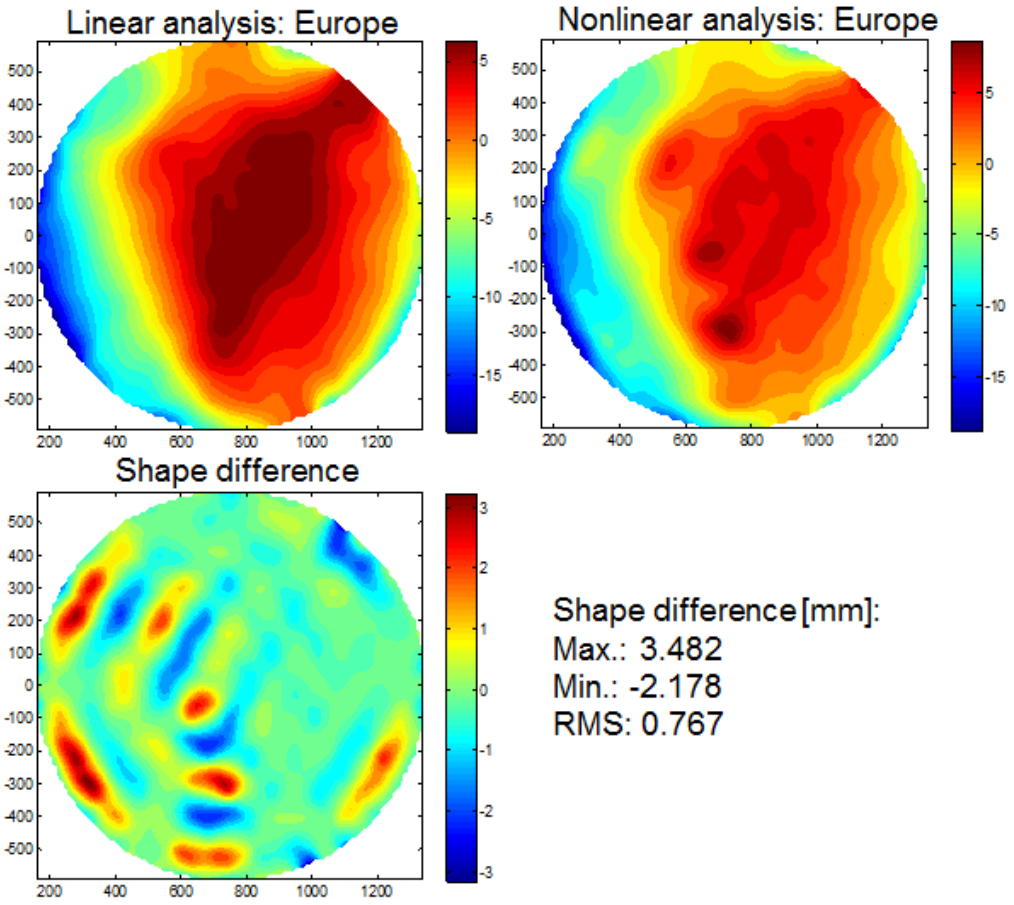

Figure 6.10.: Linear and nonlinear reshaping analyses of the task Europe

As a potential approach to reduce the high computation cost in the coupled analysis, a multi-step linear analysis with stepwise geometry update can be performed. The procedure of this approach is explained as follows.

In the first step, the linear least square method is performed to obtain the preliminary stroke lengths. The achieved shapes using the obtained stroke lengths, in both linear and nonlinear reshaping, are already close to the target shape. Benefit by the material design, the shape difference between the linear and nonlinear analyses shall be relative small as well. As inputs to the second step, the geometry is updated through applying the obtained stroke lengths on the first step in geometry nonlinear analysis. By this update, the shape difference between the start geometry on the second step and the target shape has been reduced, which means the required reshaping amplitude for the second step is also reduced.

As a positive consequent of the reduced reshaping amplitude, the stroke lengths for the second step will be reduced correspondingly. As known from theory of thin plate/shell, the difference between linear and nonlinear behavior is mainly depending on the amplitude of applied deflection. The reshaping with small stroke lengths shall be quite the same in both linear and nonlinear analyses. Therefore the shape difference between the linear and nonlinear analyses on the second step shall be considerably reduced as compare with the first step (see also Figure 6.11). Extending the process to more steps, the reshaping difference between them can be eventually reduced to be ignorable. Following this approach, a nonlinear reshaping analysis can be replaced by multi-step linear analyses containing stepwise geometry update, which has advantages of low computation complexity and cost.

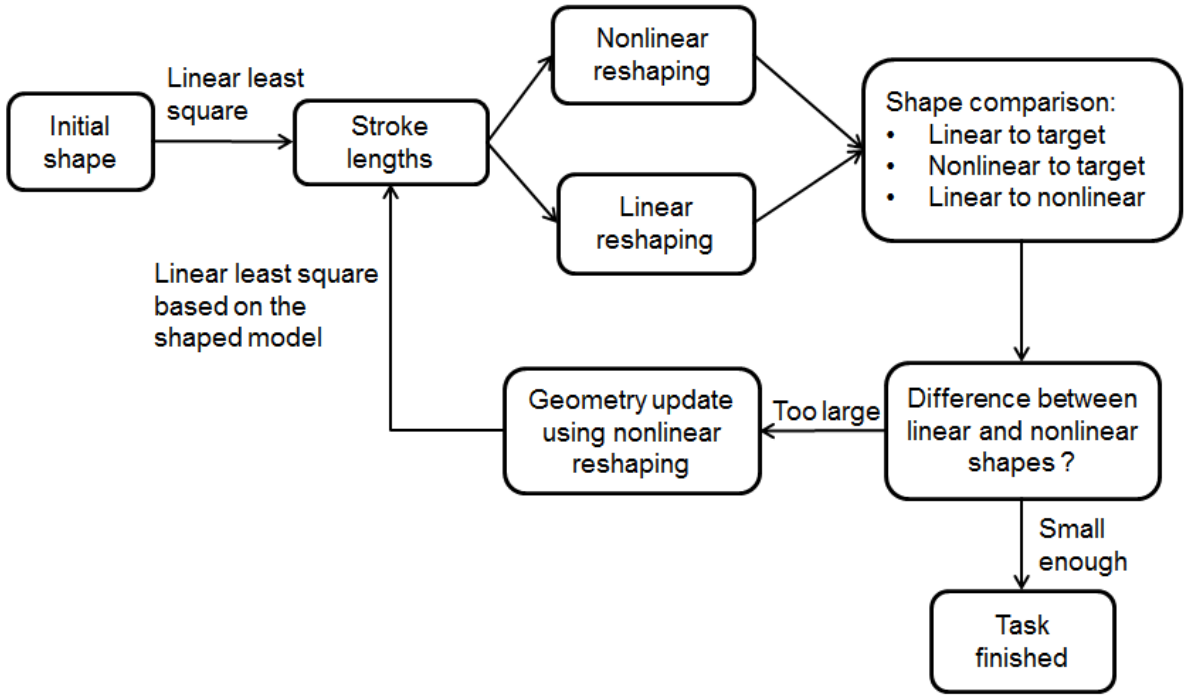

Figure 6.11.: The flowchart of multi-step linear analysis

Since the shape difference on the first step is usually around 1 mm on these defined tasks, a sufficient small shape difference can be achieved by just performing two or three steps linear reshaping analyses. This approach will be further demonstrated and verified in details through numerical and experimental analyses on the demonstrator.

6.3. Technology Demonstrator and Reshaping Results Correlations

A technology demonstrator is build based on the engineering model. The reshaping tests are performed on the demonstrator and the results are correlated with the corresponding numerical results. The applied correlation and correction methods about the reshaping results are presented in the following sections.

6.3.1. Demonstrator Model Description

The demonstrator is the center part extracted from the engineering model with a hexagonal rim (see Figure 6.12). The projected diameter of the truncated hexagonal rim is 660 mm. The demonstrator contains 19 regularly placed actuators, which are driven by electric stepper motors.

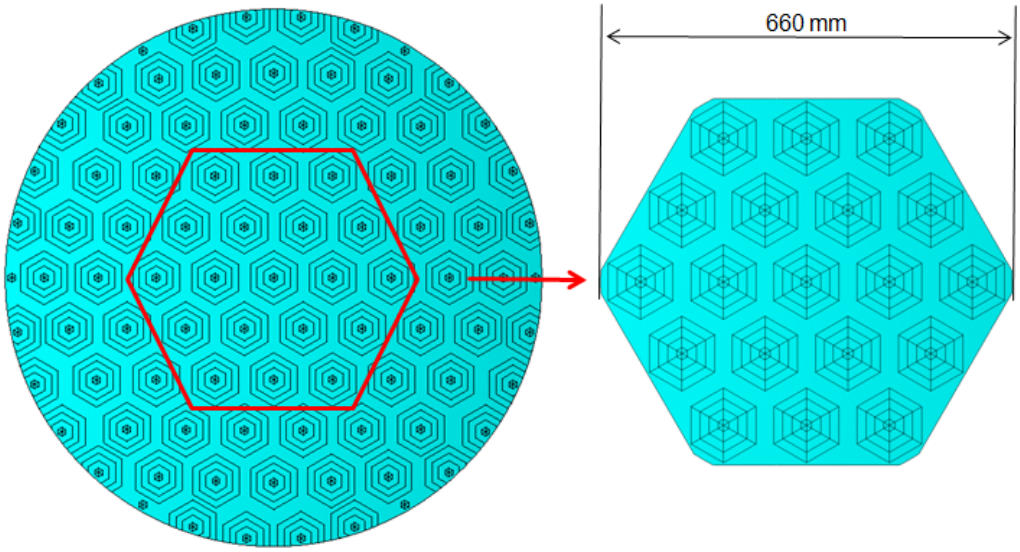

Figure 6.12.: The FEM model of the demonstrator (top view)

The designed morphing skin is implemented in the engineering model with a CB surface layer. The CFRP tubes connect with electric stepper motors, which are mounted in the flat aluminum backplate. The defined boundary conditions as in the numerical analyses are realized through placing guiding components around the actuators. A photo of the demonstrator is shown in Figure 6.13.

The stroke length inputs are controlled through a control unit and a program implemented in MATLAB. Limited by the available number of control channel, only one actuator can be activated at one signal input. The simultaneous actuating as presented in the numerical analyses can not be realized in tests. Instead, the required stroke lengths are divided into small values according to defined steps. In each step, actuators are activated sequentially with small inputs. As verified through numerical analyses, as long as the step number

more than 5, the difference between simultaneous actuating and multiple steps sequential actuating is negligible.

Figure 6.13.: The technology demonstrator [Endler et al. (2014)]

6.3.2. Reshaping Tests and Results Correlations

To evaluate the performance of the demonstrator, two target shapes are derived from the coupled mechanical and RF analyses by TAS. The optimized stroke lengths of the reshaping tasks Europe and Brazil are actuated on the numerical and laboratory models for shape comparison and correlation. The shaped surface of the demonstrator model is measured through photogrammetric measurements. As the measurement positions for the photogrammetric, there are 521 markers regularly placed on the reflector surface (see Figure 6.14).

Sensitivity and Repeatability

In order to identify the reshaping repeatability of the demonstrator, a repeatability study is performed. There are two major sources of reshaping deviations in tests, actuator positioning and resolution of the measurement system. It is observed, the mean deviation of actuator positioning is around ± 0.05 mm and the resolution of the applied photogrammetric system is around 0.02 mm.

The demonstrator is placed with a inclination angle as defined in the offset antenna configuration. The reference shape is defined as the shape with zero stroke length inputs under gravity. The surface deformation under the gravity load as well as some shape deviations introduced by manufacturing and handling are contained in the reference shape. The measured shape is compared with the shape provided by FEM analyses. Since the number of measurement nodes in the FEM model is significant larger than those in the demonstrator, the data comparison is performed through an extrapolation approach. The predicted values

in Z direction of the measured nodes are extrapolated from the results of FEM analyses using their in-plane coordinates. The surface difference is estimated through comparing the Z coordinates between the measured and extrapolated values.

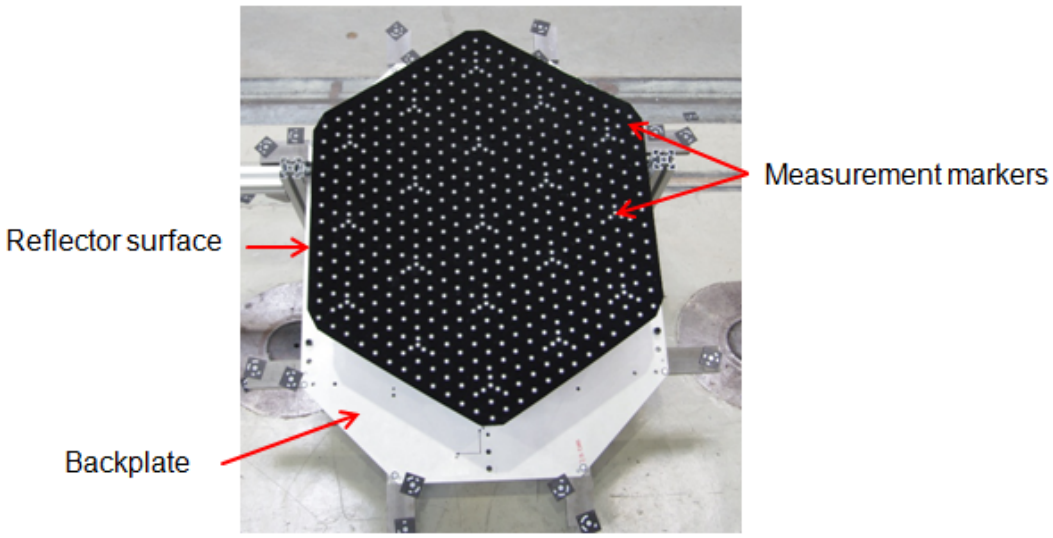

Figure 6.14.: The demonstrator with measurement markers (top view) [Endler et al. (2014)]

Totally the reference shapes are measured five times with different reshaping tasks between every two measurements. The surface difference in terms of RMS among the different measurements is less than 0.02 mm, which is acceptable as accuracy tolerance of the measurements (see Table B.9 in Appendix B.3).

Reshaping Results Correlations

The optimized stroke lengths are in the range of -10 to +10 mm in the Brazil and Europe tasks of the demonstrator. The laboratory model is first activated to the defined Brazil task. After the surface measurement, it returns to the reference shape first and then be reshaped to the defined Europe task for the second measurement. Visual results are presented in Figure 6.15 and Figure B.3 (in Appendix B.4). The RMS between the target and measured shapes in the Brazil task is 0.92 mm and in the Europe task is 0.6 mm. Both of them are not satisfied to an acceptable surface difference within 0.3 mm. The relative large difference presents in 3 full layers region, which seems to be "mountains" and "valleys" between actuators. This clearly indicates the bending stiffness on the demonstrator is less than the numerical model. The sources of the reduced stiffness are mainly from geometry distortions of the reflector surface.

The geometry distortions of the reflector surface are mainly introduced in assembling process. The CFRP pads are bonded with biax-CFRS full layers by the adhesive red silicone S691 (quite similar to S690, [Chemie]). In bonding of the CFRP pads, the thickness of the adhesive layers (around 1 mm) can be varied widely according to applied pressing forces. Sometimes the CFRS layers could be even pressed into the flexible CB front layers. These over pressing in assembling can cause surface distortions in magnitude of -1 to +1 mm.

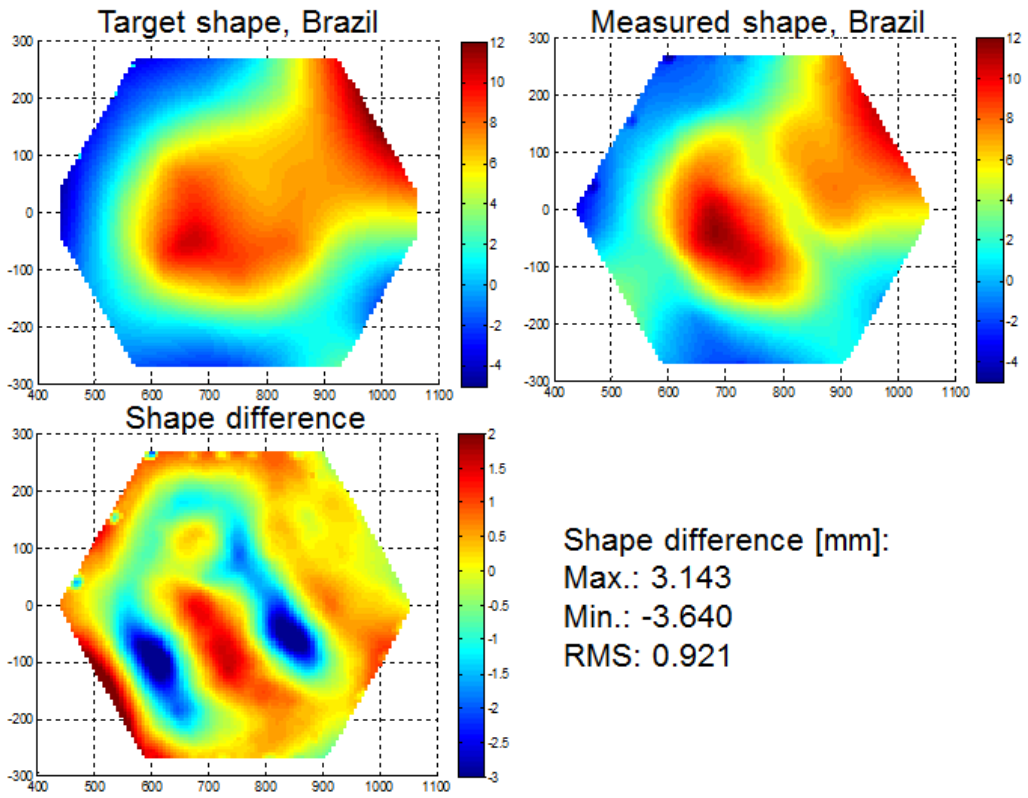

Figure 6.15.: Predicted and Measured shapes of the Brazil task

To figure out the influence of geometry distortions on reshaping results, numerical investigations are performed. In the analyses, geometry distortions are introduced into numerical models as update of the initial shape. Then the reflector model with the updated initial geometry is actuated with the same stroke lengths as applied on the demonstrator for shape comparison.

Initial Geometry Distortions

Geometry distortions, especially when its magnitude is on the same level of thickness of thin shells/plates, can significantly influence the reshaping results. The amplitude of the geometry distortions is propagated rapidly with reshaping amplitude growing and eventually the desired reshaping pattern will be noticeably changed. The exact geometry distortions of the reflector surface can't be accessed since it is covered by the CB front layer. As an approximation, the geometry distortions are generated through detailed observations of the shape difference between the predicted and measured shapes.

The surface difference of the predicted and measured shapes for the Brazil and Europe tasks is presented in Figure 6.16. Their shape difference is quite similar in the pattern distributions but different in magnitude. An initial shape pattern can be roughly estimated though combining these two shapes with weighting factors. According to their RMS values, the weighting factor for the Brazil task is 0.6 and is 0.4 for the Europe task. Afterwards, the combined shape is scaled down with a factor of 0.4 to generate the initial geometry distortions within reasonable magnitude. The surface shape variations of the initial geometry distortions are in the range of -1 to 0.6 mm.

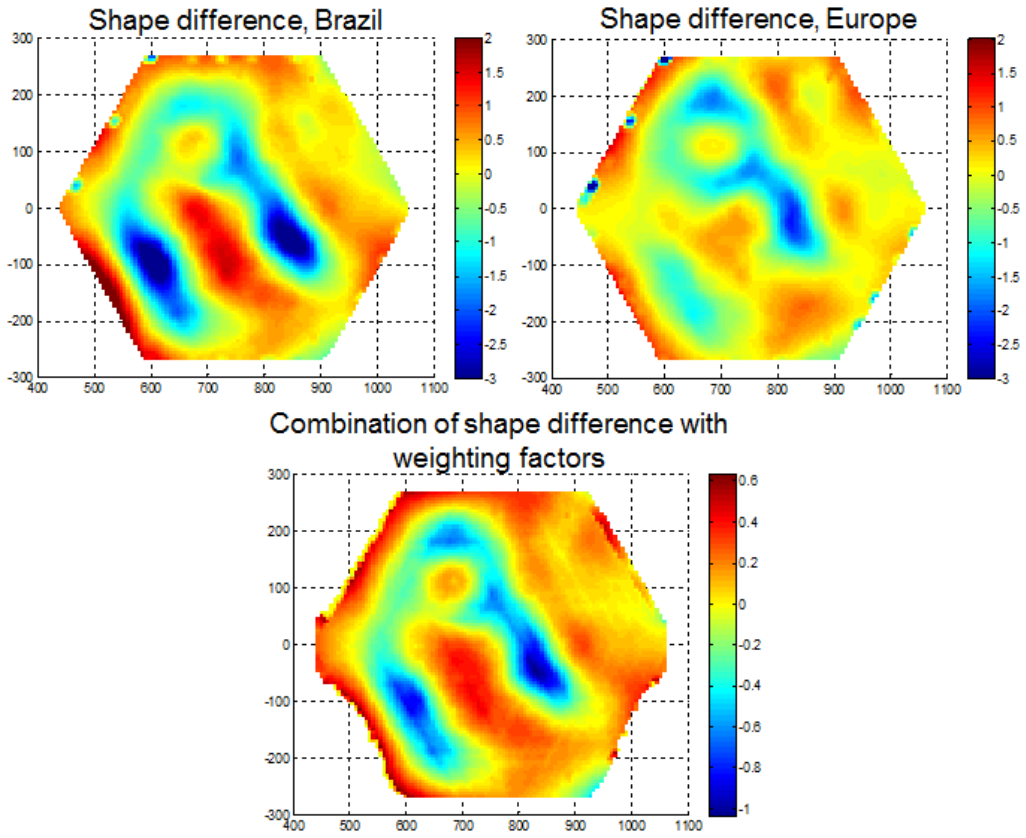

Figure 6.16.: Shape pattern of the initial geometry distortions

The geometry of the FEM model is then updated with introducing the initial geometry distortions. The reshaping results of both tasks are clearly improved as compare with the previous results (see Table 6.7). These improvements indicate the hypothesis of geometry distortions in the demonstrator model is correct.

Table 6.7.: Improvements of correlations between the numerical and measured shapes

Analysis description	Brazil task RMS [mm]	Europe task RMS [mm]
Initial FEM model	0.921	0.605
FEM model with initial geometry distortions	0.367	0.335

Update Analyses and Measurements

Based on the fact of existing geometry distortions on the demonstrator, the FEM model is updated correspondingly. Two types of updated FEM models are applied for the coupled mechanical and RF analyses. The first type is the model with the initial geometry distortions, which is the same to the demonstrator. The coupled mechanical and RF analyses are

performed again based on the updated FEM model through geometry nonlinear analyses. The second type is the shaped model, which is the model type 1 reshaped with the previously defined stroke lengths through geometry nonlinear analyses. In the coupled analyses of the second type model, the adjustment of stroke lengths is performed through geometry linear analyses. The purpose of the second model is verifying the mentioned multiple-step linear approach.

Target shapes are also updated through the coupled mechanical and RF analyses on the updated FEM models. The stroke lengths for the FEM model type 1 are varied up to 2 mm in the Brazil task and up to 0.5 mm in the Europe task. The updated stroke lengths are then given to the demonstrator for updating reshaping and measuring. The shape difference between the updated predicted and measured shapes is improved to be 0.47 mm in the Brazil task and 0.36 mm in the Europe task. It can be clearly observed from the visual descriptions in Figure 6.17 (and also Figure B.4 in Appendix B.4), the target and the measured shapes are correlated quite well.

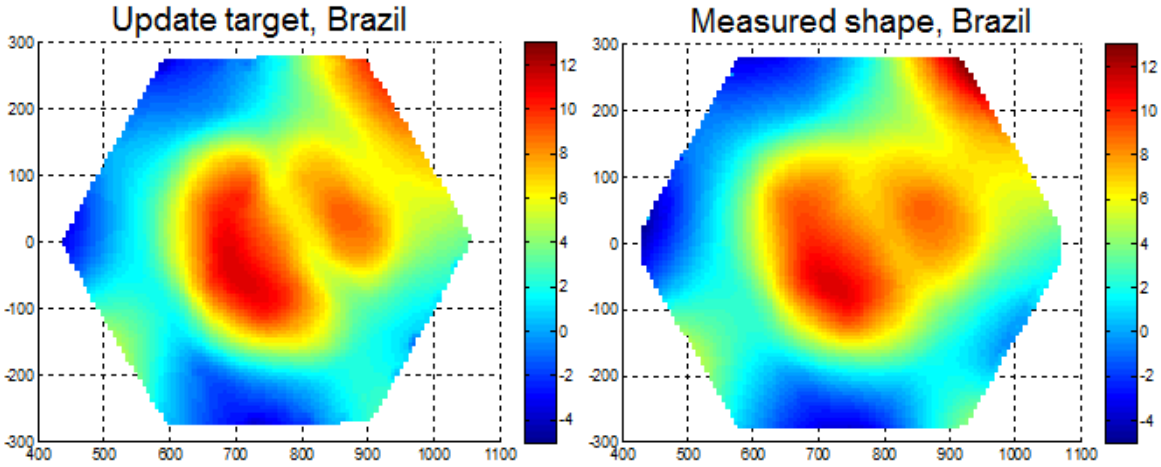

Figure 6.17.: The updated measured and predicted shapes of the Brazil task

Similar improvements are also found at the updated results based on the second type model, which is 0.47 mm in the Brazil task and 0.34 mm in the Europe task (see Table 6.8). The adjustments of stroke lengths for the shaped models have similar effect on improving reshaping results to restarting of the stroke length optimization as in model type 1. Moreover it has obvious advantage on computation cost, which is the quite important feature demanded on the engineering application.

From these investigations several conclusions can be draw. The shape difference between the updated predicted and measured shapes is around 50% reduced as compare with the previous results. These results can strongly support the argument of existing initial geometry distortions in the demonstrator. Further, the multi-step linear stroke length optimization with stepwise geometry update can offer quite the same results to those obtained by fully nonlinear analyses.

Table 6.8.: Reshaping results using the updated FEM models and measurements

Analysis description	Brazil task RMS [mm]	Europe task RMS [mm]
Initial results	0.921	0.605
Coupled analyses using the FEM model type 1	0.471	0.360
Coupled analyses using the FEM model type 2	0.466	0.343

Applying the updated FEM models on the coupled analyses, target shapes are considerably changed as compare with the previous defined ones. The improved RMS results are still larger than the required values 0.3 mm, which indicate satisfactory RF performance is hardly to be achieved using this demonstrator. Limited by the reshaping results accuracy, the RF performance tests are not suggested in this stage.

Short Conclusions about the Demonstrator

Through these investigations about the demonstrator, broader insights about the reflector morphing skins on numerical and experimental aspects are obtained.

The sensitivity and repeatability tests are performed on the demonstrator, which present remarkable features of the demonstrator. The biax-CFRS materials, the actuation system as well as the photogrammetry measurement system demonstrate their robustness and reliability in more than 20 tests.

Geometry distortions of the reflector surface are introduced in the manufacturing and assembling process. Because of that, reshaping results can't be well correlated with the measured ones. To improve the shape correlations, approaches like introducing geometry distortions in the initial geometry model are taken. It is found applying the updated FEM model in the coupled analyses, around 50% improvements on RMS values are achieved. However, further improvements on shape correlations for the demonstrator are quite difficult to be achieved for insufficient information of the geometry distortions.

Lessons learned from the investigations on the demonstrator are on manufacturing, analysis, and concept design aspects. On the manufacturing aspect, introducing of geometry distortions shall be minimized. The functional CB filled silicone layer can be removed from the demonstrator, which will be quite helpful to reduce the risk of geometry distortions. Furthermore the assembling of CFRP pads shall be carefully handled to reduce the sources of geometry distortions. On the analysis aspect, the proposed multi-step linear analyses with stepwise geometry update shall be followed. As shown in the updated investigations of FEM analyses and measurements, the results of multi-step linear analyses are quite similar to those of geometry nonlinear analyses. The approach of multi-step linear analysis is the key to reduce the high computation costs in the full size engineering models.

In the end, the sensitivity to geometry distortions and the local convex on the 3 full layers region indicate insufficient bending stiffness locally. Updates of the concept are proposed, which can be either enlarging the patch size to reduce the 3 full layers region or using the 7 or 8 full layers concept as investigated on the medium size models.

7. Sailplane Wings and Their Morphing Skins

The methods of morphing skin design are further explored on the application of sailplane morphing wings. In this chapter, contents like approaches to derive morphing skin concepts, morphing skin material design, correlations with the manufactured specimens, and numerical investigations about morphing wings are presented.

7.1. Objectives and Approaches of Morphing Wing Skin Design

7.1.1. Objectives of Morphing Wing Skin Design

As consequents of different application environments, the objectives of sailplane morphing wing skin design are not focusing on high reshaping accuracy but on realizing relative large amplitude reshaping, carrying the complex loads from aerodynamics and actuations, and maintaining the smoothness of surface contour. As side requirements, the demands of actuation energy, system complexity and reliability, and maintenance cost of the morphing wing system shall be in acceptable ranges.

7.1.2. Approaches of Morphing Wing Skin Design

The morphing wing skin design starts from determining a proper principle concept of morphing wing and skin according to the specific applications. In order to accomplish the mentioned task, a simplified representative numerical model of morphing wing shall be initialized based on task definitions at first. With help of the representative model, concepts of skins, actuations, interface systems and boundary conditions can be briefly accessed and determined.

As outputs of the investigations on the representative model, the desired material properties of morphing skins can be estimated. Afterwards, potential skin concepts can be briefly selected/determined based on existed concepts and engineering experience. In the next step, the desired material properties of morphing skin concepts will be realized through compound material design in terms of proper combining design parameters like materials, geometry, and configurations.

The estimated skin concepts from the morphing wing skin design will be correlated with

experimental results at first. Then the detailed performance e.g. the mechanical performance of the implemented morphing skin, actuation and interface systems will be evaluated (see Figure 7.1).

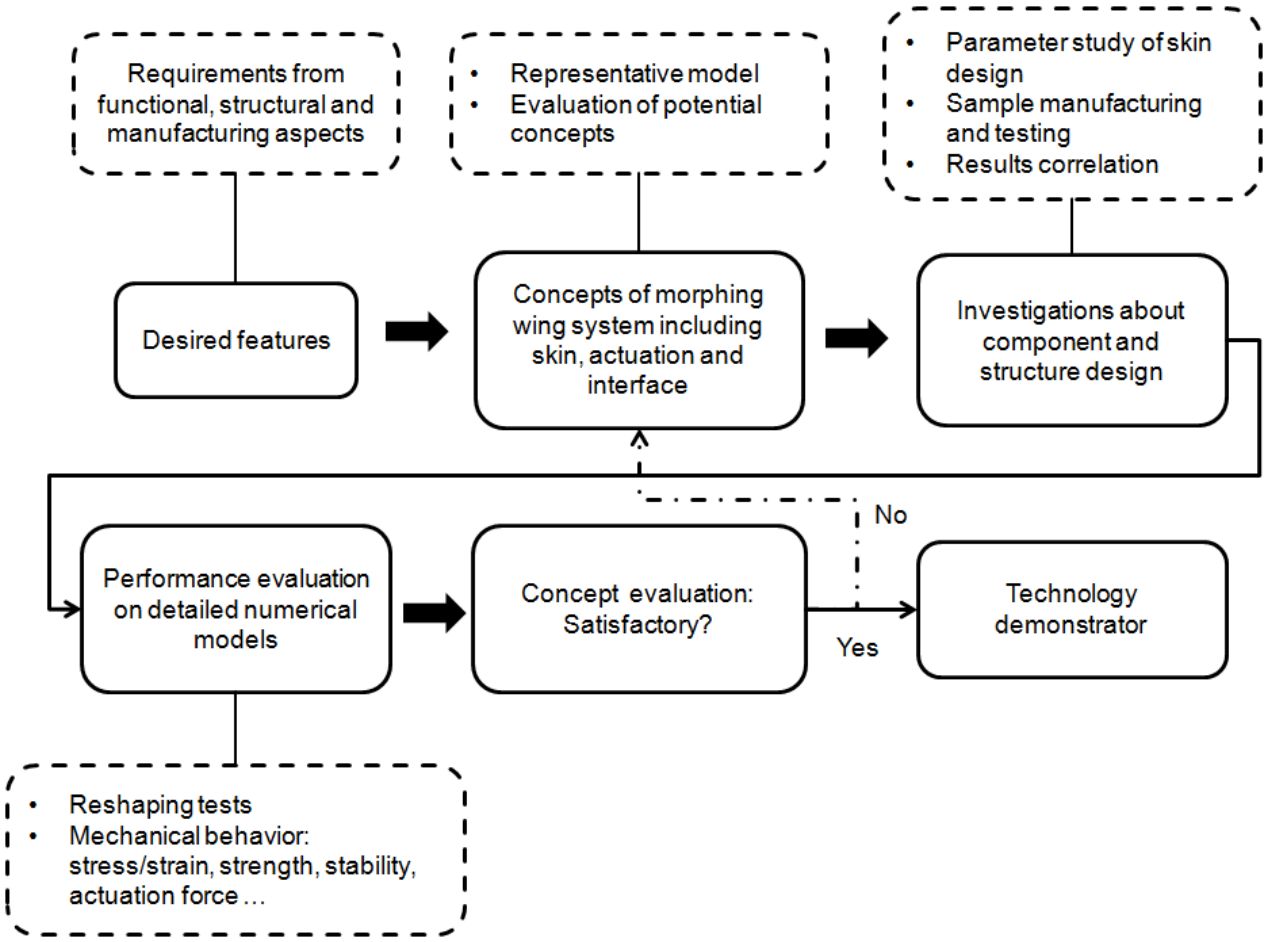

Figure 7.1.: Flowchart of morphing wing skin design

7.2. Morphing Wing Skin Design

7.2.1. Preliminary Analyses

Representative Model

The representative model is defined based on the works of Wießmeier. The geometry of the modified sailplane leading edge is around 200 mm in chordwise and 60 mm in height. Compare with the existed morphing concepts of the civil transport aircraft wings [Monner et al. (2009) and Müller (2000)], the available space for placing actuation and interface systems is quite limited for the sailplane wing.

As the defined functional requirement to the morphing wing [Chapter 3.3.2], the leading edge shall be able to deflect downwards 10 degree without open gap on skins.

Based on the defined geometry and functional requirements, potential concepts of actuation and interface systems are reviewed through the published works at first. Among the potential concepts of actuation and interface systems, the eccentuator concept, which is simple and applicable in the narrow construction space, has highest priority. Referring to the eccentuator concept of Müller (2000), the eccentuator (horn) can be made from CFRP with glass-PTFE fabric coating to reduce surface frictions. In the interactive area between the leading edge and horn, thin steel plates are placed in a discrete manner to reinforce the loading area and distribute actuation forces smoothly. Furthermore, as stated by Matteo et al. (2010), additional spars shall be added to sustain the profile contour of the airfoil in reshaping (see Figure 7.2). These spars are connected to skins with flexible hinges to allow certain degree of freedoms for smooth reshaping.

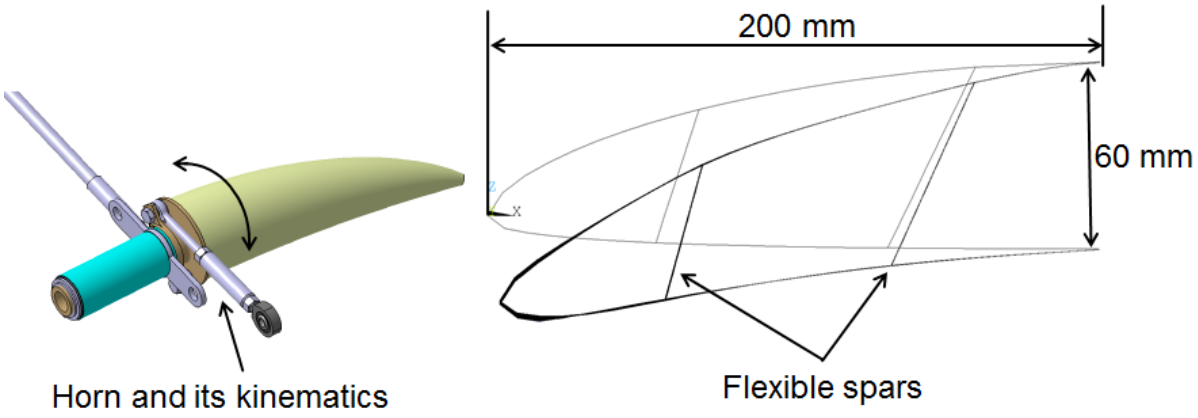

Figure 7.2.: The CFRP horn as the eccentuator [Wießmeier] and the idealized deflection of the sailplane morphing leading edge

With these definitions, a representative model can be created accordingly. In the representative model, the flexible spars are implemented but no contact interactions between the horn and skins are considered. Instead, the reshaping of the leading edge is realized through applying the required displacements on the contact region of the lower skin. With

this simplification, investigations can be focusing on deriving concrete morphing skin concepts rather than solving the complex contact analyses.

Morphing Skin Concepts

In order to figure out the desired stiffness characters of morphing skins, two representative examples of skin concepts, which are the full compliant membrane skin and the stiff metal panel skin, are implemented in the representative model for reshaping analyses. In these analyses, the desired deflections are applied on the contacting region of the lower skin. As boundary conditions, the edges of both upper and lower skins are fixed in translations but free in rotations.

In the first analysis, the skin is idealized as full flexible to be able to accommodate any kinds of deformation. Using the representative model created in ANSYS, an illustration of the idealized deflection can be presented as in Figure 7.2. Observing the deformed leading edge, the upper skin is bended and extended in the longitude direction and the lower skin is mainly bended. The contour of the nose is changed due to the combined deformations of upper and lower skins. From this analysis, a conclusion about these highly flexible skin concepts such as corrugated laminates and flexible sandwiches can be made. They shall be capable to realize the required reshaping but probably have weakness on surface quality especially when carrying aerodynamic loads.

In the second analysis, the skin is set as thin aluminum with 0.3 mm thickness. In the deformed leading edge, the nose is highly distorted caused by the nonlinear bending (see Figure 7.3). This phenomenon is called as "Brazier effect" [Matteo et al. (2010)], which relates to thin-walled, cambered and long structures under large bending loads. The smooth shape transformation of the droop nose using stiff hybrid composite skins as presented in Monner et al. (2009) can't be achieved in the sailplane wing mainly due to its narrow airfoil configuration.

As the conclusion obtained from these two studies, one of the most promising and simplest concepts of the morphing leading edge is containing only certain high flexible region to accommodate the required smooth reshaping. The advantages of this concept are less stiffness reductions of the rest skins and less difficulties in design and manufacturing. The flexible region can be either at the end edge of upper or lower skin or at the nose. Since the deflection is downwards, a flexible upper skin is preferred for the tension status, which can add additional geometry stiffness on the skin.

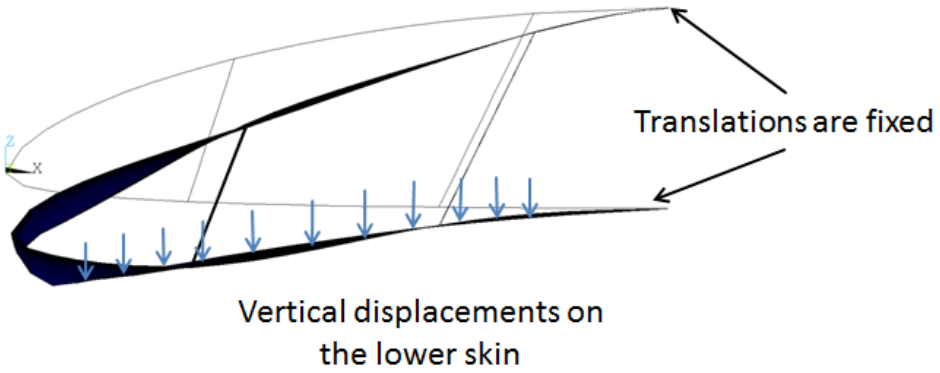

Figure 7.3.: The deflection profile of a closed leading edge

About the requirements to the flexible skin, it shall be able to deform in a relative large amplitude within material elasticity while in the same time to carry aerodynamic loads without noticeable shape degeneration.

Start with the determined basic morphing skin concept, the further task is determining the dimension of the flexible skin zone. On the one hand, the area of the flexible skin is preferred to be as small as possible to limit stiffness reductions on skins. But on the other hand, the flexible skin shall be sufficient large to accommodate the deformation without large strain on materials. As simplification in the preliminary assessment, the flexible skin is taken as elastomer and the rest of skins are assumed to be thin aluminum. Through a parameter study, it is found the most promising concept is applying the flexible skin at the region after the second spar. In this concept, the length of the flexible skin is around 40 mm, which seems to be a minor change in the leading edge.

Observed in the deformed contour of the proposed morphing leading edge concept (Figure 7.4), most of the airfoil is quite smoothly deformed. Due to lacking of bending stiffness at the flexible skin, it is stretched only in the in-plane direction, whose surface shape is not optimal for aerodynamics. It is believed that the profile quality of the flexible skin can be considerably improved by introducing certain level of bending stiffness. As potential skin concepts for the flexible skin, which should be able to deform up to 30% elastic strain, flexible sandwiches and corrugated laminates are recommended.

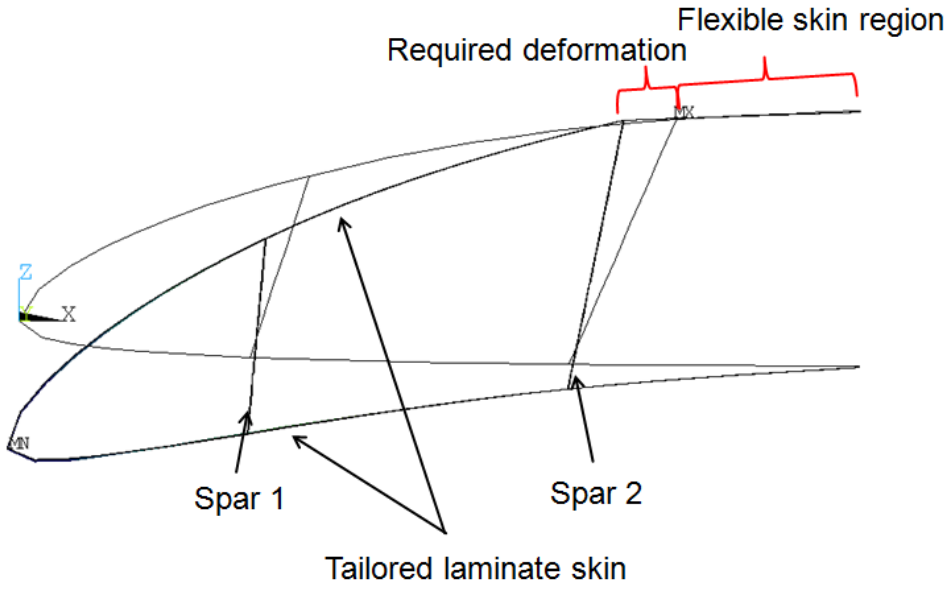

Figure 7.4.: The proposed morphing skin concept of the morphing leading edge

About the skin concept of the rest skins, the discussion starts from the current skin of sailplane wings, which is a sandwich skin consisted of two layers CFRP face sheets and foam core. However, this concept is not available for applying on the morphing wing due to the large strains on the face sheets. To reduce the large strains on skins but still maintain its equivalent bending stiffness, the skin concepts can be updated as tailored thin laminates consisting of CFRP, GFRP or hybrid laminates of both. Since for sailplane wings there is neither strict impact resistance nor large loading requirements. The CFRP laminate is selected as the baseline for its high structural performance.

As the short conclusion of the preliminary analyses, the morphing skin concept of the leading edge is tailored CFRP laminates with one section flexible sandwich.

7.2.2. Detailed Analyses and Correlations with Tests

The proposed morphing skin concept contains flexible sandwich and tailored thin laminate these two parts. In following sections, the numerical and experimental investigations about the flexible sandwich design will be presented at first. Then a brief discussion about the CFRP laminate design will be followed. In the end, a detailed morphing leading edge model containing designed morphing skins, actuation and interface system will be created and the results of the reshaping performance are to be presented.

Flexible Sandwich Design

As concluded in the skin concept study, the essential requirements to the flexible skin are low in-plane stiffness and sufficient out-of-plane stiffness. The requirement of low in-plane stiffness in concrete means that the skin is capable to be deformed to 30% elastic strain without material and structural failures. And the requirement of sufficient out-of-plane stiffness means the skin should be able to carry typical aerodynamic pressures without noticeable degenerations of surface quality.

Review of the existed materials, the typical maximal elastic stretching strain of materials like metals could be up to 0.3% and materials like plastics could be up to 3%. Although the hyperelastic materials like elastomer can be elastically deformed to more than 100%, their stiffness are generally over low, which are not the ideal candidates of morphing skins. Not limiting to these homogeneous materials, solutions to satisfy the conflicting requirements of compliance and stiffness can be the sandwiches and corrugated laminates. Compare these two skin concepts to each other, the sandwich has more freedoms in material design and can provide better surface quality for aerodynamics. Therefore the flexible sandwich is taken as the baseline and will be discussed in the further study. The concept of corrugated laminates is also a feasible solution but it will not be discussed in scope of the thesis.

The flexible sandwich is consisted of two elastomer face sheets and a honeycomb core (see Figure 7.5). As suggested by Bubert et al. (2010), in order to bond with the elastomer face sheets conveniently, the height of the inclined walls is designed to be slightly less than the vertical walls in the honeycomb core.

The geometry of the honeycomb core can be tailored to satisfy the required in-plane and out-of-plane material properties. Moreover, its Poisson's ratio can be designed to be zero, which is ideal for the one dimensional morphing wings. The honeycomb core with zero Poisson's ratio is called as accordion core, which is often discussed in the one dimensional morphing skin concepts. Material properties of the according core can be tailored through varying the geometry parameters like length of wall, cell angle, and thickness of wall. In the analytical equations derived by Gibson and Ashby (1997), the non-dimensional parameters are used to tailor the desired material properties. A figure of the accordion core is shown in Figure 7.6 and its geometry parameters are presented in Table 7.1.

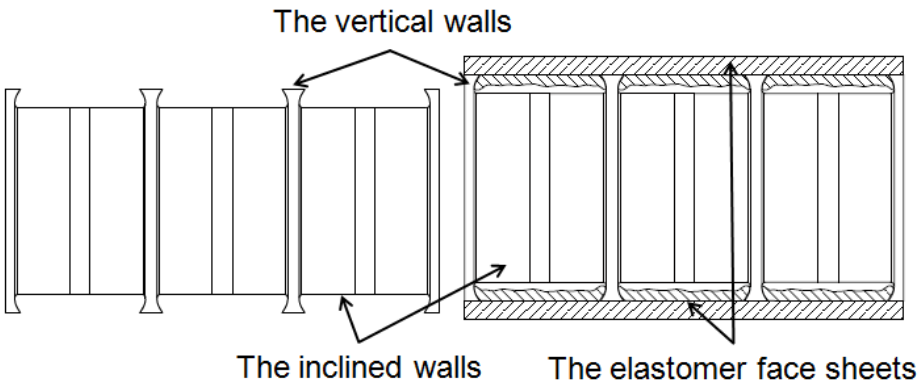

Figure 7.5.: The flexible sandwich concept [modified from Weinzierl (2013)]

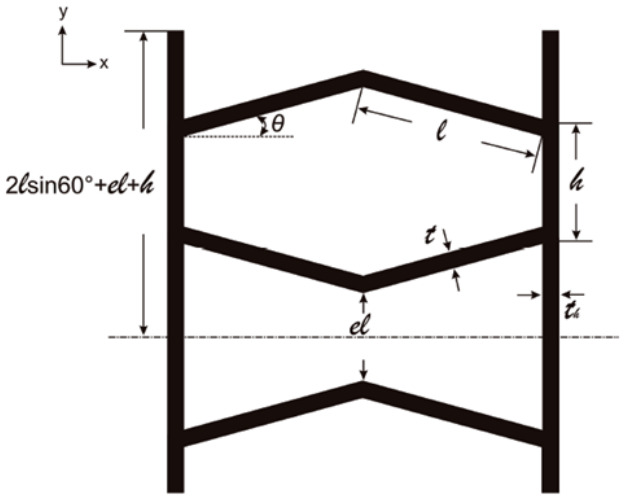

Figure 7.6.: The unit cell of the accordion honeycomb core [Xu (2012)]

Table 7.1.: Geometry parameters of the accordion honeycomb core

	Geometry parameters		Non-dimensional parameters
l	length of the inclined wall	$\alpha = \frac{h}{l}$	cell aspect ratio
h	length of the vertical wall	$\beta = \frac{t}{l}$	inclined wall thickness ratio
θ	cell angle	$\eta = \frac{t_h}{t}$	vertical wall thickness ratio
t	thickness of the inclined wall	$\gamma = \frac{b}{l}$	depth ratio
t_h	thickness of the vertical wall	e	interval distance ratio between unit cells

One important feature of the accordion honeycomb core is it can be stretched with relative large in-plane strain while maintaining small strain on materials, which is realized by bending of the internal walls. Depending on the chosen geometry parameters, the amplification factor of global to local strain can be varied from several to twenty or even more. According to the analytical equations of the strain amplification (Eq. 7.1 and 7.2), the strain

amplification factor is determined by three geometry parameters such as cell angle θ, ratio of inclined wall length to thickness β, and a constant κ related to Poisson's ratio. A large strain amplification factor can be realized by applying a large cell angle and a small ratio of inclined wall length to thickness.

$$\frac{\varepsilon_x^{global}}{\varepsilon_x^{local}} = \frac{|sin\theta|}{3\beta cos\theta} + \frac{1 + (\kappa + cot^2\theta)\beta^2}{1 + \frac{\beta}{3}|cot\theta|} \tag{7.1}$$

$$\kappa = 2.4 + 1.5\nu \tag{7.2}$$

In which, ν is the Poisson's ratio of the applied basic material.

To realize a 30% in-plane strain while maintaining material strain below 3%, the strain amplification factor should be larger than 10 and as preference to be around 30. The range of the design parameters can be briefly defined according to the geometry definitions of the flexible sandwich as follows. Considering the total length of the defined flexible skin is only 40 mm, the range of wall length is defined from 5 to 20 mm and the thickness range of the inclined wall is set from 0.5 to 1.5 mm. Additionally, the cell angel is defined in the range of 50 to 85 degree for the requirement of large strain amplification factor.

The results of the accordion core design are presented based on the student project of LLB [Weinzierl (2013)]. Totally three sets of parameter study are performed to estimate the proper parameter combination. In the first study, the thickness and the length of the inclined wall are constant ($t = 1\,mm,\ l = 10\,mm$) while varying only the cell angle. The material local strain is greatly influenced by the cell angle. It can be observed in Figure 7.7 (a), with more than 70 degree cell angle the local strain can be smaller than 3% as required. In the second study, the cell angle is set to 79 degree and the inclined wall length is 10 mm. The local strain can be further reduced to be below 1% when the wall thickness is varied to be 0.5 mm. In the third study, two constants are the cell angle 79 degree and the inclined wall thickness 0.5 mm. Through varying the wall length from 5 to 20 mm, it is found a local strain below 1% can be easily achieved by applying more than 10 mm inclined wall (Figure 7.7 (b)).

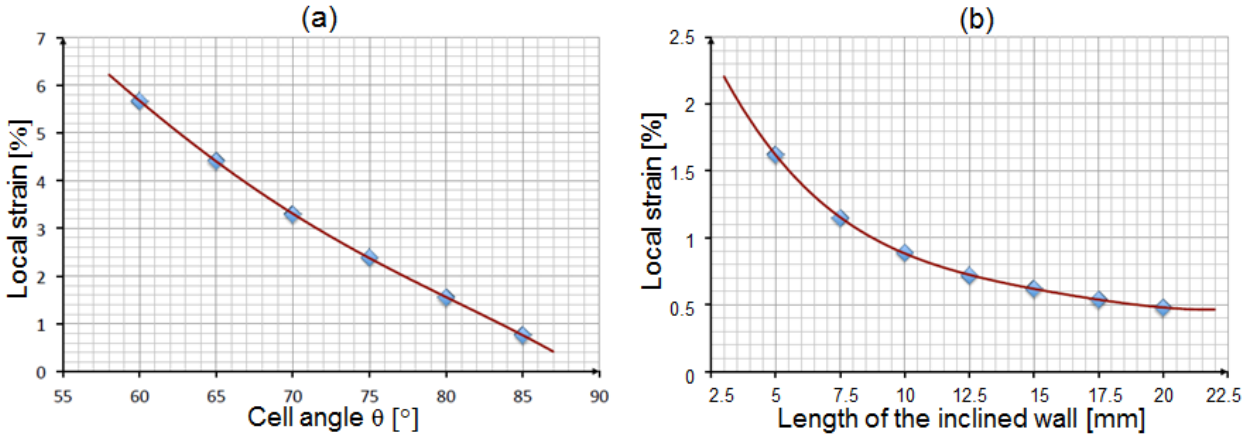

Figure 7.7.: The value of local strain related to the cell angel (a) and the inclined wall length (b) [Weinzierl (2013)]

Through these parameter studies, the geometry parameters are estimated as cell angle 79 degree, wall thickness 0.5 mm and wall length 16 mm as the most promising solution. Under the defined parameter combination, the maximal material strain is around 0.6% for 30% in-plane structural stretching, which indicates a strain amplification factor of 50. Benefit by the large strain amplification factor, plenty of basic materials for the accordion core can be selected to accommodate the elastic strain requirement. For instance, a potential material for the honeycomb core is thermal plastic PA2200. It has satisfactory mechanical properties and can be easily manufactured by the 3-D print technology. Some essential material parameters of PA2200 are tensile modulus 1700 MPa, failure strain 24% and yield strain around 2.8%.

Based on the determined geometry, a numerical model is created. There are five unit cells placing in the chord direction to fit the defined 40 mm flexible region and also five unit cells in the span direction with dimension of 250 mm (Figure 7.8).

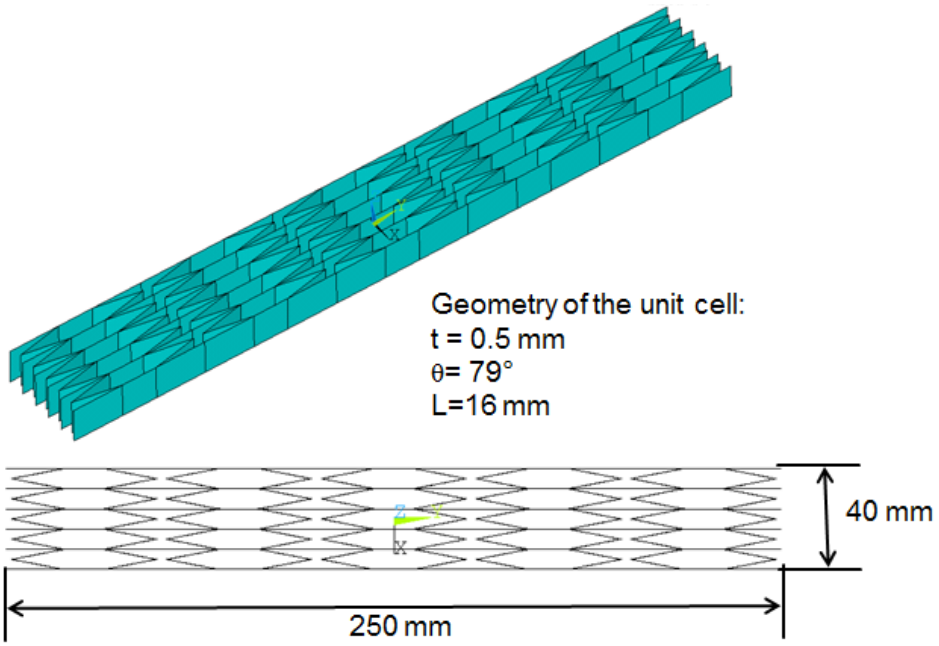

Figure 7.8.: The designed accordion honeycomb core

After fulfilling the requirement of in-plane compliance, the tailoring of out-of-plane stiffness is performed. The aerodynamic pressure on the skin is assumed to be 450 N/m^2, which is twice of the dynamic pressure under the condition of maximal gliding speed 200 km/h at 1000 m. This pressure should be carried by the flexible sandwich containing two silicone face sheets. The major parameter to determine the out-of-plane stiffness of the flexible sandwich is its thickness. In a parameter study with varying thickness from 4 to 15 mm, the maximal deflection is reduced from 0.39 to 0.07 mm accordingly. Since there is no specific requirement to the maximal surface deflection on skins. An empirical assessment of the maximal allowable deflection under 0.1 mm is set here. To satisfy the maximal deflection requirement, the thickness of the sandwich is taken as 10 mm. But actually, the thickness of the sandwich is preferred to be as thin as possible for better integrations with the conventional skins.

In the end, these parameters are further tuned through bending tests of the designed flexible sandwich. In these tests, the cell angle and the inclined wall length are set as constant

and the wall thickness and the honeycomb core thickness are design variables. The bending test is defined based on the reshaping behavior of the flexible skin region in the leading edge. In which, one side of the flexible skin is fully fixed and the other side is applied with in-plane tension and out-of-plane bending. These loads are represented as 5.4 mm in-plane displacement and 9.4 mm vertical displacement. Confirmed through the bending tests, the most promising skin parameters are 10 mm honeycomb thickness and 0.5 mm inclined wall thickness. With the parameter combination, the maximal strain on the honeycomb core is around 0.8% in the numerical tests (see Figure 7.9).

Based on these parameter studies, the parameters of the accordion honeycomb core are basically determined. A demonstrator of the flexible sandwich will be manufactured and tested in the further stage.

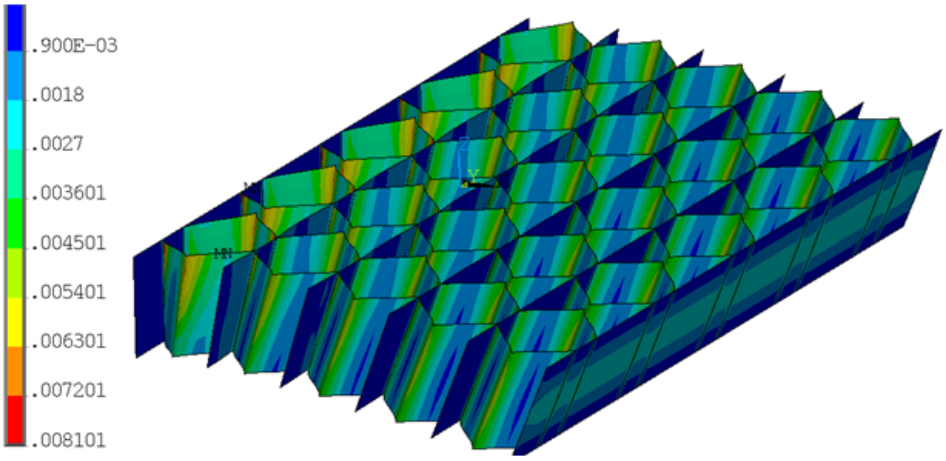

Figure 7.9.: The maximal strain on the designed accordion honeycomb core

Correlations with Tests

In order to verify the mechanical behavior of the designed flexible sandwich, tensile and bending tests are planned for the manufactured specimens. The set up of the tensile test is referred to DIN527-4. According to the standard, the length of the specimen is taken as 235 mm referring to its 10 mm thickness. Its width is estimated to equal to one unit cell width of 40 mm (see Figure 7.10).

The applied loading cell has measurement range up to 20 N with resolution of 0.01 N, which is appropriate for the tests of the compliant accordion honeycomb core. As the planned tests, three loading/unloading cycles up to around 30% strain are performed on three specimens at first, then an extreme large stretching to material rupture is performed on one of the specimens.

Observed from the stress and strain relations of specimens, the relation of stress and strain presents linearity up to 30% strain. The residual strain is observed in the cycle tests, which is around 3% between the first and the second cycle. Converting the residual strain to the material strain, it is actually only around 0.06% as a result of the strain amplification factor 50. Estimated from the tests, the tensile modulus of the designed accordion honeycomb core is 0.0095 MPa, which can be quite well correlated with the analytical and numerical re-

sults (Table 7.2). One specimen is stretched to more than twice of its initial length but still no crack on the specimen is observed (Figure in section B.5 of Appendix). As presented in the large stretching test, the linear relation of stress to strain can be extended to be around 150%.

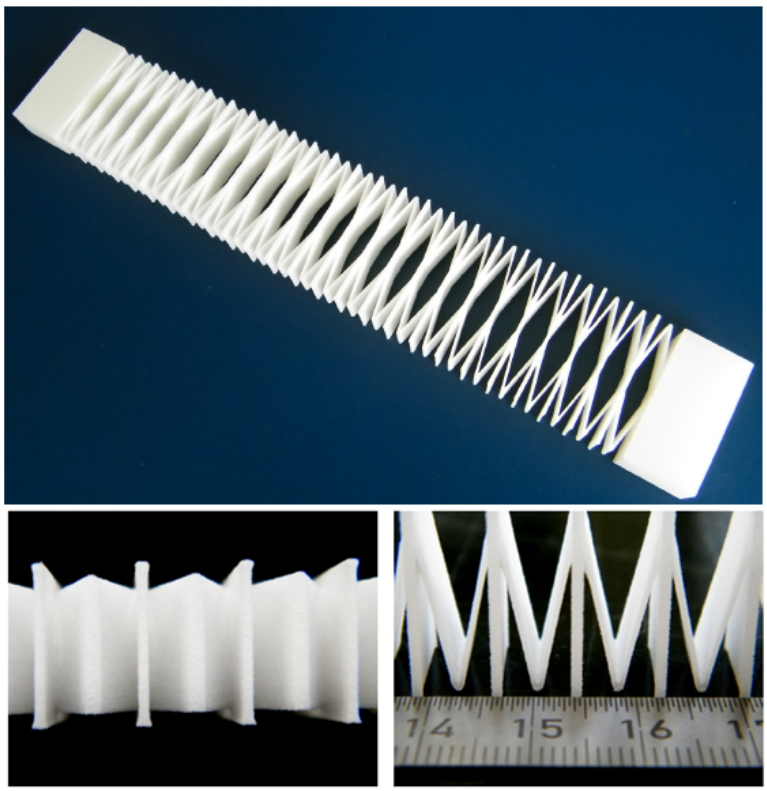

Figure 7.10.: The manufactured accordion honeycomb core for tensile tests [Weinzierl (2013)]

As shown in the tensile tests, the designed accordion honeycomb core demonstrates its compliance with quite low tensile modulus. Due to the fact of over low stiffness, performing bending test of the accordion honeycomb core is quite difficult. Actually in the flexible sandwich, the accordion honeycomb core is mainly used to provide the distance between two elastomer face sheets to achieve a sufficient bending stiffness. Therefore it is not necessary to perform bending tests on the accordion honeycomb core.

Table 7.2.: Tensile modulus of the designed accordion honeycomb core

Analytical result	Numerical result	Experiment result
0.0102 MPa	0.0092 MPa	0.0095 MPa

After the experimental verifications of the accordion honeycomb core, a demonstrator of the flexible sandwich is manufactured (see Figure 7.11). The width of the demonstrator is 40 mm as defined and the length is around 150 mm due to the dimension limitation of the 3-D print technology. With the elastomer face sheets, the flexible skin demonstrates a sufficient bending stiffness through a simple cantilever test under its own weight (see the Figure B.6 of Appendix).

Verified through the numerical and experimental investigations about the flexible sandwich, the requirements of in-plane compliance and out-of-plane stiffness can be considered as been satisfied. The focus of the following works is on tailoring the thin CFRP laminate and evaluating the performance of the designed morphing wing systems.

Figure 7.11.: A demonstrator of the flexible sandwich [Weinzierl (2013)]

Detailed Numerical Analyses

As mentioned before, the conventional sandwich skin of the sailplane wing is to be replaced by the tailored CFRP laminates for the reason of relative large bending deformation. The selected UD-CFRP laminate consists of carbon fiber T300 (HT) and epoxy matrix with fiber volume fraction of 45%, which can be manufactured through hand lamination. The material properties of the selected laminate are listed in Table 7.3. It should be mentioned that the values of yield strengths and strains are quite conservative in the definitions of Luftfahrt-Bundesamt (LBA).

The tailoring of fiber orientation and stack sequence is following the methods mentioned in Herencia et al. (2006) and Andrykowski (2012). Plies in the middle are oriented in the chord direction to provide the necessary in-plane stiffness and the outer plies are orientated in the span direction for providing sufficient spanwise bending stiffness. The flexible spar has to sustain the airfoil shape in reshaping and its roots should be flexible for bending. To realize these functions, a layout design of the flexible spar contributed by Müller (2000) is followed here. The laminate layouts of the tailored skin and the flexible spar are listed in Table 7.4.

Table 7.3.: Material properties of the UD-CFRP laminate (referring to the definitions of Luftfahrt-Bundesamt (LBA))

		Yield strength [MPa]		Yield strain [%]	
E_{11}	86000 MPa	$\sigma_{11,t}$	420	$\varepsilon_{11,t}$	0.55
E_{22}	5000 MPa	$\sigma_{11,c}$	420	$\varepsilon_{11,c}$	0.55
ν_{12}	0.28	$\sigma_{22,t}$	13.6	$\varepsilon_{22,t}$	0.55
G_{12}	3000 MPa	$\sigma_{22,c}$	34	$\varepsilon_{22,c}$	1.00
		τ_{12}	19.6	γ_{12}	0.70
t : tensile load					
c : compressive load					

Table 7.4.: Laminate layout design

Tailored CFRP skin	90/0/0/90
Tailored CFRP skin, in the interaction region	90/90/0/0/90/90
Flexible spar	0/+45/-45/-45/+45/0
1. For the tailored skin: 0 degree is the chord direction, see Figure 7.12	
2. The interaction region is reinforced with 0.5 mm steel plate	
3. For the flexible spar: 0 degree is the span direction	

With the above definitions, a detailed leading edge model is then created in ABAQUS with involving the interactions between the horn and skin (Figure 7.12). The software ABAQUS is chosen for its advanced performance in geometry nonlinear and contact analyses. The dimension of this model is 1000 mm in the span direction, which is chosen for placing two horns. The profile of the horn's cross section is created through an interpolation between the defined initial and final configurations of the leading edge (see Figure 7.13).

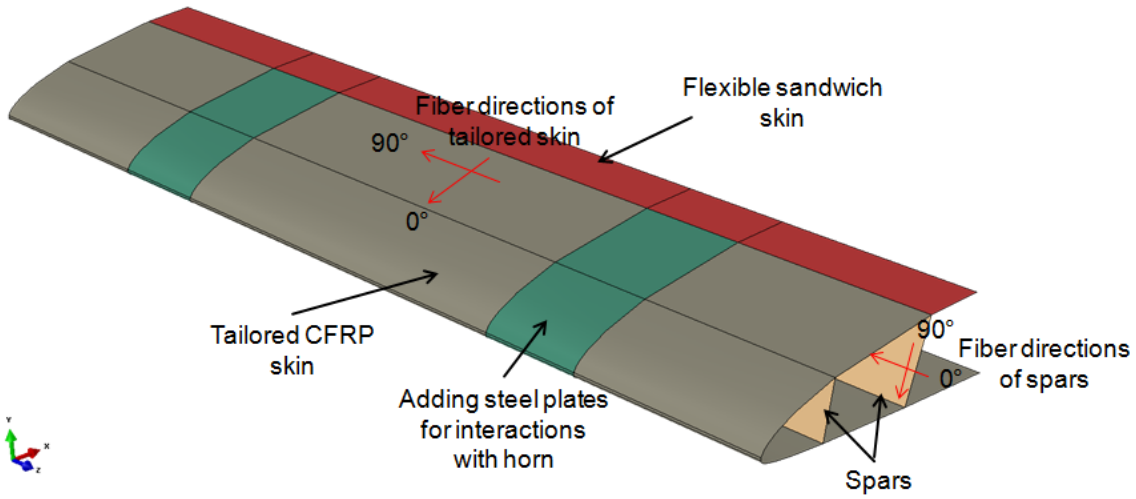

Figure 7.12.: The detailed morphing leading edge FEM model [Kraus (2013)]

As boundary conditions, the upper and lower skins are fully clamped at their sides connecting with the main spars. Both horns are rotated to 90 degree around their middle axes to actuate the reshaping.

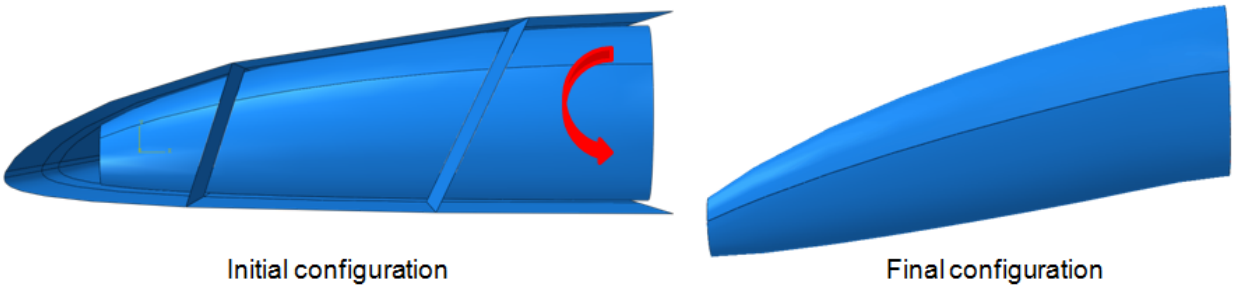

Figure 7.13.: The implemented horn in the FEM model

The results of the detailed FEM analyses are presented based on the work of Kraus (2013), which is a student project guided by author. The analysis results demonstrate the required the deformation can be achieved using the proposed morphing skin (see Figure 7.14). Slightly local out-of-plane convex can be observed on the contact region caused by the loading of the stiff horns. The maximal in-plain strain on the flexible sandwich is around 20%, which is actually lower than the predicted value in the preliminary analyses. It can be concluded from the reshaping analyses, the designed flexible sandwich can well satisfy the functional and structural requirements.

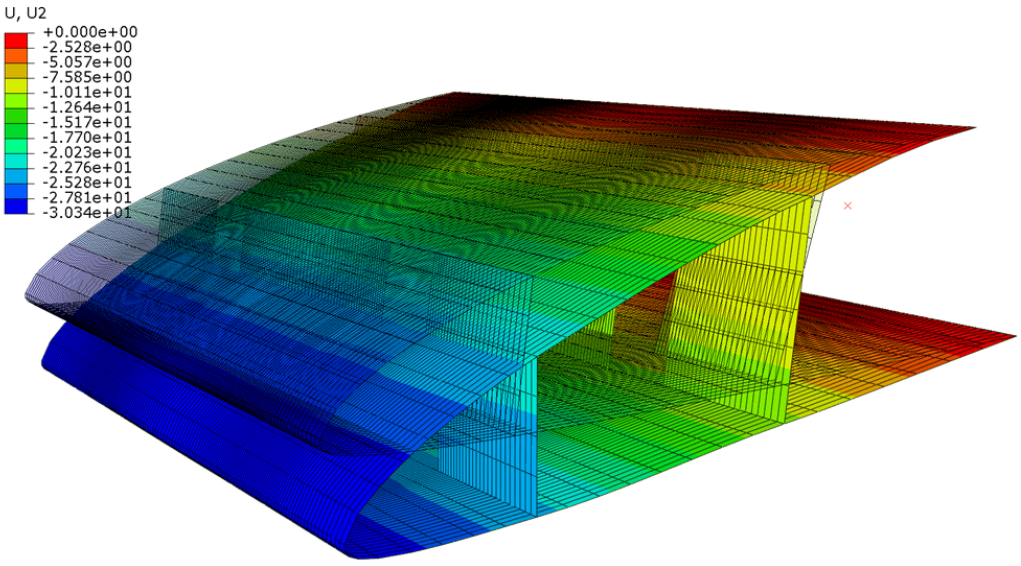

Figure 7.14.: The deformation of the morphing leading edge

Observing the stress and strain results of the tailored CFRP skins and the flexible spars in the whole reshaping procedure, it is found the extreme values are presented at the horn

tip and the nearby skin in the initial contact stage. The maximal stress in the fiber direction is quite close to the defined yield strength, and the value in the transverse direction is even beyond the yield strength (tables in section B.6 of Appendix). These extreme values are concentrated at the contact region in the initial phase only. With the contact area increasing they are reduced to be quite low values (Figure 7.15). The local over large stress and strain values are mainly related to the not accurate horn profile design. To avoid the strength problem, the cross section of the horn shall be slightly adjusted to achieve smoother contacts and larger contact areas.

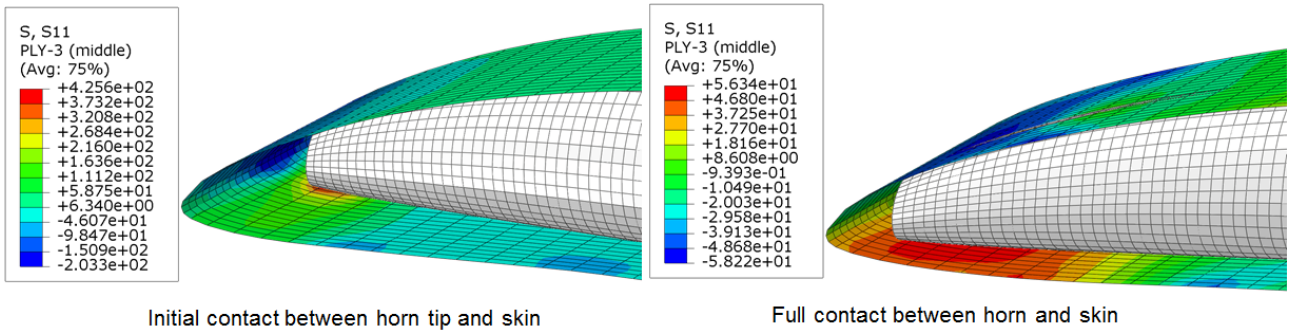

Figure 7.15.: The stress distribution at the contact region in different reshaping stages

Through this numerical study, two disadvantages of the actuation method using eccentuators are found. First, the requirements of geometry accuracy on design and manufacturing of the horn shall be quite high to avoid the local stress concentration in the contact areas. Second, the horn introduces a local loading at the skin, which causes local small convex and degenerations of the surface quality. Based on these two facts, the actuation concept of eccentuator seems to be less appropriate than the alternative concept of hinged kinematic structures.

About the actuation force, the peak value is around 1200 N, which is presented in the initial contact stage. The maximal actuation force presents only shortly in the initial deforming stage. With increasing of the contact area, the actuation force is rapidly reduced and reaches around 70 N in the final configuration.

7.2.3. Summary

With help of the defined representative model, a hybrid morphing skin concept is derived for the sailplane morphing leading edge. Thanks to the high freedoms on material tailoring of the flexible sandwich concept, the desired in-plane compliance and sufficient out-of-plane stiffness are realized readily. More important, the numerical results can be well correlated with the experimental investigations of specimens.

With the growing understanding of the functional and structural requirements on the flexible sandwiches, the accordion core could be further adjusted to be smaller in cell size and height. By doing so, the difficulty of integration with the leading edge will be reduced.

The bonding between the accordion core and the elastomer face sheets is not well solved in the investigation. As observed in the medium amplitude stretching tests, some local

debonding on the manufactured sandwiches is appeared, which requires further improvements.

8. Conclusion and Outlook

The morphing skin design is actually an inverse design process with knowing objectives derived from functional, structural and manufacturing requirements to determine the design parameters range from geometry, boundary conditions and material properties. One of the major difficulties in the handling of this task is lacking of appropriate methods to correlate design variables with the objectives, which is developed in this thesis. Besides, the related works like numerical analyses to derive morphing skin concepts, experimental characterizations of morphing skin materials, and correlations of the numerical predictions with testing results are also investigated.

Mechanically Reconfigurable Reflectors

In most published works, the morphing skins of mechanically reconfigurable reflectors are mostly derived through qualitative analyses and assessments based on engineering experience. To reduce the dependence on experience and make the assessments of different kinds of design parameters conveniently, the correlation method with combining mathematic shape expressions and strain energy expressions is developed, which is one of the major contributions of the thesis. As complements to the correlation method, representative models are also initialized, which are used in combing with the correlation method to define the design parameters of morphing skins.

The developed method is fully demonstrated on the reflector morphing skin design of the mechanically reconfigurable reflector. As the first step, the morphing skin design is performed on the unit cell models, in which the major design parameters such as size, thickness, configuration, boundary conditions, and material properties are evaluated to figure out feasible design solutions. Then the derived preliminary morphing skin concepts are further evaluated and adjusted on the medium size models with considering complexer reshaping scenarios. In the end, the the most promising morphing skin concept is implemented on the full size models and tested through reshaping tasks derived from practice applications for gaining further insights.

One of the highlights in the reshaping analyses is the comparison between the linear and nonlinear behavior of the designed morphing skin. Although the structural performance of the designed concept has high similarity between its geometry linear and nonlinear analyses, the nonlinearity in structural performance can't be ignored especially for the reason of high reshaping accuracy. In oder to save the high computation cost in the tasks of stroke length optimization, the method of multi-step linear analyses with stepwise geometry update is developed. As verified through the numerical and experimental analyses, the developed method offers quite the same results to the stroke length optimization with full nonlinear analyses and demands significant less computation cost.

On the material characterizations of the selected reflector morphing skin biax-CFRS composites, bending and shear tests are performed for the interested in-plane and out-of-plane material properties. The presented results have shown the biax-CFRS has a relative large

ratio of bending to shear stiffness as preferred, which indicates the biax-CFRS is one of the most advantageous materials for the reflector morphing skin. To offer more options to the reflector morphing skin concepts, other fabrics with larger area density and larger space between fiber bundles shall be characterized in future. As not finished works in the thesis, the observed fiber microbuckling in the bending tests should be further investigated to identify the influence of different parameters like fabric geometry and different manufacturing processes. These analyses will be quite helpful to find out better reflector morphing skin material candidates with larger tolerance to fiber microbuckling.

According to the designed reflector morphing skin concept, a scale down technology demonstrator of the mechanically reconfigurable reflector is manufactured correspondingly. The reshaping tests are performed on the demonstrator and the numerical model for result correlations. Initially the reshaping results between them are not highly correlated due to geometry distortions on the demonstrator introduced in manufacturing and assembling. Afterwards with introducing the geometry distortions to the numerical model, the updated reshaping results are then quite well correlated with the experimental results. Through the investigations on the demonstrator, the feasibility of the proposed reflector morphing skin and the interface and actuation systems are validated. A further technology demonstrator, on which the update skin concept and improvements on manufacturing and assembling shall be applied, is proposed for the next stage.

Morphing Aircraft Wings

On the extending application of the sailplane wing morphing skin design, material design methods are further explored. The correlations between the design parameters and reshaping performance are also performed on the representative model derived from the specific functional and structural requirements. With help of the representative model, a hybrid morphing skin concept of tailored CFRP laminate and flexible sandwich is defined. In the tailoring of the flexible sandwich, geometry parameters of the sandwich core are varied to realize the required features of in-plane compliant and out-of-plane stiff. In sample tests of the designed sandwich core, the latest prototype manufacturing technology 3-D print is applied, which indicates great potentials in exploring further morphing skin concepts. In the detailed numerical model, the designed morphing skin, actuation and interface systems are all implemented and their performance are evaluated in reshaping analyses. As the major output of the analyses, the feasibility of the proposed skin concept is proved. Besides, problems like skin debonding failures and high actuation force are also pointed out, which are mainly related to the proposed actuation and interface systems. In short, the technology maturity level of the proposed morphing skin concept is still low and building a demonstrator is not recommended in this stage. To drive the technology maturity level to be higher level, other morphing skin concepts like corrugated laminates and actuation systems like hinged kinematic mechanisms and compliant structures shall be investigated and compared in further investigations.

Outlook

As the outlook to morphing skin development, the gained knowledge and developed methods shall be further developed on broader applications. For instance, morphing automotive skin, which can be reshaped according to actual aerodynamic conditions and aesthetic design, is one of the potential applications. A further potential application of morph-

ing wings is morphing automotive spoiler. Compare with the morphing aircraft wing, the critical structural requirements can be released on this application, which enable a shorter developing period and more radical design concepts. Benefits of the application are the aerodynamics and drive dynamics could be considerably improved. With these various applications, the technology of morphing structures will be developed to be higher technological readiness level and be presented on more and more practice applications in future.

A. Bibliography

Online resource, a. URL http://www.akaflieg.tu-darmstadt.de/geschichte/d-40/.

Online resource, b. URL http://www.deutsches-museum.de/flugwerft/sammlungen/segelflugzeuge/mue-27/.

Online Resource, c. URL http://www.akaflieg.vo.tu-muenchen.de/index.php/mue-31.

Online resource, d. URL http://www.uni-stuttgart.de/akaflieg/projekte/die-fs-projekte/fs-29-tf.html.

ACARE. Acare 2008 addendum to the strategic research agenda. URL http://www.acare4europe.com/docs/ACARE_2008_Addendum.pdf, 13-03-2009.

N. C. Albertsen, K. Pontoppidan, and S. B. Soerensen. Beam optimization by means of a reconfigurable reflector with true bending stiffness. In *IEE conference publication*, 1994.

G. Doro Altan and F. Rispoli. Multi-shaped beams antennas design and technology for futrther communication satellites. *ANN TELECOMMUN*, Vol. 44:489–500, 1989.

Martin Andrykowski. Inverses Materialdesign eines hybriden Faserverbundlaminats für eine formvaribale Flügelhaut. Semester thesis, Inverses Materialdesign eines hybriden Faserverbundlaminats für eine formvaribale Flügelhaut, 2012. Student Project Supervised by Author.

Antenna-Theory. Online source. URL www.antenna-theory.com.

Manuel Armbrüster. Entwicklung eines nachgiebigen Rippendesigns für eine flexible Tragflügelhinterkante. Diploma thesis, Technische Universität München, 2012. Student Project Supervised by Author.

D. Baker and M.I. Friswell. Design of a compliant aerofoil using topology optimization. In *Smart Materials and Structures*, Toronto, Ontario, Canada, 2006.

Constantine A. Balanis. *Antenna Theory: Analysis Design*. ISBN 0-471-66782-X. John Wiley & Sons, Inc., 2005.

S. Barbarino, W. G. Dettmer, and M. I: Friswell. Morphing trailing edges with shape momory alloy rods. In *21st International Conference on Adaptive Structures and Technologies (ICAST)*, 2010.

M. R. Barnes. Form finding and analysis of tension structures by dynamic relaxation. *International Journal of space structures*, Vol. 14, No.2:89–104, 1999.

J.D. Bartley-Cho, D.P. Wang, C.A. Martin, J.N. Kudva, and M.N. West. Development of high-rate, adaptive trailing edge control surface for the smart wing phase 2 wing tunnel model. *J Intell Mat Sys and Struc*, Vol 15 (4):279–291, 2004.

E. A. Bubert, B. K. S. Woods, K. Lee, C. S. Kothera, and N. M. Wereley. Design and fabrication of a passive 1d morphing aircraft skin. *Journal of intelligent material systems and structures*, Vol. 21:1699–1717, 2010.

D. Cadogan, T. Smith, F. Uhelsky, and M. MacKusick. Morphing inflatable wing development for compact package unmanned aerial vehicles. In *American Institute Aeronautics and Astronautics*, 2004.

L.F. Campanile. *Adaptive Structures: Engineering Applications*. John Wiley & Sons, Ltd, 2007.

C. Cappellin. Flexible reflector antennas in the context of european telecommunications strategy, a feasible study. Technical report, TICRA engineering consultants, 2007.

C. Cappellin and K. Pontoppidan. Feasibility study and sensitivity analysis for a reconfigurable dual reflector antenna. In *3rd European Conference on Antennas and Propagation (EUCAP)*, volume 1, pages 2017–2021, 2009.

C. Cappellin, K. Pontoppidan, and H. H. Viskum. Reconfigurable dual reflector for a realistic mission scenario in ku band. In *31st ESA Antenna Workshop Digest*, 2009.

Wacker Chemie. Silicone rubber adhesives for outer space. Online resource. URL http://www.wacker.com/cms/media/publications/downloads/6427_EN.pdf.

P.J.B. Clarricoats and H. Zhou. Design and performance of a reconfigurable mesh reflector antenna, part 1: antenna design. *IEE Proceedings-H*, Vol. 138:485–492, 1991a.

P.J.B. Clarricoats and H. Zhou. Design and performance of a reconfigurable mesh reflector antenna, part 2: antenna performance. *IEE Proceedings-H*, Vol. 138:493–496, 1991b.

P.J.B. Clarricoats, A.D. Monk, and H. Zhou. Array-fed reconfigurable reflectors for spacecraft systems. *Electronics Letters*, Vol. 30(8):613–614, 1994.

L. da Rocha-Schmidt and H. Baier. Morphing skins and gap covers for aerodynamics control surfaces. In *Deutscher Luft- und Raumfahrtkongress*, 2013.

L. Datashivili, H. Baier, and N. Natrath. The deployable precision shell-membrane reflector smart. In *Proc. Euro. Conf. on Antennas and Propagation, Eucap 2006*, Nice, 2006.

L. Datashivili, H. Baier, and J. Schimitschek. Massive shape adaptivity in shell-membranes. In *Proc. Int. Conf. on Comput. and Exp. Science*, 2008.

L. Datashvili. Orthogonal wire grid modeling and fem investigations (reconfigurable reflector concept by ticra). Technical report, Technical Note TN-LLB-Recora-LD-014, 2008.

L. Datashvili. Review and evaluation of the existing designs / technologies for space large deployable apertures. In *nternational Scientific Conference on Advanced Lightweight Structures and Reflector Antenna*, 2009.

L. Datashvili and H. Baier. Space applicable antenna reflectors with flexible shell-membrane reflecting surface. In *International Scientific Conference on Advanced Lightweight Structures and Reflector Antennas*, 2009.

L. Datashvili, H. Baier, J. Schimitschek, M. Lang, and M. Huber. High precision large deployable space reflector based on pillow-effect-free technology. In *48th AIAA/ASME/ASCE/AHS/ASC Structures, Structural Dynamics, and Materials Conference*, 2007.

L. Datashvili, H. Baier, and J. Hoffmann. Mechanically reconfigurable and massively shape morphing space structures. In *11th European Spacecraft Structures, Materials and Mechanical Testing Conference (ESSMMT)*, 2009.

L. Datashvili, H. Baier, B. Wei, J. Hoffmann, E. Wehrle, L. Schreider, C. Mangenot, J. Santiago-Prowald, L. Scolamiero, and J.-C. Angevain. Mechanical investigations of in-space-reconfigurable reflecting surfaces. In *ESA Antenna Workshop 2010, Noordwijk*, 2010.

L. Datashvili, H. Baier, B. Wei, S. Endler, and L. Schreider. Design of a morphing skin using flexible fiber composites for space-reconfigurable reflectors. In *54th AIAA/ASME/ASCE/AHS/ASC Structures, Structrual dynamics, and Material Conference*, 2013.

The design of morphing aircraft. Online source, 2007. URL http://www.aer.bris.ac.uk/research/morphing/morph-main.html.

J. Diani, B. Fayolle, and P. Gilormini. A review on the mullins' effect. *European Polymer Jounral*, Vol. 1:601–612, 2009.

DIN14125. Fiber-reinforced plastic composites – determination of flexural properties.

DIN527-4. Bestimmung der zugeigenschaften din 527-4.

DIN53362. Testing of plastic films and textile fabrics (excluding nonwovens), coated or not coated with plastics - determination of stiffness in bending - method according to cantilever.

DIN65466. Aerospace-fibre reinfored plastics-testing of unidirectional laminates-determination of shear strength and shear modulus in tension.

Yubiao Du. FEM investigations about actuator distribution of reconfigurable antenna with concept orthogonal wire mesh. Semester thesis, Technische Universität München, 2010. Student Project Supervised by Author.

S. Endler, H. Baier, and L. Datashvili. Nano-fillers in fiber reinforced polymers for performance enhancement of satellite structures. In *European Conference on Spacecraft Structures, Materials & Enviromental Testing*, Noordwijk, Netherlands, 2012.

S. Endler, B. Wei, M. Friemel, N. Maghaladze, G. Reinicke, and L. Datashvili. Reconfigurable reflector demonstrator manufacturing and shape measurements, technical note TN9. Technical report, Lehrstuhl für Leichtbau, Technische Universität München, 2014.

J. S. Flanaganl, R. C. Strutzenberg, R. B. Myers, and J. E. Rodiran. Development and flight testing of a morphing aircraft, the nextgen mfx-1. In *48th AIAA/ASME/ASCE/AHS/ASC Structures, Structural Dynamics, and Materials Conference*, 2007.

Jonathan P. Gardner, John C. Mather, Mark Clampin, Rene Donyon, Matthew A. Greehouse, Heidi B. Hammel, and etc. The James Webb Space Telescope. *Space Science Reviews*, Vol. 123:485–606, 2006.

A. Gasser, P. Boisse, and S. Hanklar. Mechanical behaviour of dry fabric reinforements. 3d simulations versus biaxial tests. *Computational Materials Science*, Vol. 17:7–20, 2000.

Lorna J. Gibson and Michael F. Ashby. *Cellular Solids Structure and Properties*. Cambridge University Press, 1997.

S. Govindjee and J. Simo. A miro-mechanically based continuum damage model for carbon black-filled rubbers incorporating mullins' effect. *Journal of the Mechanics and Physics of Solids*, Vol. 39:87–112, 1991.

Gridshell. Online resoure. URL http://www.aaron-grey.com/.

Kaijun Gu. High performance dual shaped reflector antennas for earth stations. Master's thesis, Faculty of Engineering and Applied Science, Memorial University of Newfoundland, 1995.

JAC Harwood and AR. Payne. Stress softening in nature rubber vulcanizates. iv. unfilled vulcanizates. *J Appl Polymer Sci*, Vol. 10:1203–1211, 1966.

Julian Heim. Auslegung eines Compliant Mechanism für eine formvariable Flügelverderkante. Semester thesis, Technische Universität München, 2012. Student Project Supervised by Author.

J. E. Herencia, P. M. Weaver, and M. I. Friswell. Local optimization of long anisotropic laminated fibre composite panels with t shape stiffeners. In *47th AIAA/ASME/ASCE/AHS/ASC Structures, Structure Dynamics, and Materials Conference*, number 2171, 2006.

Sebastian Von Hoerner and Woon-Yin Wong. Improved efficiency with a mechanically deformable subreflector. *IEEE transactions on antennas and propagation*, Vol. AP-27:720–723, 1979.

Jügen Hoffmann. *Charakterisierung faserverstärkter Elastomere für formvariable Strukturflächen*. PhD thesis, Technischen Universität München, 2012.

Denis Howe. *Aircraft conceptual design synthesis*. ISBN 1 86058 301 6. Professional Engineering Publishing, 2000.

IEEE. Ieee standard definitions of terms for antennas. *IEEE Transactions on Antennas and Propagation*, Vol. AP-31, No.6, Part II:–, 1983.

Intermodulation. Online resource. URL http://en.wikipedia.org/wiki/Intermodulation.

A.K. Jha and J.N. Kudva. Morphing aircarft concepts, classifications, and challenges. In *Smart structures and materials and nondestructive evalutaion for health monitoring and diagnostics conference*, 2004.

F. L. Jimenez. *Mechanics of thin carbon fiber composites with a silicone matrix*. PhD thesis, California Institute of Technology, 2011.

Robert M. Jones. *Mechanics of Composie Materials*. ISBN 1-56032-712-X. Taylor & Francis, Inc., 1998.

M. Kintscher, H.P. Monner, and M. Wiedemann. First results of the groundtest of a fibre reinforced continuous flexible gap and stepless smart droop nose for high lift applications. In *Deutscher Luft- und Raumfahrtkongress*, pages 475–485, 2011.

S. Kota, J. Hetrick, R. Osborn, D. Paul, Ed Pendleton, P. Flick, and C. Tilmann. Design and application of compliant mechanisms for morphing aircraft structures. *Smart Structures and Materials 2003: Industrial and Commerical Applications of Smart Structures Technologies*, Vol. 5054, 2003.

S. Kota, J. Hetrick, F. Russel, and R. Osborn. Adaptive structures: Moving into mainstream. In *Aerospace America*, 2006.

David Kraus. Auslegung einer formvariablen Tragflügelvorderkante eines Hochleistungssegelflugzeugs. Semester thesis, Technische Universität München, 2013. Student Project Supervised by Author.

J.N. Kudva. Overview of the darpa smart wing project. *J intell Mat Sys and Struc*, Vol 15 (4): 261–267, 2004.

Peter R. Lawson and Jui Lin Yen. A piecewire deformable subreflector for compensation of cassegrain main reflector errors. *IEEE transactions on antennas and propagation*, Vol. 36: 1343–1350, 1988.

Lockheed. Online resource. URL http://www.lockheedmartin.com/skunkworks.

A.-C. Long, editor. *Design and manufacturing of textile composites*. Woodhead Publishing, 2005.

M. H. Love, P. S. Zink, R. L. Stroud, D. R. Bye, S. Rizk, and D. White. Demonstration of morphing technology through ground and wing tunnel tests. In *48th AIAA/ASME/ASCE/AHS/ASC Structures, Structural Dynamics, and Materials Conference*, 2007.

N. Di Matteo, S. Guo, S. Ahmed, and D. Li. Desgin and analysis of a morphing flap structures for high lift wing. In *51st AIAA/ASME/ASCE/AHS/ASC Structures, Structural Dynamics, and Materials Conference*, Orlando, Florida, April 2010.

Bob Matthews. Composite materials (analysis). Online soure. URL http://www.structsource.com/pdf/composite.pdf.

C. K. Maucher, B. A. Grohmann, P. Jänker, A. Altmikus, F. Jensen, and H. Baier. Actuator design for the active trailing edge of a helicopter rotor blade. Online resource. URL http://www.researchgate.net/publication/228659818_Actuator_design_for_the_active_trailing_edge_of_a_helicopter_rotor_blade.

Microwave. Online source. URL www.en.wikipedia.org/wiki/Microwave.

H.P. Monner, D. Sachau, and E. Breitbach. Design aspects of the elastic trailing edge for an adaptive wing. In *RTO AVT specialists' meeting "Structure Aspects of flexible Aircraft Control"*, Canada, 1999.

H.P. Monner, M. Kintscher, T. Lorkowskin, and S. Storm. Design of a smart droop nose as leading edge high lift system for transportation aircrafts. In *50th AIAA/ASME/ASCE/AHS/ASC Structures, Structural Dynamics, and Materials Conference*, 2009.

R. Morishima, S. Guo, and S. Ahmed. A composite wing with a morphing leading edge. In *51st AIAA/ASME/ASCE/AHS/ASC Structures, Structural Dynamics, and Materials Conference*, Orlando, Frorida, April 2010.

Dietmar Müller. *Das Hornkonzept Realisierung eines formvariablen Tragflügelprofils zur aerodynamischen Leistungsoptimierung zukünftiger Verkehrsflugzeuge*. PhD thesis, Fakultät Luft- und Raumfahrttechnik der Universität Stuttgart, 2000.

Michael Müller. *Modeling of the structure-optics-interaction in large astronomical telescopes*. PhD thesis, Technischen Universität München, 2005.

L. Mullins. Softening of rubber by deformation. *Rubber Chem Technol*, Vol. 42:339–362, 1969.

L. Mullins and NR. Tobin. Theoretical model for the elastic behavior of filled reinforced vulcanized rubbers. *Rubber Chem Technol*, Vol. 30:555–571, 1957.

K.R. Olympio and F. Dandhi. Zero-ν cellular honeycomb flexible skins for one-dimensional wing morphing. In *48th AIAA/ASME/ASCE/AHS/ASC Structures, Structural Dynamics, and Materials Conference*, 2007.

K.R. Olympio and F. Dandhi. Flexible skins for morphing aircraft using cellular honeycomb cores. *Journal of intelligent material systems and structures*, Vol.21:1719–1735, 2010.

D. A. Perkins, J.L. Reed, and E. Havens. Morphing wing structures for loitering air vehicles. *American Institute Aeronautics and Astronautics*, 2004.

K. Pontoppidan, J. P. Boisset, and G. A. E. Crone. Reconfigurable reflector technology. *IEE Colloquium on Satellite Antenna Technology in the 21st Century*, Vol. 1:10/1–10/5, 1991.

K. Pontoppidan, C. Cappellin, N:C. Jessen, and H. U. Noergaard-Nielsen. Latest achievements on reconfigurable reflector antennas modelling. In *32nd ESA Antenna Workshop on Antennas for Space Applications Digest*, 2010.

Y. Rahmat-Samii, L. I. Williams, and R. G. Yoccarino. The ucla bi-polar planar-near-field antenna measurement and diagnostics range. *IEEE Antennas & Propagation Magazine*, Vol. 37, No.6:–, 1995.

RG. Technical data sheet. Online Resource, a. URL `http://www.ezentrumbilder.de/rg/pdf/td_de_ECC_Style447_D.pdf`.

RG. Online Resource, b. URL `http://shop1.r-g.de/art/190239-125`.

RG. Technical data sheet. Online resource, c. URL `http://www.ezentrumbilder.de/rg/pdf/td_de_ECC_493_Deutsch.pdf`.

B. W. Rosen. Fiber composite materials. *Metals Park*, 1965.

John Ruze. Antenna tolerance theory - a review. *Proceedings of the IEEE*, Vol. 54, NO. 4: 633–640, 1966.

H. J. Schek. The force density method for form finding and computation of general networks. *Journal of computer methods on applied mechnanics and engineering*, Vol. 3:115–134, 1974.

L. Schreider, S. Depeyre, P. Lepeltier, and P. Voisin. TN1 Actuator based reconfigurable reflector antenna, technical requirement document. Technical report, Thales Alenia Space, 2007.

M. Scott, J. D. Jacob, S. W. Smith, L. T. Asheghian, and J. N. Kudva. Development of a novel low stored volume high-altitude wing design. In *50th AIAA/ASME/ASCE/AHS/ASC Structures, Structural Dynamics, and Materials Conference*, 2009.

C.O.A. Semprimoschnig, D. Pueyo, J.R. Williamson, C. Mooney, C. Zimmermann, M.v. Eesbeek, and S. Taylor. Elastosil s690 - a space qualified european silicone material. Online resouce. URL http://esmat.esa.int/materials_news/isme09/pdf/4-New/S7%20-%20Semprimoschnig.pdf.

Ole Sigmund. Tailoring materials with presribed elastic properties. *Mechanics of Materials*, Vol. 20:351–368, 1995.

W. H. Theunissen, H. T. Yoon, W. D. Burnside, and G. N. Washington. Recofigurable contour beam-reflector antenna synthesis using a mechanical finite-element description of the adjustable surface. *IEEE transactions on antennas and propagation*, Vol. 49:272–279, 2001.

C. Thill, J. Etches, I. Bond, K. Potter, and P. Weaver. Morphing skins. *The Aeronautical Journal*, Vol. 112:117–139, 2008.

S. Timoshenko and J. M. Gere. *Theory of elastic stability*. McGRAW-HILL BOOK COMPANY, INC., 1963.

S. Timoshenko and S. Woinowsky-Krieger. *Theory of Plates and Shells*. McGRAW-HILL BOOK COMPANY, INC., 1959.

Torayca. T300 data sheet. Online resouce. URL http://www.toraycfa.com/pdfs/T300DataSheet.pdf.

S. W. Tsai, editor. *Composite Materials, Testing and Design*. American Society for Testing and Materials, 1979.

H. H. Viskum, S. B. Soerensen, and K. Pontoppidan. A dual reflector system with a reconformable subreflector. *Antennas and Propagation Society International Symposium, IEEE transactions on antennas and propagation*, Vol. 2:840–843, 1998.

H. H. Viskum, C. van't Klooster, F. Zocchi, P. Binda, and R. Wagner. Corrective subreflectors for millimetre and sub-millimetre wave applications. In *21 st AIAA International Communications Satellite Systems Conference and Exhibit*, Yokohama, Japan, 2003.

G. Washington. Smart aperture antennas. *Smart Mater. Struct.*, Vol. 5:801–805, 1996.

G. Washington, H. S. Yoon, M. Angelino, and W. H. Theunissen. Design, modeling, and optimization of mechanically reconfigurable aperture antennas. *IEEE transactions on antennas and propagation*, Vol. 50, No.5:628–637, 2002.

Dominik Weidmann. Material design of a reconfigurable reflector surface used in satellite communications. Master thesis, Technische Universität München, 2014. Student Project Supervised by Author.

Matthias Weinzierl. Design der hochelastischen Sektion einer formvaribalen Tragflächenverderkante der Mü3X Wölbfips. Semester thesis, Technische Universität München, 2013. Student Project Supervised by Author.

P. Weiss. Wings of change - shape-shifting aircarft may ply future skyways. *Science News*, pages 359–367, 2003.

M. Wießmeier. Konzept einer formvariablen tragflügelvorderkante bei einem segelflugzeug mit innenliegender austeuerung über ein rotary drive system (rds). Akaflieg München e.V.

J. Wittmann, M. Hornung, and H. Baier. Mission performance optimization via morphing wing-tip devices. In *Proceeding of DGLR Kongress*, Hamburg, Germany, 2010.

R.W. Wlezien, G.C. Horner, A.R. McGowan, S.L. Padula, M.A. Scott, R.J. Silcox, and J.O. Simpson. The aircarft morphing programm. In *International Society for Optical Engineering*, 1998.

Xinxue Xu. Morphing skin design for form variable airfoil cambers using a sandwich concept. Master thesis, Technische Universität München, 2012. Student Project Supervised by Author.

T. Yokozeki, S. Takeda, T. Ogasawara, and T. Ishikawa. Mechanical properties of corrugated compoistes for candidate materials of flexible wing structures. *Composites: Part A applied science and manufacturing*, Part A 37:1578–1586, 2006.

Hwan-Sik Yoon. *Design, modeling, and optimization of a mechanically reconfigurable smart reflector antenna system*. PhD thesis, The Ohio state University, 2002.

Shihang Zhou. Mikromechanische Analyse vom orthogonalen Metallgewebe. Semester thesis, Technische Universität München, 2011. Student Project Supervised by Author.

B. Appendix

B.1. Results of Reshaping Analyses on the Medium Size Models

Table B.1.: Shape difference in the reshaping case 1

Center actuator +10 mm			
[mm]	Model 1	Model 2	Model 3
Max.	0.636	0.631	1.519
Min.	-0.745	-0.972	-1.871
RMS	0.331	0.480	0.962

Table B.2.: Shape difference in the reshaping case 2

Center actuator -10 mm			
[mm]	Model 1	Model 2	Model 3
Max.	0.294	0.474	1.111
Min.	-0.669	-0.993	-2.325
RMS	0.184	0.255	0.556

In the case 1 and 2, the RMS results of the model 1 are the most promising with values smaller than 0.2 mm. The model 2 have slightly worse results than the model 1 while the results in the model 3 are almost three times larger than the results in the model 1 and 2. The initial geometry stiffness from the shell configuration has slightly influence on the model 1 and 2 but relative large influence on the model 3.

Table B.3.: Shape difference in the reshaping case 3

Center and adjacent actuator +10 mm			
[mm]	Model 1	Model 2	Model 3
Max.	1.131	0.948	3.219
Min.	-0.631	-1.419	-3.786
RMS	0.261	0.309	1.129

Table B.4.: Shape difference in the reshaping case 4

Center and adjacent actuator -10 mm			
[mm]	Model 1	Model 2	Model 3
Max.	0.998	0.548	3.925
Min.	-1.064	-0.796	-5.418
RMS	0.350	0.318	1.198

Table B.5.: Shape difference in the reshaping case 5

Center actuator +10 mm, adjacent actuator -10 mm			
[mm]	Model 1	Model 2	Model 3
Max.	2.223	1.462	5.431
Min.	-2.367	-1.817	-5.426
RMS	0.563	0.530	1.535

Table B.6.: Shape difference in the reshaping case 6

Random values: mean = 0 mm, std.= 3 mm			
Test 1			
[mm]	Model 1	Model 2	Model 3
Max.	1.267	1.038	2.790
Min.	-2.696	-0.869	-2.843
RMS	0.419	0.304	0.872
Test 2			
[mm]	Model 1	Model 2	Model 3
Max.	1.322	1.131	2.267
Min.	-1.378	-0.749	-2.081
RMS	0.293	0.276	0.762
Test 3			
[mm]	Model 1	Model 2	Model 3
Max.	1.417	1.543	2.258
Min.	-1.580	-0.895	-2.731
RMS	0.439	0.301	0.883

Table B.7.: Shape difference in the reshaping case 7

Random values: mean = 5 mm, std.= 3 mm			
Test 1			
[mm]	Model 1	Model 2	Model 3
Max.	1.036	1.398	5.690
Min.	-1.499	-1.307	-4.193
RMS	0.295	0.340	1.195
Test 2			
[mm]	Model 1	Model 2	Model 3
Max.	1.281	1.705	3.325
Min.	-1.630	-0.828	-2.674
RMS	0.402	0.276	0.777
Test 3			
[mm]	Model 1	Model 2	Model 3
Max.	2.151	0.835	1.987
Min.	-2.202	-1.594	-3.387
RMS	0.611	0.240	0.686

Table B.8.: Shape difference in the reshaping case 8

Random values: mean = -5 mm, std.= 3 mm			
Test 1			
[mm]	Model 1	Model 2	Model 3
Max.	1.955	1.344	2.934
Min.	-1.233	-0.904	-3.795
RMS	0.384	0.349	1.327
Test 2			
[mm]	Model 1	Model 2	Model 3
Max.	0.835	0.896	1.431
Min.	-0.370	-0.747	-2.722
RMS	0.149	0.202	0.618
Test 3			
[mm]	Model 1	Model 2	Model 3
Max.	1.607	1.239	2.396
Min.	-1.584	-0.700	-1.453
RMS	0.367	0.196	0.542

B.2. Results of Reshaping Analyses

The reshape figures for the Brazil and ConUS tasks are presented as follows.

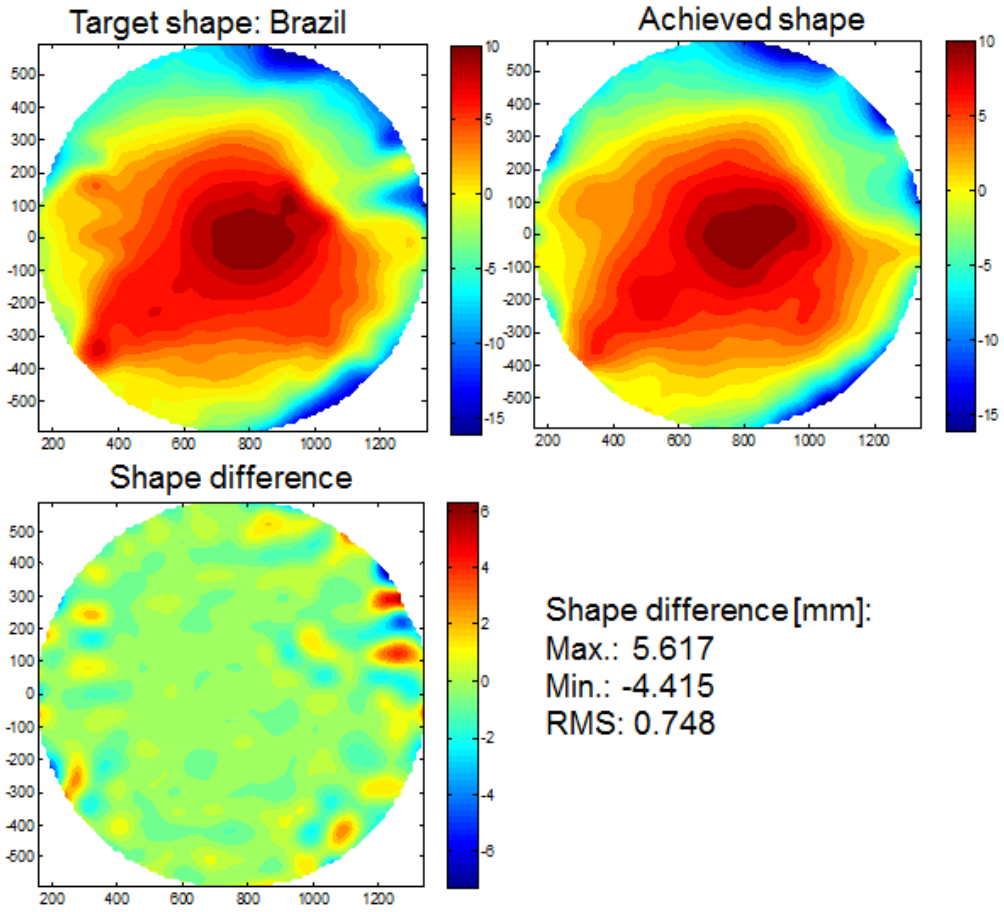

Figure B.1.: Target and achieved shapes of the task Brazil

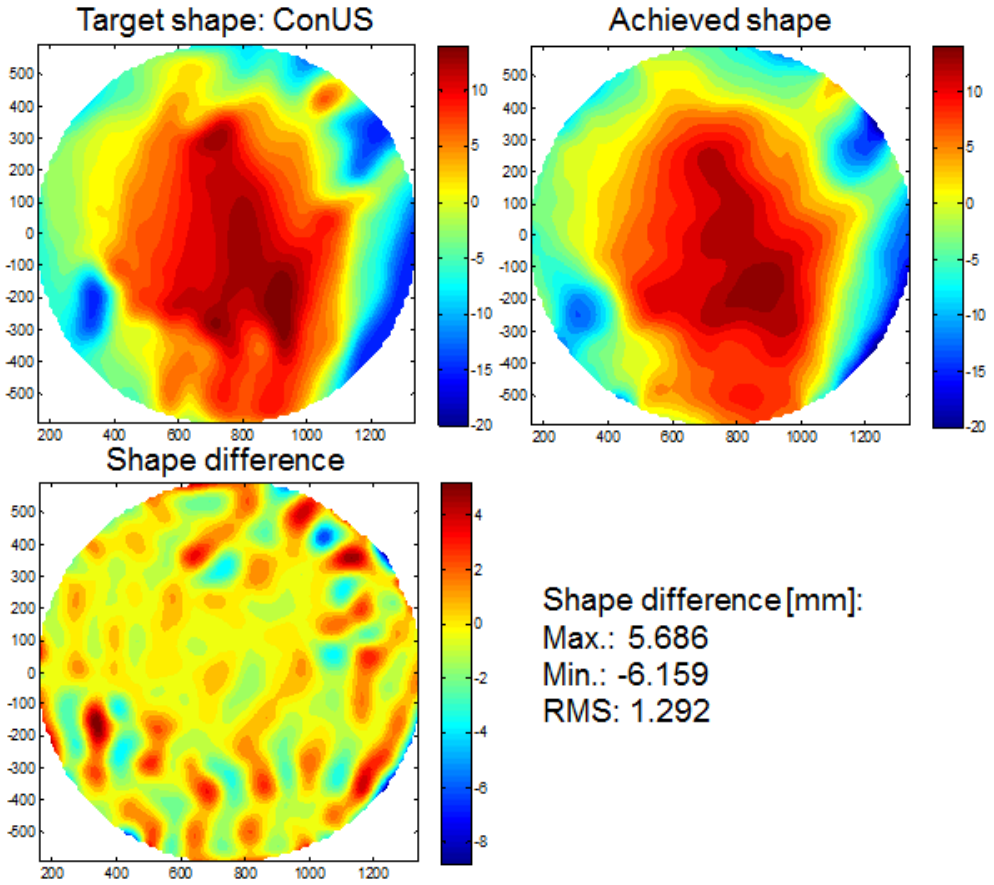

Figure B.2.: Target and achieved shapes of the task ConUS

B.3. Sensitivity Study on Demonstrator

The reference shapes are measured five times with different reshaping tasks between every two measurements, and their results are following:

Table B.9.: Comparison of measured and predicted reference shapes

Measurement description	RMS [mm]
1. Initial reference shape	0.084
2. Reference shape after Brazil task, measured immediately	0.105
3. Reference shape after Brazil task, measured one hour later	0.092
4. Reference shape after Europe task, measured immediately	0.098
5. Reference shape after Europe task, measured one hour later	0.089

B.4. Results of Shape Correlation on Demonstrator

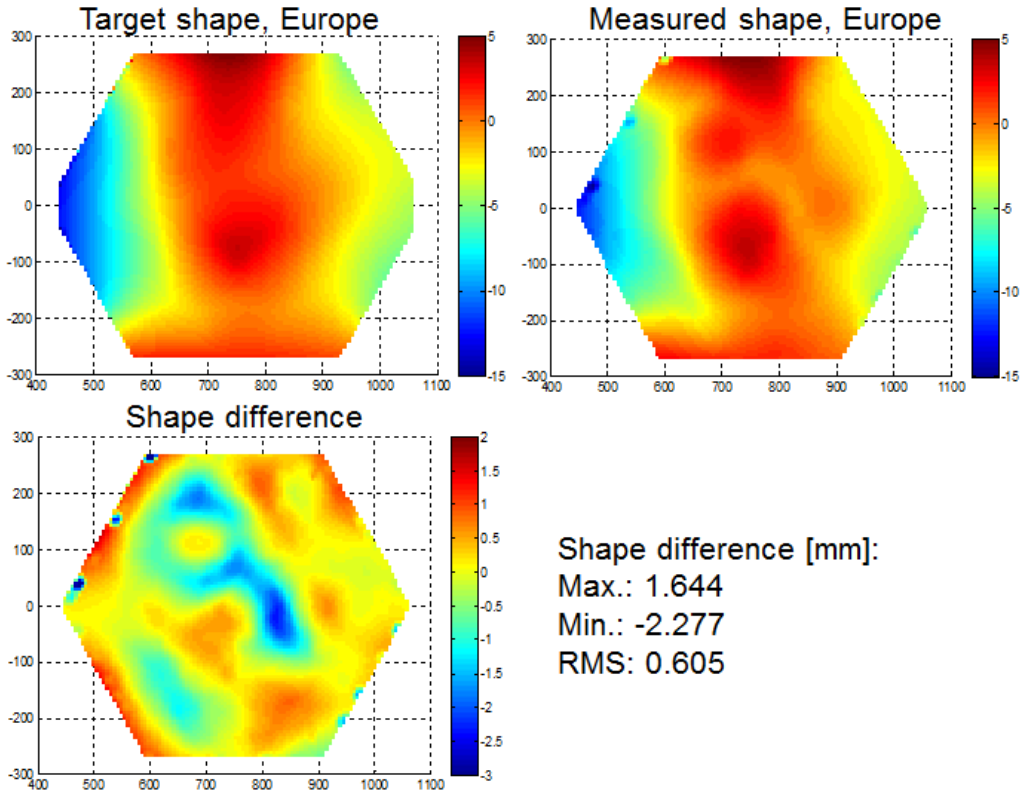

Figure B.3.: Predicted and measured shapes of the Europe task

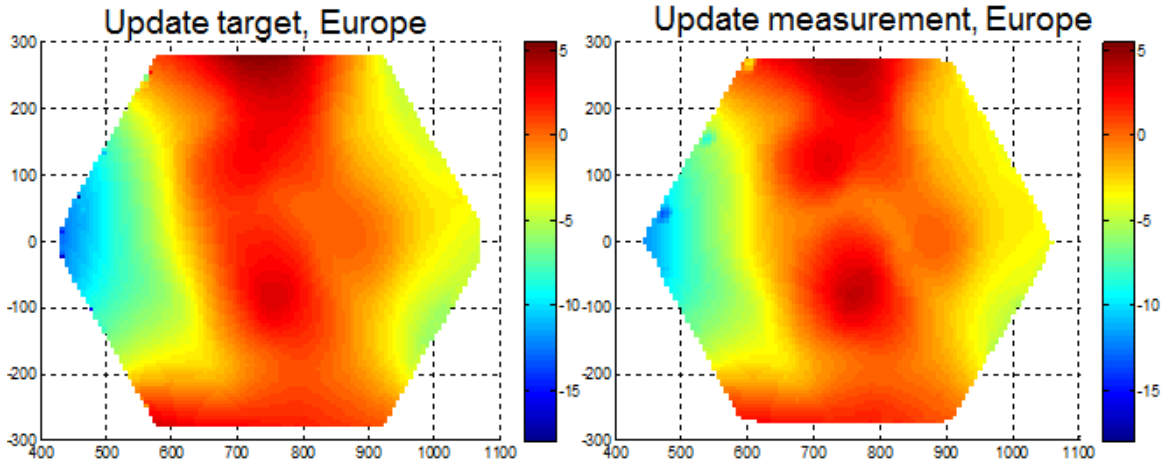

Figure B.4.: Update measured and predicted shapes of the Europe task

B.5. Experiments of Flexible Sandwich

One of the accordion cores is stretched to more than 200% of its own length. A close view of the accordion core and the curve of stress to strain relation are presented here.

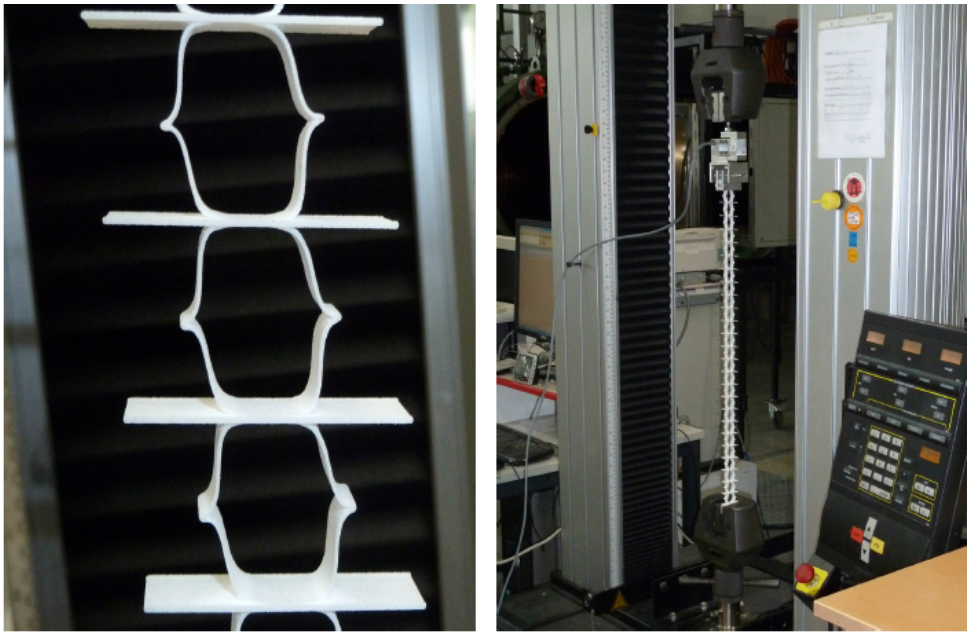

Figure B.5.: The manufactured according core with extreme large strain [Weinzierl (2013)]

The cantilever test of the manufactured flexible sandwich has demonstrated a sufficient bending stiffness as shown in the following figure.

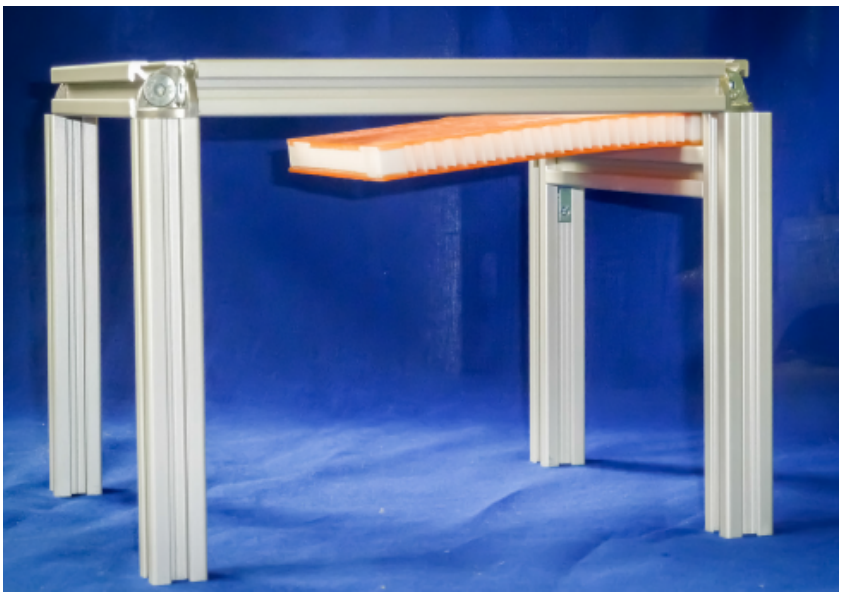

Figure B.6.: The demonstrator of the flexible sandwich [Weinzierl (2013)]

B.6. Results of Stress and Strain of the Tailored CFRP Laminates

Table B.10.: Extreme stresses (MPa) in reshaping of the leading edge, skin at the contact region

Time step	Max. in S_{11}	Min. in S_{11}	Max. in S_{22}	Min. in S_{22}	Max. in S_{12}	Min. in S_{12}
0.15	416	-254	38	-23	10	-16
0.30	437	-210	40	-19	7.7	-11
0.50	369	-148	33.8	-14	6.2	-5.6
0.75	201	-83	18	-7.5	2.9	-2.9
1.00	65	-68	5.5	-5.6	2.7	-2.8

Table B.11.: Extreme strains in reshaping of the leading edge, skin at the contact region

Time step	Max. in ε_{11}	Min. in ε_{11}	Max. in ε_{22}	Min. in ε_{22}	Max. in ε_{12}	Min. in ε_{12}
0.15	0.0048	-0.0029	0.0068	-0.0044	0.0033	-0.0054
0.30	0.0050	-0.0024	0.0071	-0.0036	0.0026	-0.0036
0.50	0.0042	-0.0017	0.0060	-0.0026	0.0020	-0.0018
0.75	0.0012	-0.0003	0.0036	-0.0016	0.0010	-0.0009
1.00	0.0007	-0.0008	0.0011	-0.0011	0.0009	-0.0009

Table B.12.: Extreme stresses (MPa) in reshaping of the leading edge, skin without interactions

Time step	Max. in S_{11}	Min. in S_{11}	Max. in S_{22}	Min. in S_{22}	Max. in S_{12}	Min. in S_{12}
0.15	143	-159	13	-18	20	-9
0.30	152	-184	15	-22	19	-9.7
0.50	106	-162	12.6	-16.6	13	-8.6
0.75	53	-84	11.3	-9.8	3.6	-4.1
1.00	24	-63	8.2	-8.8	3.9	-3.7

Table B.13.: Extreme strains in reshaping of the leading edge, skin without interactions

Time step	Max. in ε_{11}	Min. in ε_{11}	Max. in ε_{22}	Min. in ε_{22}	Max. in ε_{12}	Min. in ε_{12}
0.15	0.0018	-0.0026	0.0026	-0.0039	0.0069	-0.0033
0.30	0.0017	-0.0021	0.0025	-0.0040	0.0064	-0.0032
0.50	0.0012	-0.0018	0.0024	-0.0030	0.0044	-0.0029
0.75	0.0006	-0.0009	0.0022	-0.0018	0.0012	-0.0014
1.00	0.0003	-0.0007	0.0016	-0.0017	0.0013	-0.0012